AN EVALUATION OF INTERPOLATION TECHNIQUES AND COMMONLY USED DIGITAL ELEVATION MODELS FOR FLOODLINE MAPPING IN A SOUTH AFRICAN ENVIRONMENT

Completed in accordance with the requirements of a Masters in Geography (MSc) degree

By

Prevlan Chetty

200723276

Supervisor: Professor Solomon G. Tesfamichael

Department of Geography, Environmental Management and Energy Studies

Faculty of Science University of Johannesburg

March 2021

ABSTRACT

Flooding accounts for a large proportion of property loss and damage all over the world. Flood frequencies associated with intense periods of rainfall show increasing trends in both South Africa and globally. As a result, preventative measures to mitigate property loss and damage play an increasingly important role in the built environment. In hydrology terms, flood-lines refer to the maximum extent of a flood event that can either be measured retrospectively after a rainfall event of significance through in-situ measurements or proactively simulated through a digital representation of the assessment area. The proactive approach has inherent benefits of being able to run a multitude of volumes to illustrate the effect of various rainfall events on a river system but is dependent on the quality of data being fed into the system itself. A key component to the data input includes elevation information that defines the topographical environment around the river system. There are several elevation sources and methods of interpolating to create continuous elevation surfaces that can be utilized for an area-based flood modelling scenario. The usage and application of many of these sources are affected by the cost and time factors which often place restrictions on the level of detail and accuracy that the digital representation of the river system captures. Due to the multitude of variables with regards to the elevation data inputs, there is a need to 1) identify the best-suited interpolation techniques to accurately represent a hydrological environment; and 2) to identify an optimal elevation source to accurately depict a flood-line output.

The research investigated the accuracy of the Inverse Distance Weighting (IDW), Nearest Neighbour (NN), kriging, spline and Topo to Raster (ANUDEM) interpolation techniques as applied to a 5 m interval elevation contours obtained from the Chief Directorate: National Geospatial Information (NGI) for a hydrological setting in the Roodepoort Region in Johannesburg, South Africa. A 50 cm resolution aerial Light Detection and Ranging (LiDAR) point cloud was used as a baseline dataset to compare the five interpolations techniques. The findings from the interpolation assessment found that the Topo to Raster technique yielded the most accurate results with the least amount of variation. The spline interpolation showed the highest level of variation to the baseline LiDAR, followed by the IDW technique. The location-based analytics in the form of a standardised residual outlier identification allowed for the identification of significant elevation outliers that were produced in the interpolation process when evaluated using the LiDAR, and it was noted that most of the outliers across all techniques coincide with areas that showed frequent topographical changes.

The second main objective of the research aimed at comparing different Digital Elevation Model (DEM) sources, including the NGI's 5 m contour, the 30 m resolution Shuttle Radar Topography Mission (SRTM) and the Advanced Land Observation Satellite (ALOS) World 3-

D 30 m (referred to as the AW3D30) to delineate flood-line extent outputs. To achieve this objective, the Topo to Raster interpolation technique was applied to produce continuous DEM surfaces, while the LiDAR-derived flood extent was used as a reference. The flood-line models were run for two scenarios, representative of short duration and lower volume 10-year period, and a longer duration and higher volume 100-year period. The results indicated that while the NGI DEM consistently produced outputs that provided the highest coverage area of the flood-line, the accuracy of the NGI DEM in comparison to the AW3D30 and SRTM DEMs was lower. While the SRTM DEM produced the best relative accuracy in terms of mean distance differences to the baseline LiDAR, the poor coverage output of the SRTM DEM source shows its unsuitability for flood-line applications, particularly in lower return period conditions (10-year period) with low water volumes. The results showed that the AW3D30 DEM source has the best performance when taking the output area and overall accuracy into account. The AW3D30 DEM performed consistently well in both 10-year and 100-year scenarios with an increase in performance with longer return periods and larger associated volumes. Using a location-based standardised residual analysis, significant outliers were identified in areas where large amounts of surface change occur further illustrating the influence of temporal resolution in DEM data. The study presents an interesting dynamic between spatial resolution versus timely acquired data and highlights the importance of having access to more frequently acquired elevation data sources in environmental modelling applications.

ACKNOWLEDGEMENTS

I would like to thank my parents and my wife for all the support and encouragement throughout this journey. I am passionate about Remote Sensing and GIS and over the course of my career thus far, I have been fortunate to have identified gaps in the consulting industry which has ultimately led to the content of this MSc. The MSc is extremely significant to me, with a decade since the last graduation that I missed (I got the dates all mixed up). I am hopeful that this time around, I will have a graduation photo to show to my family and prove that I did indeed graduate.

I would also like to thank the companies that I have had the pleasure of working for over the course of this MSc: Digby Wells Environmental, and Groundwater Consultancy Services, for allowing me the time to dedicate the required attention to this research, along with the provision of the resources needed to complete this study.

Finally, a huge thank you to my friend and supervisor Professor Solomon Tesfamichael for your counsel, guidance and support through this journey. My gratitude is also extended to Robert Verger, a friend and colleague that has assisted me in understanding the hydrological modelling environment. This journey has given me perspective and a sense of immense respect towards the field of hydrology. Notable mentions also need to be made towards Alan Brower and Shayna-Anne Cuthbertson for their assistance and guidance.

PLAGIARISM DECLARATION

I hereby declare that the work contained in this dissertation is my original work. Sources referred to in the creation of this work have been appropriately acknowledged by the usage of explicit references.

Signature:  Date: 22/03/2021

TABLE OF CONTENTS

TABLE OF FIGURES

LIST OF TABLES

PUBLICATION

The following manuscript modified from Chapter 2 of the dissertation has been submitted and accepted to the *GISTAM 2021* conference.

A comparison of interpolation techniques in producing a DEM from 5 m contours

The following manuscript modified from Chapter 3 of the dissertation has been submitted to the journal *Water SA*.

A comparison of flood-line models derived from multiple DEM sources

ABBREVIATIONS AND ACRONYMS

ALOS	Advanced Land Observation Satellite
ANUDEM	Australian National University Digital Elevation Model
ASCII	American Standard Code for Information Interchange
ASTER	Advanced Spaceborne Thermal Emission and Reflection Radiometer
AVNIR	Advanced Visible and Near Infrared Radiometer
AW3D30	Advanced Land Observation System 30 m resolution
COJ	City of Johannesburg
CSIR	Council for Scientific and Industrial Research
DEM	Digital Elevation Model
DMC	Dual Mass Camera
DRDLR	Department of Rural Development and Land Reform
DSM	Digital Surface Model
DTM	Digital Terrain Model
DWS	Department of Water and Sanitation
GIS	Geographic Information Systems
GNSS	Global Navigation Satellite Systems
GPS	Global Positioning System
GSD	Ground Sample Distance
IDW	Inverse Distance Weighting
IMU	Inertial Measurement Unit
JAXA	Japanese Aerospace Exploration Agency
LiDAR	Light Detection and Ranging
NASA	National Aeronautics and Space Administration
NGI	Chief Directorate for National Geospatial Information
NN	Nearest Neighbour
PALSAR	Phased Array type L-band Synthetic Aperture Radar
PRISM	Panchromatic Remote-sensing Instrument for Stereo Mapping
RGB	Red, Green, Blue
RMSE	Root Mean Square Error
SAR	Synthetic Aperture Radar
SAWS	South African Weather Service
SDF	Standard Design Flood
SRTM	Shuttle Radar Topography Mission
TIN	Triangulated Irregular Network
WRC	Water Resources Commission
XS	Cross Section

CHAPTER 1

INTRODUCTION

1.1 Background

Flooding is recognised as one of the most damaging types of natural disaster in South Africa (ASSAf, 2020; Merolla, 2012). Research into rainfall trends in South African between 1921 and 2015 has revealed that the intensity of daily rainfall has been increasing for most of the country (Kruger *&* Nxumalo, 2017). Other research conducted on a global scale corresponds to the South African trend (Easterling *et al.,* 2000; Donat *et al.,* 2013), further providing context to the threat of flooding. Flood inundation is a term that refers to a flooded area, where water would extend onto land that would otherwise have been dry (Teng *et al.,* 2017). Flood-lines, or flood inundation extents, refer to the maximum extent of a flood inundation that is derived to determine the extent that a hydrological system (that is a river and/or stream) will flood, with specific flooding likelihoods that are related to periodic intervals (Sanders, 2007).

There are two popular methods for deriving the extent of flood-lines which either includes: 1) physically demarcating the extent of a flood shortly after a significant rainfall event/significant volumetric change in the river system, or 2) the deterministic method of simulating the extent of flooding along cross sections along the river with historical rainfall data through computer-aided models (Belayneh *et al.*, 2009). The physical demarcation of a flood extent is a reactive approach, where flood-line extents are recorded constantly after each significant rainfall event. While a field verification of flood-line extents associated with a flood has occurred is accurate, the approach is labour intensive and cannot offer predictive insight into flood-line extents for specified volumes of water (Teng *et al*., 2017). The deterministic method allows for the modelling of a hydrological environment in a digital framework and allows for the simulation of the impact a specified volume of water will have on a hydrological environment. The success of the deterministic method is heavily dependent on the quality of the data that is used to create the digital framework, which includes rainfall data; the physical demarcation of the hydrological system; the hydrological properties that determine the coefficients of flow and resistance across the surface; and elevation data that defines the river geometry and surroundings in the form of a Digital Elevation Model (DEM) (Brunner, 2008).

The focus of the present research is placed on DEM data inputs that define the hydrological environment in the deterministic approach and close attention is paid to the effect that the elevation data input has on the flood-line extent outputs. The South African hydrological modelling setting is fortunate to have access to a variety of DEM sources based on where the

area of assessment is located within the country. Most major metropolitan regions have been surveyed with high-resolution aerial based platforms including Light Detection and Ranging (LiDAR), while the rest of the country is supplemented by medium- to low-resolution datasets that are promoted for use in assessments for strategic decision making by the relevant authorities. The Department of Rural Development and Land Reform (DRDLR) releases a 5 m ground sample distance (GSD) contour dataset to the public that is produced by the Chief Directorate for National Geospatial Information (commonly referred to as the NGI) which forms a large component of the medium-resolution supplementary data available in South Africa. Online sources that include the Shuttle Radar Topography Mission (SRTM), Advanced Spaceborne Thermal Emission and Reflection Radiometer (ASTER) and the Advanced Land Observation System (ALOS) 30 m resolution (AW3D30) account for large components of the low-resolution DEM data available to the public.

While there is a need for high-resolution elevation data inputs to derive accurate flood-line results, access to this kind of elevation information is often restricted by the costs and time involved in obtaining this information. It is therefore common practice for hydrological modelling to be based on free and readily available online and publicly distributed elevation data sources with a significantly lower resolution and often lower associated accuracies. To use the elevation data source as an input in the flood-line modelling process, the elevation source needs spatial continuity which is achieved through a process of interpolation.

1.2 Spatial interpolation algorithms and their associated relative accuracy

Spatial interpolation refers to the prediction of a series of unknown values that occur between a limited number of sample points (Manuel, 2004). Interpolation is commonly used for geographic data that is defined as points or lines, with elevation attributes, to create a continuous surface referred to as a DEM. There are numerous routines available for interpolation which have been widely applied and tested (Arun, 2013; Erdogan, 2009; Salekin *et al.,* 2018). The interpolation techniques apply the basic principle of Tobler's first law of geography, where closer objects share a greater relationship than farther ones (Arun, 2013). Interpolation techniques are commonly grouped into local/global, deterministic/geostatistical and exact/approximate (Erdogan, 2009).

Local methods of interpolation include Inverse Distance Weighting (IDW) and the Nearest Neighbour (NN) technique. IDW is a non-linear, deterministic interpolation technique that computes a weighted average of a value from sample points in close vicinity to determine the value of non-sampled points (Robinson & Metternicht, 2003). The main parameter for this interpolation methodology is the sample points' distance to the non-sampled point. The NN interpolation model is a method based on the Sibson interpolation model, where values are assigned to un-sampled points based on the construction of Voronoi cells which work together to form areas of overlap (Sibson, 1980). Weights are applied to the Voronoi cells which are then used to determine the values of unknown points. The formula used for the NN interpolation is identical to IDW, with the only difference coming from the method used to calculate the weightings. The output from the NN interpolation does not produce peaks, pits and valleys that were not already defined in the known sample points.

Geostatistical methods of interpolation include the kriging method, which uses the spatial location rather than relying on attribute values only (Arun, 2013; Matheron, 1963). Kriging is a stochastic local interpolation technique that computes the value of non-sampled points in a similar way to IDW, with the exception that there is more control on the weighting system that determines unknown values based on distance (Robinson *et al.,* 2003).

The spline interpolation model creates a smooth raster surface from the known sample points using a 2-D minimum curve technique (Robinson *et al.,* 2003). The resulting surface passes through all known sample points. The spline method is mathematical in nature and takes the form of a cubic equation whereby each known data point has a cubic equation through which all splines pass (Robinson *et al.,* 2003).

Different interpolation techniques applied to the same set of data can result in varying DEM outputs (Arun, 2013). There is therefore a need to evaluate the suitability and accuracy of these interpolation techniques across a variety of elevation data sources. Erdogan (2009)

investigated the relative accuracy of various interpolation algorithms for an area in Turkey with high topographical variance. The research utilised deterministic procedures to evaluate various interpolation algorithms against a baseline survey-grade dataset. The best results are obtained using the thin-plate spline algorithm, a derivative of the spline algorithm itself. Zimmerman *et al*. (1999) presented research that compared the outputs of the IDW versus the kriging methodology and showed that the kriging method was able to adjust to the spatial variability of the data and by doing so, yielded better estimation of altitude for unknown sample points (Zimmerman *et al.,* 1999). Aguilar *et al*. (2005) presented findings from a study in Almeria, Spain, that indicated that the IDW method was marginally better than the accuracy from the kriging model output.

In the 1980s, a study done by Mark (1984) proposed an algorithm for automatically delineating a drainage network from DEM data. This study gave rise to the need for hydrological correction algorithms in the DEM interpolation process which includes the development of the Australian National University Digital Elevation Model (ANUDEM). ANUDEM is also known as the Topo to Raster feature in ESRI's ArcGIS software (ESRI, 2019) which aims to generate elevation models that are hydrologically conducive to network extraction (Callow *et al.,* 2007). The ANUDEM method creates an interpolated surface that preserves the critical geometry components required to define a hydrological system which includes ridgelines and stream networks (Arun, 2013).

1.3 Digital elevation model sources and their effect on the flood-line modelling environment

A DEM is described as a numerical data file that represents the topography over an area at a grid interval (Erdogan, 2009). A DEM can be differentiated into a Digital Surface Model (DSM), which is representative of features both on the ground and above the ground, and a Digital Terrain Model (DTM) which represents the ground only features. There are numerous methods of generating DEM data which include photogrammetry, LiDAR and Interferometry (Zhang *et al*., 2019). DEM data is often the result of an interpolation process between the height values that are stored as attributes in point or line vector files. The generation of information relating to the heights of features on the Earth's surface is affected by two parameters, namely temporal and spatial resolution. Temporal resolution is defined as the frequency of collection, while spatial resolution is defined as the GSD (Erdogan, 2009).

The input elevation data for the flood-line modelling system is one of the most important aspects of the modelling process, as the regional elevation data defines the geometry of the river and its surrounding basin (Azizian & Brocca*,* 2020). Flood-line mapping often produces

results that vary with different sources of elevation data. The outputs are affected by the vertical accuracy of the various models which is determined by the topography of the region and the spatial resolution of the DEM (Li & Wong, 2010). Sanders (2007) illustrated that higher spatial resolution sources will not necessarily provide greatly improved results in comparison to lower spatial resolution DEMs from an alternate source. Sanders (2007) also found that the temporal resolution of the DEM often played an integral role in accurately defining the geometry of a hydrologic environment.

Various studies have compared the accuracy of different elevation data sources. Elkhrachy (2017) for example, compared the accuracies of the SRTM versus ASTER over Narja City in Saudi Arabia, to determine the vertical accuracy for the two data sources. The findings from Elkhrachy indicated that the 30 m resolution SRTM DSM has a relatively high vertical accuracy measuring 16 m, which is well within the published SRTM data specifications. Li & Wong (2010) compared flood simulation results for different elevation sources and spatial resolutions along the Kansas River (part of the Missouri River in the United States of America). The study found that variations in flood-line outputs were mostly due to differences in the sources of the DSMs, rather than the varying spatial resolutions. The researchers also found that while previous sources of literature including Sanders (2007) and Schumann *et al*. (2008) argued that the SRTM DSM performs well on moderately sloped topography, the results from the Kansas River study (which has gentle topography) showed that the application of SRTM may not be acceptable. More recently, Azizian & Brocca (2020) compared the applicability of DEM sources in an applied setting for flood-line modelling in data-sparse regions, which included assessments across ASTER, SRTM and ALOS sources. The study found that the ALOS DEM source yielded the most accurate results with the cross-sectional profile of the river being the closest to those measured in-field.

While extensive research into accuracy comparisons across various elevation data sources has been conducted internationally, there have been limited instances in which commonly utilised elevation data sources in South Africa have been compared against each other. In particular, the public distribution Chief Directorate for the NGI 5 m resolution contour dataset has not been compared to the AW3D30 dataset because of the relatively new arrival and application of the latter.

In the 1990s, studies done by Grayson *et al.* (1991) demonstrated the integral role that DEM data plays in hydrological applications. In 2009, Gurnell & Montgomery (2000) illustrated the advancements in hydrological modelling concerning the models and algorithms that were being developed for the incorporation of DEM data in Geographic Information Systems (GIS) environments. While significant amounts of research have been applied to global scale

elevation models and their suitability to flood-line mapping, there is a need for localised studies that compare the suitability of elevation data sources with varying temporal and spatial resolution specifications.

1.4 Flood-line modelling environment

The process of using computer aided models to simulate the extent of a flood-line is deterministic in nature. There are various deterministic based flood inundation methodologies available to derive the extent of a flood-line which include one-dimensional flow models, two-dimensional flow models and three-dimensional flow models. The software used for the current research was the GeoHECRAS package that is distributed by CivilGEO (CivilGEO, 2019. The software package is a one and two-dimensional back-water programme which runs a series of calculations along each defined cutline running perpendicular to the river being assessed. The back-water modelling approach is commonly applied in the industry to generate flood-lines. In particular, the GeoHECRAS approach provides an opportunity to focus on the influence that individual modelling parameters (such as elevation) have on determining the flood-line extent.

The modelling environment requires the input of data describing the environment which includes the volume of water to be simulated, the geometry of the river and the DEM which describes the surrounding topography. As the focus of the research presented was to assess the influence of the DEM data on the modelling process, specific investigations were undertaken to look at the formulation of the DEM data and its associated influences, along with how different sources of this specific input affect the final outputs derived from the modelling process.

The GeoHECRAS flood-line modelling environment is able to export the obtained flood inundation and the associated flood-line extent to shapefile format which allows the analysis of the data to continue in a GIS environment. ArcGIS and Global Mapper were used to generate and facilitate the analytical components of the research, which were fed into Microsoft Excel (Microsoft Corporation, 2019) for statistical analyses.

1.5 Problem statement

A flood occurs when water flows out of the defined boundaries of a channel and influences areas that are usually dry (Merz and Blöschl, 2008) with the potential to cause significant property loss and casualties. Flood-lines represent the extent to which a hydrological system will flood; they are related to specific volumes of water from rainfall events. As part of the

Guidelines for Human Settlement, Planning and Design produced by the Council for Scientific and Industrial Research (CSIR), no urban development should be allowed in the demarcated 50-year flood-line extent (CSIR, 1999). The requirement itself originates from the National Building Regulation and Building Standards Act (Act 103 of 1997) and is solely based on safety considerations. The establishment of the extent of flood-lines therefore plays a crucial role in planning and management of any development along a river. A review of the existing literature exposes major differences and inconsistencies in performance between various DEM sources (Teng *et al*., 2017; Elkhrachy, 2017; Sanders, 2007, Schumann *et al*. 2008). These inconsistencies generally result from the defining topography, although Elkhrachy (2017) found that in contrast to previous studies, the SRTM DEM source performs well in slightly varying topographic conditions. The dependency of flood-line accuracy on DEM sources in relation to the general topographic environment means that localised assessments are required to compare various DEMs to select the optimal model in a localised context. In South Africa, there is a gap in addressing the accuracy and applicability of the NGI 5m contour data source in applied circumstances such as flood-line modelling in relation to other popularly utilised DEM sources such as SRTM. The AW3D30 data source is a relatively new DEM source with no existing literature dealing with applied accuracy assessments in South Africa. The research seeks to contribute to the body of research by comparing the flood-line outputs of different river geometry sources as per the DEMs commonly available and utilised in the South African hydrological environment. In addition, there is a significant gap in the literature in smaller, localised scale accuracy assessments of DEM interpolators for photogrammetrically derived elevation data. Previous studies have generated inconsistent results which show links to the surrounding topographical variance of the study area (Erdogan, 2009; Zimmerman *et al.*, 1999; Aguilar *et al.*, 2005). The need therefore exists to assess the accuracy of commonly utilised interpolation techniques on a localised dataset such as the South African NGI 5m contour source.

1.6 Aim and objectives

The research aims at exploring interpolation techniques and commonly utilised DEM sources for flood-line mapping for a tributary of the Wilgespruit River in Gauteng, South Africa which is covered by a variety of elevation data sources. The specific objectives of the study are to:

1) Compare various interpolation techniques including the IDW, NN, kriging, spline and Topo to Raster techniques applied to the NGI elevation data source as a precursor to flood-line modelling;
2) identify limitations associated with the interpolation accuracy of the NGI dataset;

3) compare flood-line outputs that are derived from the NGI, SRTM v3.0 and AW3D30 DEM sources in comparison to a LiDAR flood-line output; and
4) identify limitations associated with each DEM source in its application in flood-line modelling.

1.7 Significance of the study

The research sets out to report the following results. First to identify an optimal interpolation algorithm that can be used on contour lines such as those provided by the NGI contour dataset to derive spatially continuous DEM. The resultant DEM in turn provides important input for defining river geometry. Second, the research aims to report on the accuracies of digital elevation data sources for flood-line mapping. This result could contribute to the selection of the best DEM source for optimal flood-line modelling purpose. These two results therefore could contribute specifically to the knowledge of hydrological modelling techniques by focussing on spatial continuous surface creation techniques and accuracies of data sources. Selecting an optimal and publicly available data source in particular is crucial in South Africa to avoid relying on expensive data sources such as LiDAR-derived DEM.

1.8 Study area

The study area is a 5 km length of a river that is a tributary of the Wilgespruit River, between Willowbrook and Strubens Valley in Roodepoort, Johannesburg. The area has a moderate topographical range surrounding the river length, characterised by the Witwatersrand quartzite ridge outcrops. The elevation range along the 5 km river course ranges from 1500 m to 1600 m above mean sea level. According to the sub-quaternary catchment system of the Department of Water and Sanitation (DWS), the study area forms part of the A21E catchment area (DWS, 2017). The river channel width ranges between 5 and 20 m over the length of the study area and flows seasonally between October and March. The study area was selected based on the available coverage overlap between the aerial (LiDAR and NGI) and satellite-derived (SRTM and AW3D30) elevation data sources, where the assessment of the various data sources forms part of the objectives. The study area comprises urban residential land-use classes which have shown to be severely affected by flooding (Davis-Reddy & Vincent, 2017).

1.9 Organisation of the dissertation

The dissertation consists of four chapters, with Chapters 2 and 3 being standalone chapters prepared for submissions for publication. Chapter 2 compares interpolation techniques including NN, kriging, IDW, Topo to Raster and spline performed on the NGI data. The purpose of Chapter 2 is 1) to demonstrate which interpolation technique is best suited to the NGI dataset in hydrological environments using quantitative techniques and 2) to understand the limitations associated with the application of the NGI dataset with regards to the various interpolation techniques. The output and findings from Chapter 2 are used in Chapter 3 to create continuous elevation data inputs which are required for flood-line delineation. The purpose of Chapter 3 is 1) to use quantitative assessments to compare DEM sources including NGI, SRTM v3.0 and AW3D30 DEM against a baseline LiDAR DEM to delineate flood-line modelling and 2) to understand the limitations associated with the application of each DEM source by analysing significant outliers. Chapter 4 presents a synthesis of the two interlinking chapter themes with an overall conclusion of the dissertation. Limitations of the study are discussed, along with recommendations for future investigations. The chapter aims to provide recommendations to the field of research by suggesting optimal interpolation techniques for affordable DEM sources that can be used to produce acceptable flood-line maps. The research design is presented in Figure 1.1, while a schematic overview of the dissertation's processing environments is presented in Figure 1.2.

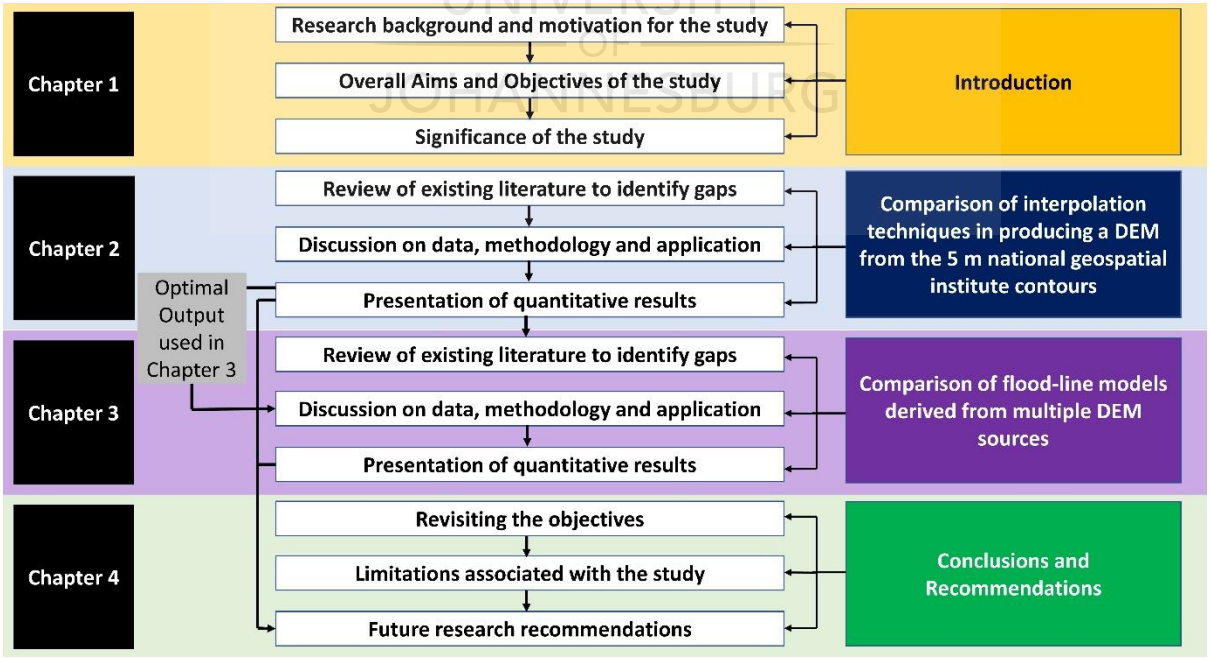

Figure 1.1: Research design

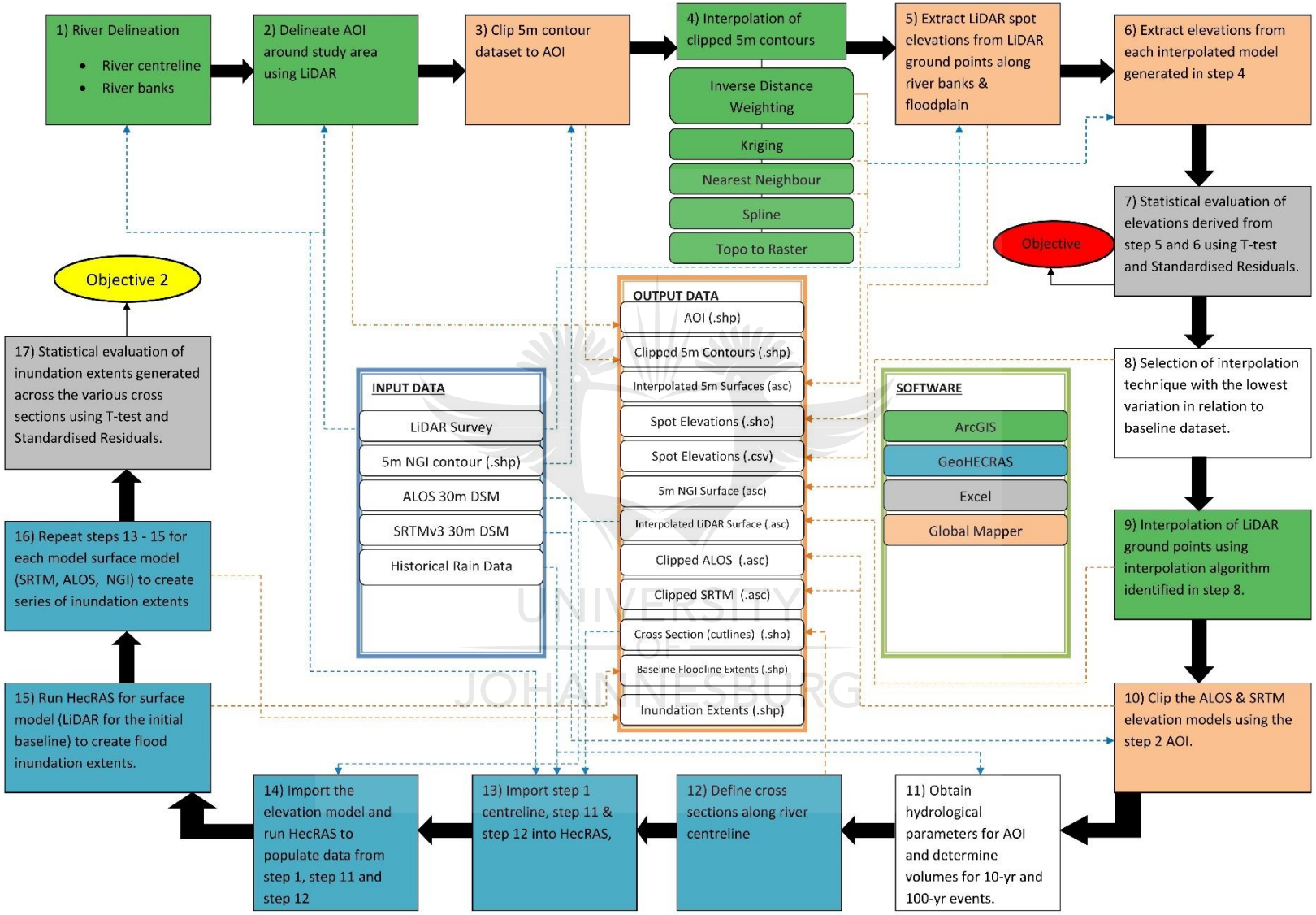

Figure 1.2: Workflow and organisation of the dissertation

CHAPTER 2

A COMPARISON OF INTERPOLATION TECHNIQUES IN PRODUCING A DEM FROM THE 5 M NATIONAL GEOSPATIAL INSTITUTE CONTOURS

2.1 Introduction

Flooding is a globally occurring phenomenon that causes property loss and casualties all around the world (Teng et al., 2017). A flood is characterised by an overflow of water that submerges land that would usually be dry which is often referred to as the flood inundation area (Merz and Blöschl, 2008). The extent to which a given river will flood to is commonly referred to as a flood-line (the maximum extent of the flood inundation area) and is related to the effect that a specific volume of water has on a hydrological system through rainfall events (Nkwunonwo et al., 2020). The statistical likelihood of a rainfall volume is commonly translated to 10-Year, 50-Year and a 100-Year flood event (Smithers, 2012). As part of South Africa's Council for Scientific and Industrial Research's (CSIR) Guidelines for Human Settlement, Planning and Design (CSIR, 1999), no urban development should be allowed in the demarcated 50-year flood-line extent. The requirement itself originates from the National Building Regulation and Building Standards Act of South Africa (Act 103 of 1997) and is solely based on safety considerations. The establishment of the flood-line extents therefore play a crucial role in any development along a river.

In deterministic computer aided techniques of demarcating a flood-line, one of the most important aspects is the input elevation data that defines the geometry of the river and its surrounding basin (Saksena & Merwade, 2015). Flood-line mapping often produces results that vary with different sources of elevation data. The outputs are affected by the vertical accuracy which is determined by the topography of the region and the spatial resolution of the elevation data (Li & Wong, 2010). In addition, the importance of interpolation algorithm accuracy is recognised as an integral component in representing the topography in numerical form (Chaplot et al., 2006). If interpolation forms an integral component of defining topography, and the topography forms an important part of the flood-line process, it can be inferred that the interpolation procedure of elevation data plays an important role in the development of flood-line extents.

For elevation data to be accurately incorporated into the flood-line modelling process, there needs to be spatial continuity in the elevation dataset by creating a raster surface referred to as a Digital Elevation Model (DEM). DEMs are derived through the process of interpolation, which refers to the prediction of a series of unknown values located between a limited number

of sample points (Manuel, 2004). Interpolation techniques, of which numerous techniques are available, are commonly used for geographic data that are represented as points or lines having elevation information. These techniques are commonly grouped into local/global, deterministic/geostatistical and exact/approximate classes (Erdogan, 2009). Local methods of interpolation include the Inverse Distance Weighting (IDW) and the Nearest Neighbour (NN) technique. Geostatistical methods of interpolation include the kriging method, which uses the spatial location of data points rather than relying on the elevation attribute values alone (Arun, 2013). The spline (sometimes referred to as rubber sheet) method is mathematical in nature and takes the form of a cubic equation whereby each known data point has a cubic equation where all splines pass through (Robinson & Metternicht, 2003).

Different interpolation techniques applied to the same set of elevation data can result in varying DEM outputs (Arun, 2013). There is therefore a need to evaluate the suitability and accuracy of these interpolation techniques for a specific data and purpose. Erdogan (2009) investigated the relative accuracy of various interpolation algorithms for an area with high topographical variance in Turkey. The research evaluated various deterministic interpolation algorithms against a baseline survey grade dataset. The best results were obtained using the thin plate spline algorithm, a derivative of the spline algorithm itself. Zimmerman et al. (1999) compared the outputs of the IDW versus the kriging methodology and showed that the kriging method was able to adjust itself to the spatial variability of the data and by doing so, yielded better estimation of altitude for unknown sample points. In contrast, Aguilar et al. (2005) presented research from their study area in Almeria, Spain, that indicated that the IDW method was marginally better than the accuracy from the kriging model output.

In 1984, Mark was the first to propose an algorithm for automatically delineating a drainage network from DEM data for specific applications in hydrological modelling (Mark, 1984). This study gave rise to the need for hydrological correction algorithms in the DEM interpolation process which includes the development of the Australian National University Digital DEM (ANUDEM), known as the Topo to Raster feature in ArcGIS, to generate elevation models that are hydrologically conducive to network extraction (Callow et al., 2007). The ANUDEM method creates an interpolated surface that preserves the critical geometry components required to define a hydrological system which includes ridgelines and stream networks (Arun, 2013). Pavlova (2017) presented research conducted in the Omsk region in Russia which evaluated the outputs from IDW, Kriging, Topo To Raster, Spline, Nearest Neighbour (NN) and the Triangulated Irregular Network (TIN) techniques. The findings indicated that on relatively flat areas, the best results were obtained using the Spline and IDW techniques. In a contrasting environment, Salekin et al. (2018) conducted research into utilising Global Navigation Satellite Systems (GNSS) as a data source to generate a DEM in a landscape with a large degree of

topographical variation in Marlborough, New Zealand. The GNSS data were used in various interpolation techniques including NN, Topo to Raster and IDW techniques. The quantitative research showed that the Topo to Raster technique showed the most accurate DEM results, while the IDW showed the least accurate results.

Chaplot et al. (2006) investigated the suitability of various interpolation techniques across a mountainous region in Laos and undulating landscapes in France. The recommendations following the results of the study indicated that the accuracy of the various interpolation techniques needs to be tested in terms of their applicability to multiple resolution data (Chaplot et al., 2006). Many studies have been focused on modelling and identifying the spatial distribution of errors associated with DEM's in order to remove DEM errors (Aguilar et al., 2010; Hu et al., 2009; Stal et al., 2012).

The above studies show that the accuracy of interpolated elevation is affected by the topography of the area of interest and the interpolation techniques used to create the continuous surface. In South Africa, the Chief Directorate for National Geospatial Information (NGI) produces a 5 m resolution elevation dataset that can be used by the public for different purposes. There is a significant gap in assessing the accuracy of the various interpolation outputs based on the NGI 5m contour dataset against survey-grade elevation data sources. The limitations associated with the application of the 5 m resolution NGI dataset needs to be understood in terms of the identification of spatial distribution errors and the circumstances that lead to these errors. This study therefore aims to compare various interpolation techniques to derive a DEM data for the eventual development of flood-lines using the 5 m NGI elevation contours in the Roodepoort region in Johannesburg, South Africa. The specific objectives of the study are to (1) compare various interpolation techniques conducted on the NGI elevation data source which includes the IDW, NN, Kriging, Spline and Topo to Raster techniques and (2) identify limitations associated with the interpolation accuracy of the NGI dataset. The performances of the interpolators will be evaluated using a high-resolution Light Detection and Ranging (LiDAR) derived DEM. It is expected that the comparisons of the various interpolators will contribute to hydrological modelling in South Africa by listing recommendations and limitations of the application of specific interpolation techniques to the 5 m NGI data source for DEM outputs.

2.2 Methods

2.2.1 Study Area

The study area focuses on a 5-kilometre length of a river that is a tributary of the Wilgespruit River, between Willowbrook and Strubens Valley in Roodepoort, Johannesburg (Figure 2.1). The study area has an urban residential composition and is amongst the land-use classes most affected by flooding (Davis-Reddy *et al.*, 2017).

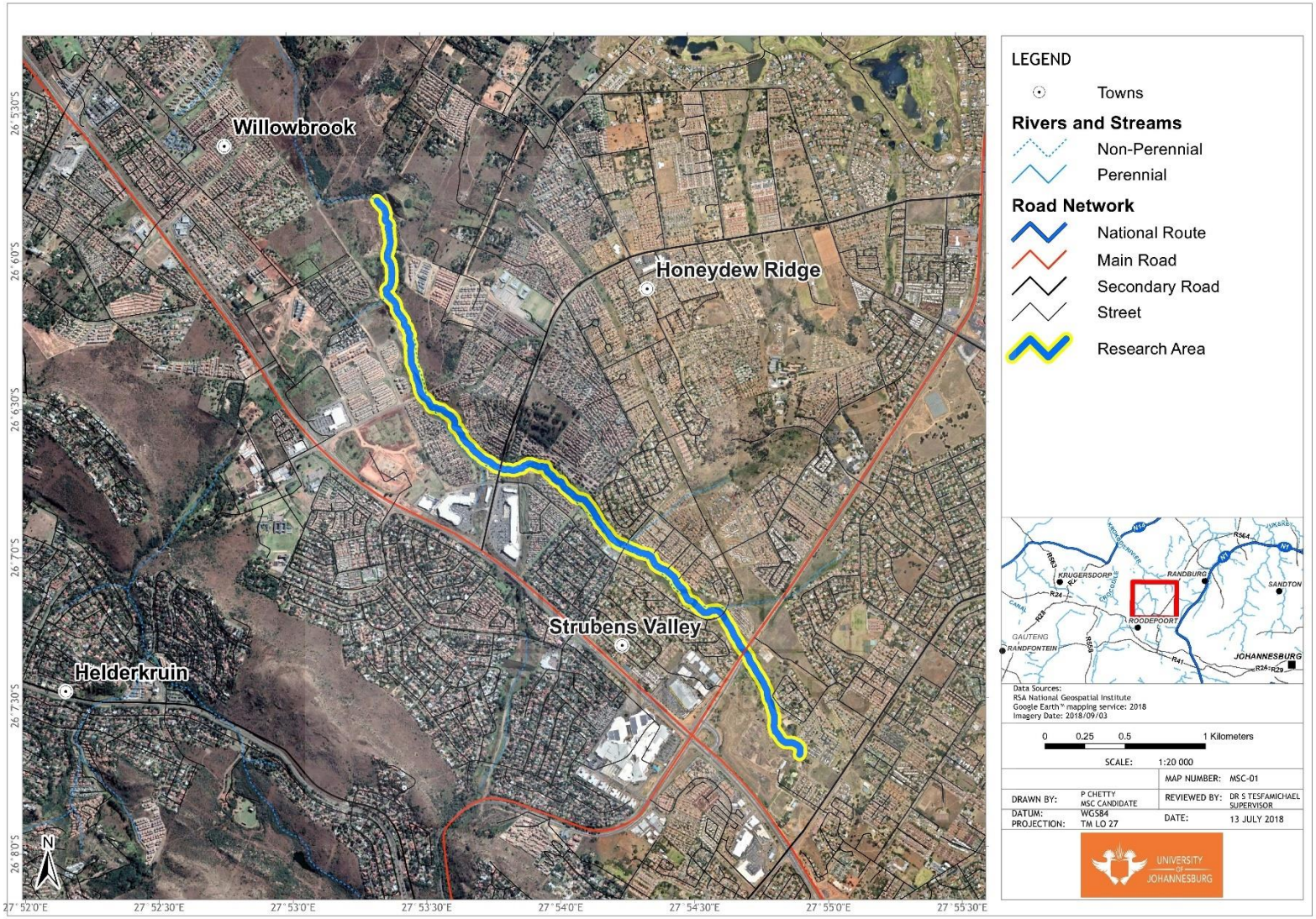

Figure 2.1: Research Area - Tributary of the Wilgespruit River, displayed in true colour Red-Green-Blue (RGB) band combination

The Roodepoort region receives approximately 610 mm of rain per year, with the majority occurring during the summer months from November to February (Climate-data.org, 2019). The region is classified as warm and temperate according to the Köppen and Geiger climate classification (Conradie, 2012). The warmest months by average temperature are between November and February. Figure 2.2 shows the annual rainfall and temperature for the Roodepoort region.

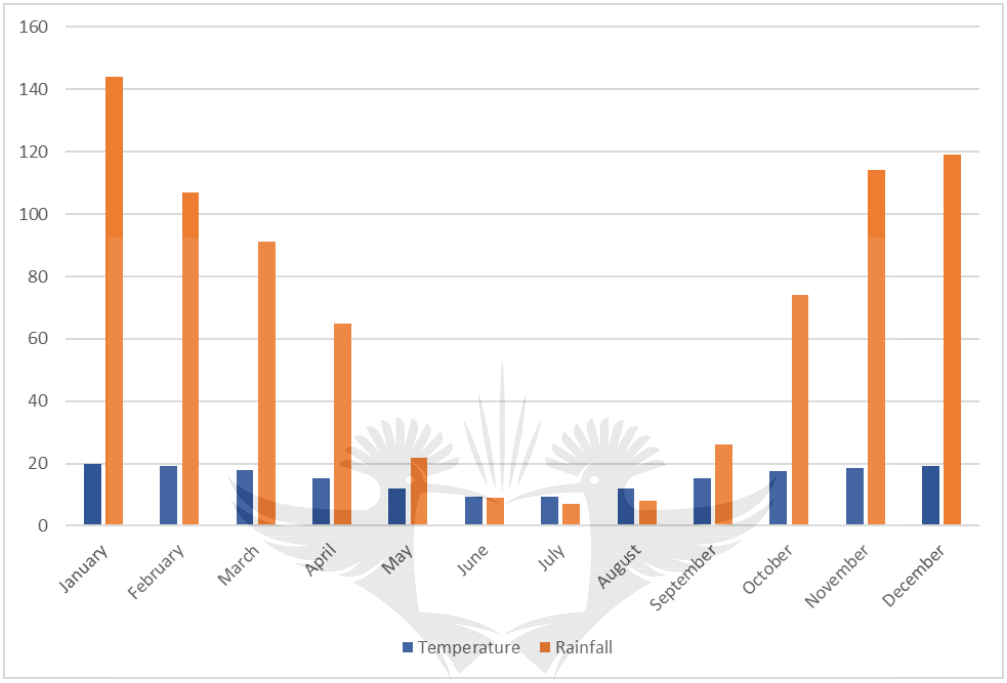

Figure 2.2: Roodepoort annual rainfall and average temperature

The geological material underlying the river and immediate area of interest includes Swazian era Halfway House granite formations that incorporate ultramafic formations extending to the uppermost section of the tributary, followed by grey medium-grained porphyritic granodiorite in the remainder of the tributary lying in a northerly direction. A shear zone comes within approximately 100 metres of the northernmost section of the tributary (Johnson *et al.,* 2006).

The land-use of the region immediately surrounding the river of interest in this research is classified as a wetland (GTI, 2014). The wetland, in turn, is surrounded by urban residential class with small pockets of grassland and thicket. Figure 2.3 shows the land-use classification of the study area and its surroundings.

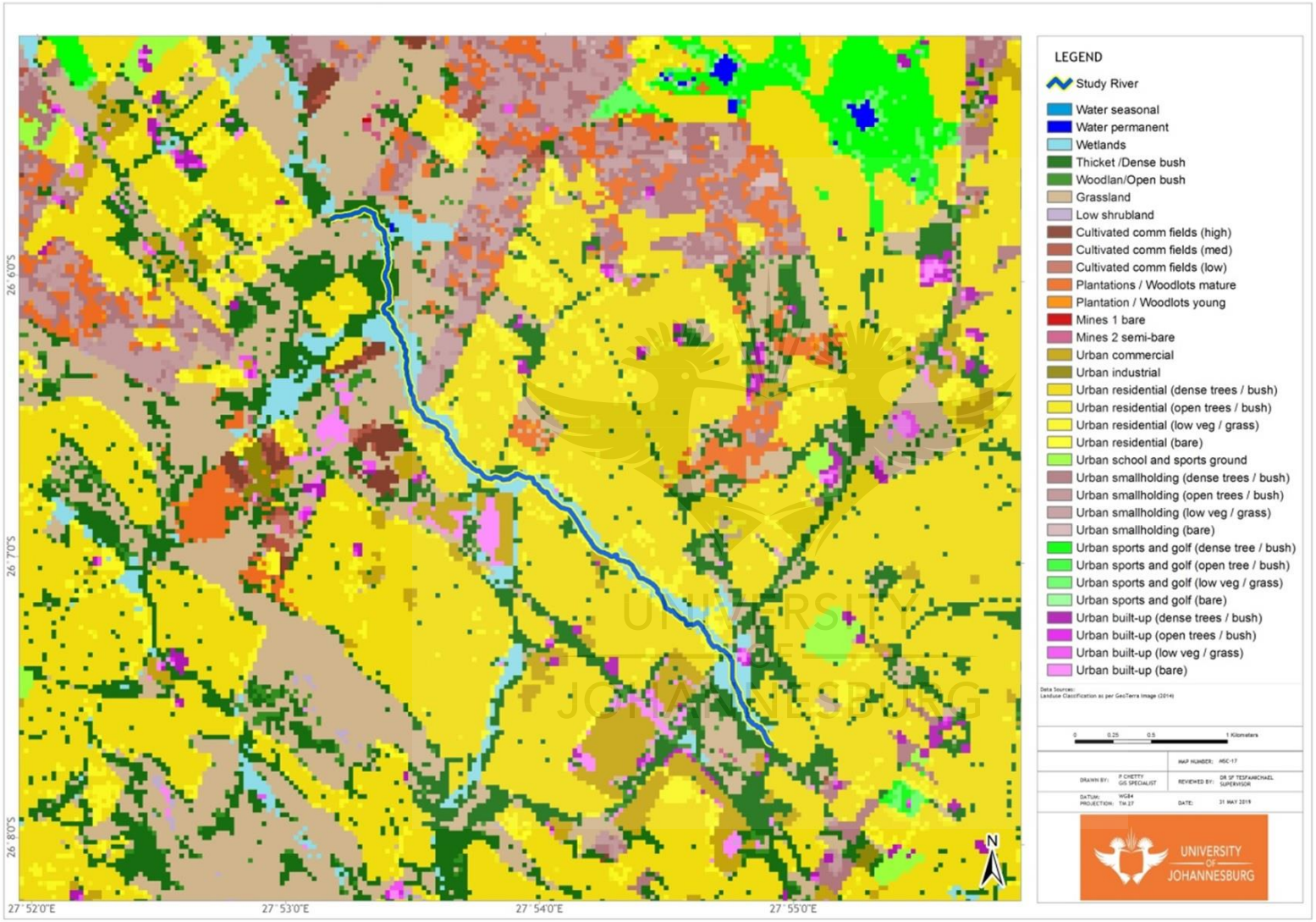

Figure 2.3: Regional land-use classification (GTI, 2014)

2.2.2 Data

2.2.2.1 5 m Chief Directorate National Geospatial Information (NGI) contours

The 5 m-resolution contour dataset from the DRDLR is generated by the Intergraph Dual Mass Camera (DMC) which captures stereo imagery at a GSD of 0.5 m (NGI, 2018). The NGI also contracts service providers with similar cameras to acquire data owing to the scale of the operation. Currently, the NGI aims to capture 40% of the country every 3 years and the remaining areas every 5 years. The dataset included in this research is the 5 m contour dataset (referred to as the NGI dataset), which was last updated 8 December 2009, for the study area.

The 5 m resolution contour dataset has the largest spatial coverage compared with more recent high-resolution survey campaigns that have been commissioned by the City of Johannesburg (COJ) Municipality. While higher resolution (that is, to smaller GSD) datasets are available for metropolitan areas in South Africa, Areas that fall outside of the designated metropolitan areas are unlikely to be covered by high resolution datasets including LiDAR and photography. Instead, these areas are covered by the 5-meter NGI dataset at best. As such, the 5 m NGI dataset is a popular choice among specialists who seek to apply topographical elements to their respective studies.

2.2.2.2 Light Detection and Ranging Point Cloud

The LiDAR data for the study area was obtained from the COJ Municipality's Corporate Geo-Informatics Department. LiDAR is a popular method of surveying that uses an active remote sensing system composed of at least three sensors, the Inertial Measurement Unit (IMU), the Global Positioning System (GPS) and the laser scanner (Csanyi & Toth, 2007). A target is illuminated by a light source through a laser beam and the time taken for the reflected beam to return to the sensor allows for the calculation of survey-grade measurements relating to the linear position of the target from the sensor (Vosselman, 2003). Advancements in optical and computing technologies have seen the emergence of LiDAR as a rapid and accurate terrain mapping tool (Lohani & Ghosh, 2017). The COJ municipality region distributes an aerial-based LiDAR dataset that is acquired by a contracted service provider every three years. The data sourced for this study was acquired in June 2012.

The native format for the LiDAR data includes American Standard Code for Information Interchange (ASCII)-based text files that contain information relating to each point's location and elevation, which collectively form a point cloud. The LiDAR point clouds used in the present study had a point density of 0.2 points per square meter with an approximate average spacing between neighbouring points of 2 m. Therefore, LiDAR is acknowledged for its survey-

grade level of accuracy (Vosselman, 2003; Lohani & Ghosh, 2017). The horizontal accuracy of the LiDAR data had a 0.048 m root mean square error (RMSE), and a vertical accuracy of 0.32 m RMSE as verified using a network of seven ground control points. The points were classified into ground and non-ground points by the data supplier, with the ground points representing the physical ground level, while the non-ground points represented all features above ground including vegetation and structures. The ground points were used in the present study to serve as the baseline dataset to evaluate the relative accuracy of the different interpolation techniques applied to the 5 m elevation contour dataset.

2.2.3 Analysis

To produce continuous digital representations of a surface, interpolation techniques were introduced to calculate the unknown values that lie between known values. In this study, five interpolation techniques conducted on the 5 m resolution NGI dataset were compared, namely IDW, NN, kriging, spline, and Topo to Raster algorithms.

IDW is a non-linear, deterministic interpolation technique that computes a weighted average of a value from sample points in close vicinity to determine the value of non-sampled points (Robinson & Metternicht, 2003). The IDW principle was first presented by Shepard (1968) for improved efficiency of the central processing unit time. Today, the IDW process is one of the most widely applied methods of interpolation in the hydrological environment. The IDW principle assumes that values which are close together are more alike than values that are further away. To calculate the value of an unknown point at a location, the weighted average of the surrounding known values is calculated and assigned to the unknown point. Known values that are closer to the location of the unknown point are given a higher weighting ranking in the calculation, and therefore have a larger influence on the determination of the unknown value, opposed to known values that are further away. Definitions of the neighbouring radius for the calculation and the power function representing the inverse distance relationship between the points are critical parameters for this interpolation method. The formula for the IDW interpolation is defined as follows.

$$Z_0 = \frac{\sum_{i=1}^{N} z_i . d_i^{-n}}{\sum_{i=1}^{N} d_i^{-n}} \qquad \text{Equation 2. 1}$$

where Z_0 = value of variable Z in point I;

Z_i = the sample in point I;

d_i = distance to the sampled point from the unknown point;

N = coefficient that defines the weight that will be based on the inverted distance function;

n = total number of predictions allowed for each validation (Shepard, 1968).

The NN Interpolation model is based on the Sibson interpolation model, where values are assigned to un-sampled points based on the construction of Thiessen polygons which work together to form areas of overlap (Sibson, 1980). The polygons are formed across all known values surrounding the unknown value by connecting all common values into a network of Thiessen polygons which represent all known values. A new Thiessen polygon is then generated over the unknown value, and the proportion of the overlap between this new polygon versus the network of intersecting polygons previously generated define the weighting system to be used. The formula used for the NN interpolation is identical to IDW, with the only difference coming from the method used to calculate the weightings. The NN interpolation formula is defined as follows.

$$\dot{Z}(u) = \sum_{i=1}^{N} \lambda(\mathrm{u}) \times \mathrm{z_i} \qquad \text{Equation 2. 2}$$

Where:

$$\lambda_\mathrm{i}(\mathrm{u}) = \frac{\text{area contributed by Polygon i}}{\text{Total area of polygon}} \qquad \text{Equation 2. 3}$$

and u = (x,y) location of query point (Rukundo & Cao, 2012).

Kriging is a stochastic local interpolation technique that computes the value of non-sampled points in a similar way to IDW, with the exception that there is more control on the weighting system that determines unknown values based on distance (Robinson & Metternicht, 2003). The kriging model was developed by Danie Krige, who formed the basis of what would later be called the kriging process in 1951 through research presented in the Journal of the Chemical, Metallurgical and Mining Society of South Africa in the 1960s (Cellmer, 2014). Krige (1951) applied the kriging technique to survey two gold mines to understand resource estimation based on borehole data. An ordinary kriging equation is defined as follows.

$$Z(s_0) = \sum_{i=1}^{n} \lambda\, \mathrm{z}(\mathrm{s_i}) \qquad \text{Equation 2. 4}$$

where, λ = weights assigned to each known value, where all weights sum to a unity which enables unbiased estimations which are defined as:

$$\sum_{i=1}^{n} \lambda_\mathrm{i} = 1 \qquad \text{Equation 2. 5}$$

The matrix equation calculating the weights is defined as:

$$C = A^{-1} \times b \qquad \text{Equation 2. 6}$$

where A = matrix of semi-variance between the known values;

b = estimated semi-variances between the known values and unknown value, represented by a vector (Krige, 1951; Krige, 1952).

The spline interpolation is a piecewise polynomial interpolation method that creates a smooth raster surface from the known sample points using a 2-D minimum curve technique (Robinson & Metternicht, 2003). The resulting surface passes through all known sample points. The spline method is mathematical in nature and takes the form of a cubic equation whereby each known data point has a cubic equation through which all splines pass (Robinson & Metternicht, 2003). Jenkins (1927) and Schoenberg (1946) can be credited with the origins of the spline method of interpolation. The spline cubic equation is defined as follows.

$$S(x,y) = T\,(x,y) + \sum_{j=1}^{n} \lambda_j R(r_j) \qquad \text{Equation 2. 7}$$

where j= 1,2,…N;

N is the number of points;

λ_j are the coefficients found by the linear equation solution; and

r_j is the distance from the point (x,y) to the j^{th} point (Meijering, 2002).

ANUDEM is based on a program developed to interpolate elevation values across a topographical surface by Hutchinson (1988). The algorithm generates elevation models that are hydrologically conducive to network extraction (Callow *et al.,* 2007). In the 1980s, a study done by Mark (1984) proposed an algorithm for automatically delineating a drainage network from DEM data. This study gave rise to the need for hydrological correction algorithms in the DEM interpolation process which includes the development of the ANUDEM. This interpolation technique provides a compromise between local interpolation methods such as IDW and global interpolation methods such as kriging, by allowing the resultant DEM values to follow abrupt changes in terrain which include streams, ridges and cliffs, thus preserving topographical continuity (Pavlova, 2017). The Topo to Raster interpolation is the only algorithm featured in ArcGIS that is preferentially applied to contour datasets. The Topo to Raster interpolation is defined by the following equation.

$$J_1(f) = \int (f_x^2 + f_y^2) dxdy$$ Equation 2. 8

where J_1 is known as a local interpolation technique that is well-suited for features with a better resolution;

$$J_2(f) = \int (f_{xx}^2 + f_{xy}^2 + f_{yy}^2) dxdy$$ Equation 2. 9

where J_2 is known to create unrealistically flat surfaces as commonly seen by global interpolation techniques. Hutchinson's ANUDEM program revolves around a compromise between $J_1 and J_2$ as follows:

$$J(f) = 0.5 \times h^{-2} J_1(f) + J_2(f)$$ Equation 2. 10

where h is the spatial resolution of the output surface model (Hutchinson, 1988).

2.2.4 Accuracy assessment

A buffer measuring 100 m was created around the river's centreline. Points were then generated at 100 m intervals along the extent of the buffer, from which LiDAR elevations were extracted within a 5 m average distance from each point, resulting in a total of 103 LiDAR spot elevations. Figure 2.4 shows the positions of the spot elevation points, plotted against a 2018 WorldView-2 derived satellite image that is rendered as a natural colour composite. These elevation values, along with their X and Y positions, represent the most accurate remotely sensed dataset available for this study and were therefore used as reference data to compare the different surfaces created using the five interpolators applied to the 5 m contour data. While a field-collected differential real-time kinematic GPS system will provide the highest level of accuracy, the intention of the research presented is to utilise practical and readily available datasets, such as the COJ distributed LiDAR. Elevation values of the five interpolated surfaces were extracted at each of the above-mentioned LiDAR spot elevation locations. The T-test and residual analysis was used to compare the interpolated surfaces against the baseline LiDAR elevation values.

2.2.4.1 Comparing the output elevations of the interpolated DEMs against the reference LiDAR elevations

The T-test is a statistical procedure that is commonly used when investigating the relationship between variables by comparing the means on the dependent variables against the baseline or independent variable (Green & Salkind, 2012). The T-test was chosen due to the flood extent comparisons involved at each measurement station, where more than one dependent set of results is be compared to the baseline LiDAR flood-line extents. The P-value from the

T-test output is used to assess the degree of difference between the means of the interpolation elevation versus the baseline LiDAR elevation. The applied T-test formula is a generalisation of a two-sample T-test (Ostertagova & Ostertag, 2013) and is defined as follows.

$$F = \frac{Mean\ square\ between\ groups\ (MSG)}{Residual\ Mean\ Square (RMS)} \quad \text{Equation 2. 11}$$

Where

$$MSG = \frac{\sum_{i=1}^{k}\left(\frac{T_i^2}{n_i}\right) - G^2/n}{k-1} \quad \text{Equation 2. 12}$$

and

$$RMS = \frac{\sum_{i=1}^{k}\sum_{j=1}^{n_i} Y_{ij}^2 - \sum_{i=1}^{k}(\frac{T_i^2}{n_i})}{n-k} \quad \text{Equation 2. 13}$$

where Y_{ij} is the observation distances from the stream centreline for each output;

T_i is the sum of each group of distances from the stream centreline;

G is the total of all observations being compared for the variance (model output being assessed versus baseline LiDAR output); and

n_i is the number of observations in group i and n is the total number of observations being analysed for the variance.

The T-test and associated P-values were calculated using Microsoft Excel (Microsoft Corporation, 2019).

The Root Mean Square Error (RMSE) is a standardized statistical metric that is commonly used in model performance assessments where the computed value is a measure of the error between two datasets (Chai & Draxler, 2014). The usage of RMSE in the field of GIS is relatively widespread, where smaller RMSE values are indicative of observed values that are closer to the baseline values of assessment. The RMSE metric does not take direction in the form of negative and positive values into account, thus providing an absolute measure of error. The RMSE is calculated using the following formula.

$$RMSE = \sqrt{\frac{1}{n}\sum_{i=1}^{n}(P_i - O_i)^2} \quad \text{Equation 2.144}$$

Where n = number of observations;

P = Baseline or predicted value; and

O = Observed value.

Mean error (ME) is a statistical metric which refers to the average of all errors between a predicted and observed dataset (Khair *et al.,* 2017). Opposed to the RMSE metric, the ME takes positive and negative values into account. In the case of ME values, the results indicate instances where an observed model on average underestimates or overestimates a baseline predictive model and to what degree. The ME is calculated using the following formula.

$$ME = \frac{1}{n}\sum_{i=1}^{n}(P_i - O_i) \quad \text{Equation 2.155}$$

Where n = number of observations;

P = Baseline or predicted value; and

O = Observed value.

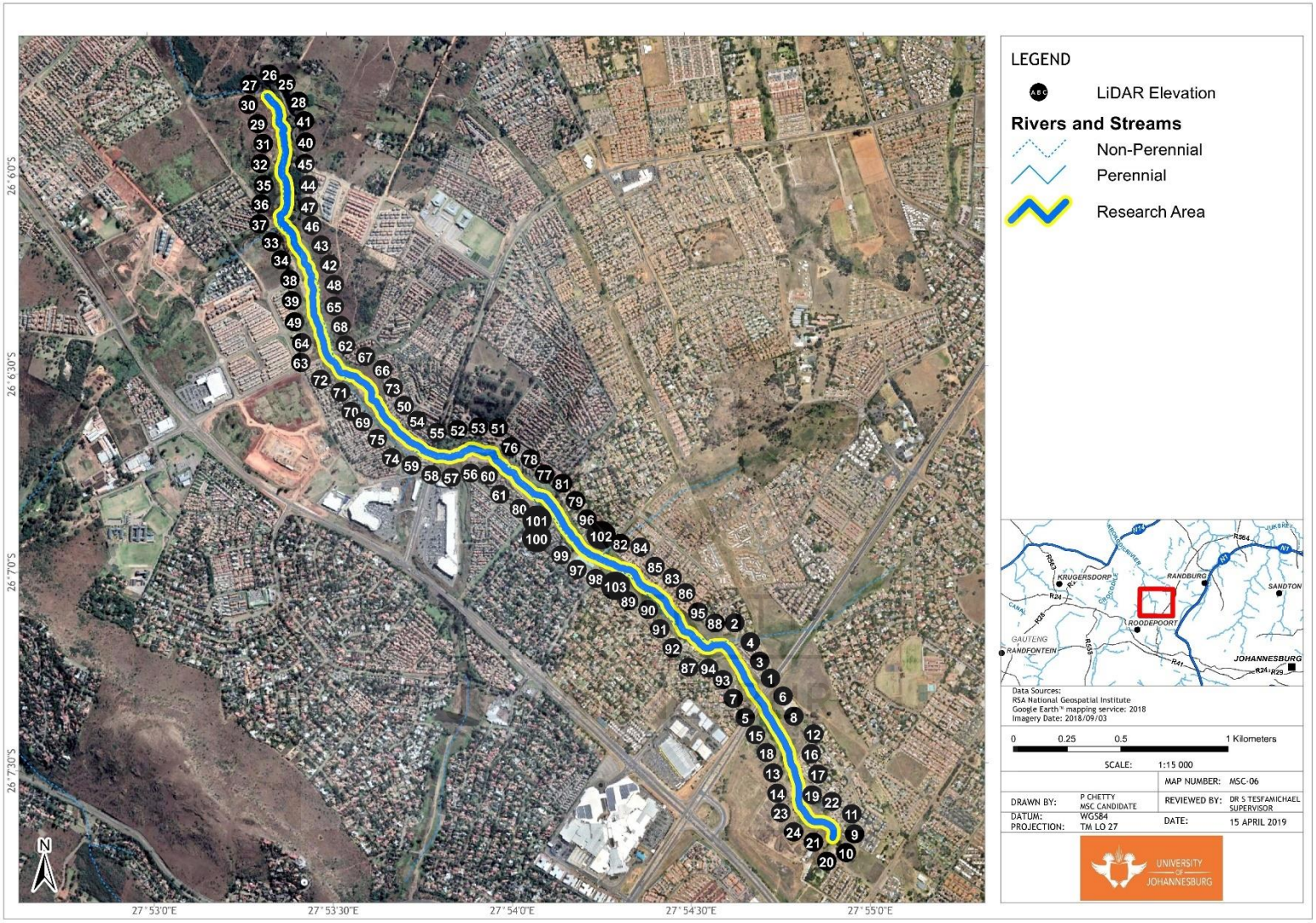

Figure 2.4: Location of observations for analysis, displayed in true colour RGB band combination

2.2.4.2 Identification of outliers from the interpolated DEMs against the LiDAR reference data

Analysis of residuals forms part of a regression analysis which is designed to assess model adequacy (Martin *et al.,* 2017). Regressions are typically applied to assess the accuracy of a predicted model against actual values (Martin *et al.,* 2017). Because the research purpose is accuracy assessment, as opposed to model fitting, regression analysis was not chosen as an accuracy assessment tool in this research. However, components of the regression analysis remain useful tools in location-based analytics, such as the residual analysis which allows for reference to a specific observation and its associated spatial location. Residuals are defined as the vertical distance (r_i) between the observed measurement and the predicted measurement represented by a linear regression line as follows.

$$(r_i = y_i - \hat{y}.) \qquad \text{Equation 2. 16}$$

In this research, the observed distance (y_i) represents the linear regression from the baseline LiDAR elevation while the predicted measurement $(\hat{y})$ represents the vertical elevation difference between the interpolation surface being assessed (Topo to Raster, kriging, NN, IDW, spline).

Outlier identifications in data have been applied successfully through the usage of standardised residuals (Sousa *et al.,* 2012; Miller, 1993, Salekin *et al.,* 2018) and are defined by the following formula.

$$r_{s=} \frac{r_i}{s} \qquad \text{Equation 2. 17}$$

where the standardised residual (r_s) is the residual value (r_i) divided by its standard deviation (s). At a 95% confidence level, it is expected that 95% of the data falls within 2 standard deviations of the mean (Sousa *et al.,* 2012). Data points falling lower than -2 and higher than 2 on the standardised residual plot will therefore represent outliers. The incorporation of a standardised residual analysis allows for the identification of interpolated elevation output observations that are significantly different to the baseline LiDAR elevation values, which in turn allows for a spatial expression of the results observed.

Figure 2.5 provides an overview of the methodology followed to achieve the objectives set in this chapter. The methodology starts with the running of the various interpolation procedures. As the focus of the assessment is on the influence of interpolation techniques on hydrological modelling environments, a streamflow analysis was run on the baseline LiDAR dataset, from which a 100 m buffer was generated. LiDAR points were then selected using proximity analyses at every 100 m interval along the extent of the buffer. Interpolated elevation values were then extracted from each interpolation process at each LiDAR elevation point every 100

m along the buffer zone. All GIS-based processing procedures were conducted using ArcGIS (ESRI, 2019). The interpolated elevation observations were then compared against the LiDAR elevations using a T-test and residual analysis in Microsoft Excel (Microsoft Corporation, 2019).

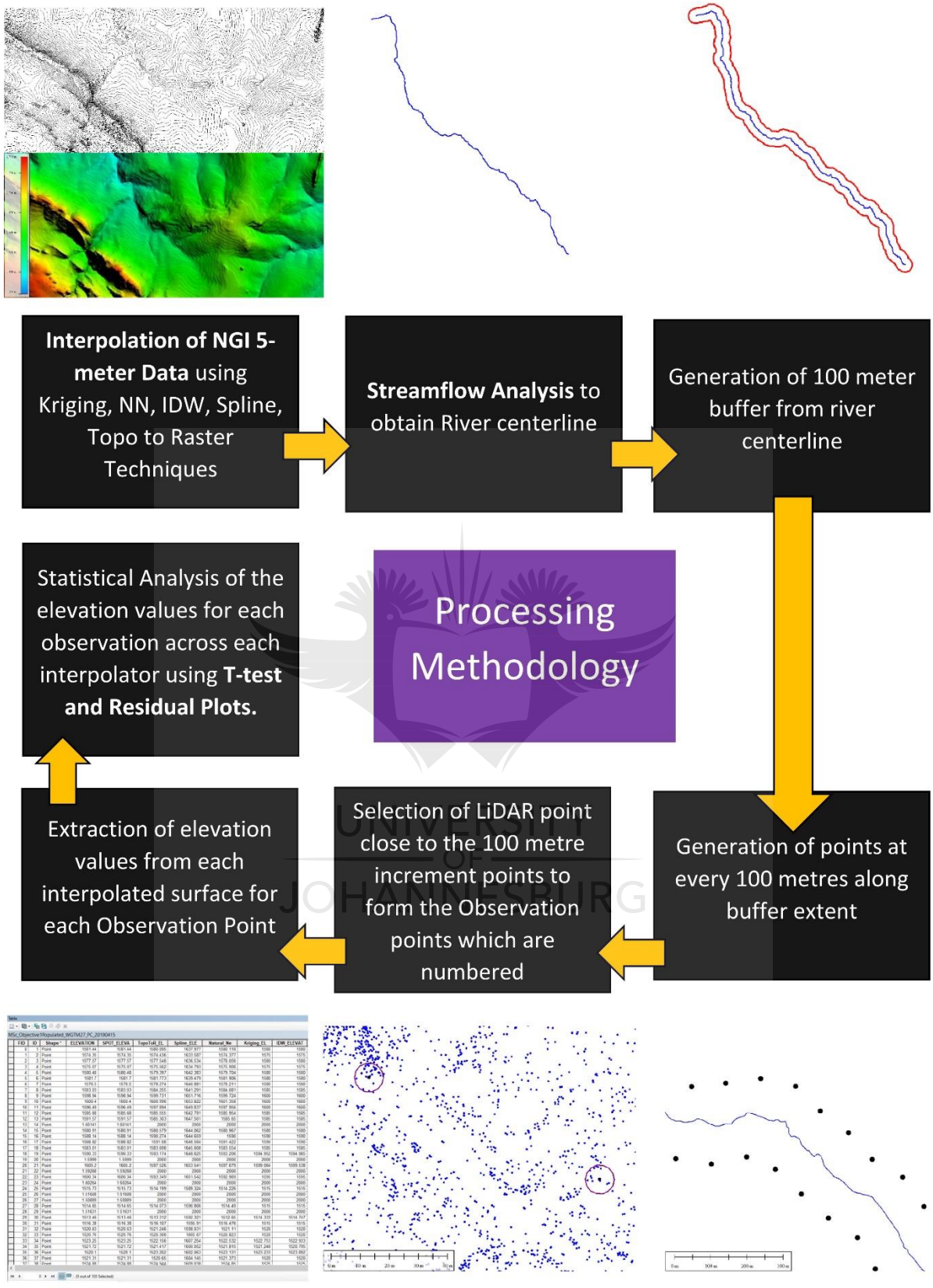

Figure 2.5: Summarised methodology for interpolation technique comparisons

2.3 Results

2.3.1 Introduction

The elevation values derived from each interpolation algorithm were extracted along the 103 spot elevation locations and compared to the LiDAR elevations through a T-test and residual value analysis. The outputs of each interpolation process are also presented as part of the results to visually depict the elevation differences seen between each model.

2.3.2 Differences between the interpolated elevations and LiDAR elevations

The T-test presented in this section yields information on the degree of variance between the elevation values obtained from each interpolation against the baseline LiDAR elevation values. The T-test was run at an alpha = 5%. The RMSE and ME values presented yield information on the adequacy of fitment of the various interpolation algorithms versus the baseline LiDAR. The outputs from the T-test, RMSE and ME for the various interpolation algorithms are presented in Table 1 which has been sorted from most accurate to least accurate.

The Topo To Raster interpolation had the highest correlation with the baseline LiDAR elevation with a P value of 0.75. The lowest P value obtained indicates a relatively strong correlation to the LiDAR baseline elevations when compared against the other interpolation techniques. The mean value from the Topo to Raster techniques elevation values are close to the mean value of the LiDAR elevations (1553.99), with the Topo To Raster interpolation generally underestimating the elevation by 1.10 m. The Topo to Raster interpolation shows the lowest RMSE value of 2.65, indicating the least difference to the baseline LiDAR elevation. The ME adversely shows the highest value amongst interpolators at 1.11, indicating that the Topo to Raster generally overestimate the LiDAR elevations by 1.11 m.

The T-test results indicate NN to have the second highest correlation to the baseline LiDAR elevation with P value of 0.78. The P value indicates a relatively good correlation to the LiDAR baseline elevations when compared against the other interpolation techniques. The mean value from the NN techniques elevation values are close to the mean value of the LiDAR elevations (1553.99), with the NN interpolation generally underestimating the elevation by 0.96 m. The Kriging T-test results show this technique to marginally be the third most accurate interpolator with results similar to the NN technique with a P value of 0.79. The IDW T-test results are within close range of the Kriging and NN interpolators, showing a relatively good correlation to the baseline LiDAR elevations with P value of 0.79. Both Kriging and IDW mean outputs indicate a general underestimation of the elevation by 0.95 m and 0.93 m respectively

in relation to the LiDAR mean value. The NN interpolation shows the second lowest RMSE value of 2.59, followed by the Kriging interpolation at 2.66 and the IDW interpolation at 2.67. The ME for the NN and Kriging interpolations results in 0.96, indicating that the NN and Kriging interpolations generally overestimate the LiDAR elevations by 0.96 m while the ME value for the IDW interpolation is 0.94, indication a general overestimation of LiDAR elevations by 0.94 m.

The spline T-test results show the highest variance to the baseline LiDAR by far with a P value of 0.00. The spline interpolation RMSE shows a value of 70.49 and with a ME of -69.83 indicating that the spline interpolation generally underestimates the LiDAR elevation by 69.83 m. The negligible P value and highest mean deviation from the LiDAR elevation with a general overestimation of -69.84 m indicate that the spline interpolation technique is unsuitable for deriving a suitable DEM from the NGI 5 m dataset.

Table 2.1: T-test, RMSE & ME results across all interpolation techniques results. Each interpolation was compared against the LiDAR mean elevation of 1553.9 m.

Interpolation Technique	Mean Elevation (metres above mean sea level)	Mean Difference between LiDAR and Interpolator (metres)	*P-value	RMSE (metres)	ME (metres)
Topo To Raster (ANUDEM)	1552.89	1.10	0.754	2.65	1.11
NN	1553.03	0.96	0.785	2.59	0.96
Kriging	1553.04	0.95	0.787	2.66	0.96
IDW	1553.06	0.93	0.791	2.67	0.94
Spline	1623.83	-69.84	0.000	70.49	-69.83

*P value was measured using 95% confidence level

2.3.3 Identification of outliers from the interpolated DEMS against the LiDAR reference data

The plotted residual results are presented for each interpolation technique in Figure 2.6. The results graphically illustrate the outliers of significance that can be related to a spatial location, which forms a platform for the subsequent discussion around the results seen. Residuals of Topo to Raster, NN, IDW and kriging share a similar distribution throughout the plot. The spline residual plot results resemble the same general distribution as the other interpolators but appear to have larger variances along the residual plot.

The Topo to Raster, NN, kriging and IDW residual points all show a dependent positive correlation to the LiDAR elevations with a wave-form trend about the Y-axis. Elevations of 1500–1540 m and 1560–1600 m show a general underestimation of elevation values by the Topo to Raster interpolation. For elevation values of 1540–1560 m, the Topo to Raster interpolation overestimates the elevations. Highly significant outliers occur at higher elevation values at around 1600 m. The IDW and kriging interpolation outputs have similar standardised residual plots, while the Topo to Raster and NN interpolation outputs share similarities in their standardised residual plots. The spline interpolation residual points also show a general dependent positive correlation to the LiDAR elevations, but in comparison to the other interpolators, the spline results have a larger residual variance. Larger underestimations in elevation values are seen at 1530–1550 m, with the same general observation of higher overestimations of elevations at 1600 m.

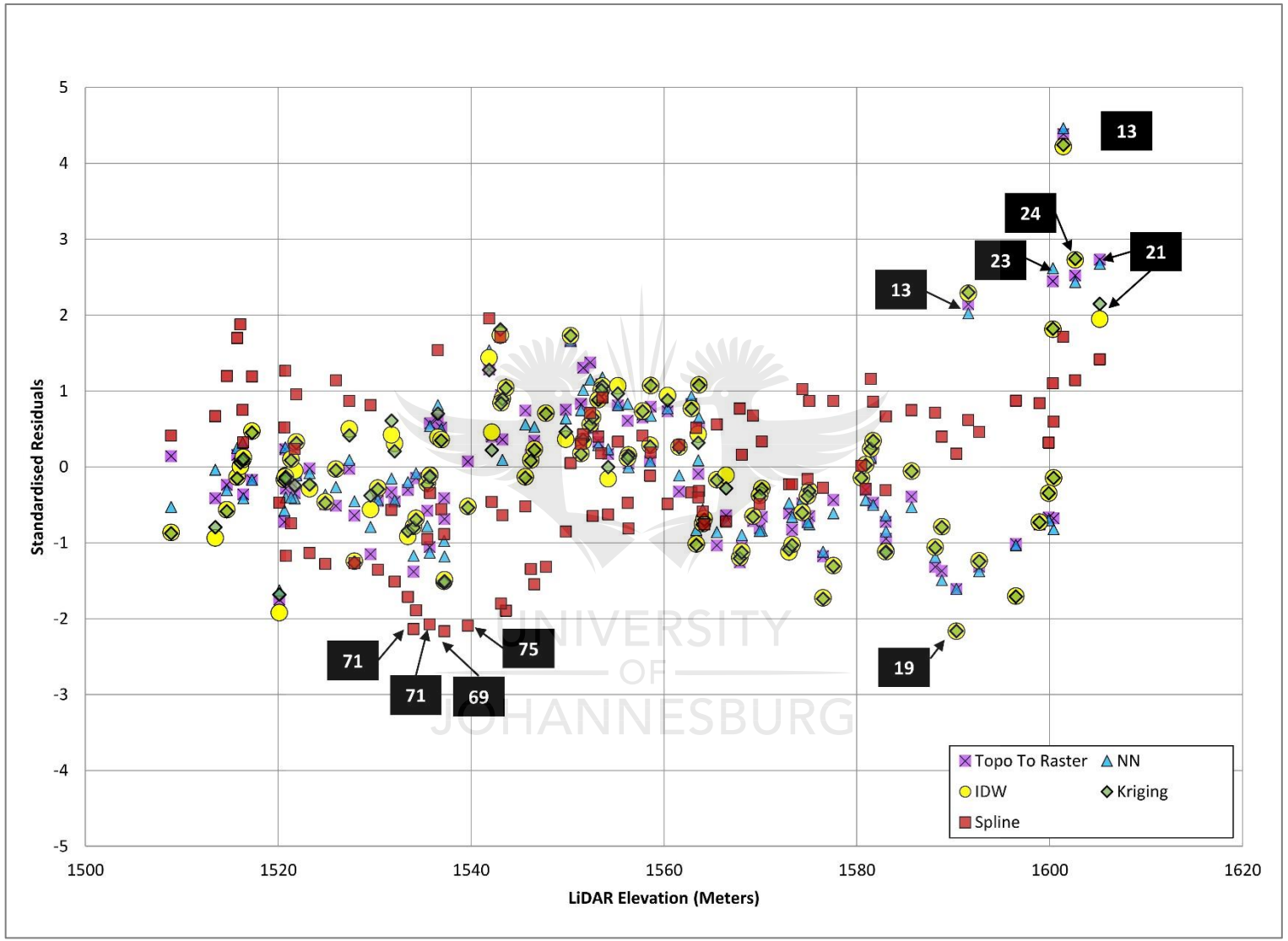

Figure 2.6: Combined standardised residuals across all interpolation techniques with significant outliers identified with a label

Table 2.2 shows the name and location of the elevation values that were identified through the residual plot shown in Figure 2.6. Observations 13, 14, 21, 23 and 24 show overestimations of the elevation across all interpolation techniques except for the spline technique. Observation 19 shows underestimations of elevation in the kriging and IDW technique while observations 69, 70, 71 and 75 show underestimations of the elevation only in the spline technique.

Table 2.2: Identified outliers from standardised residual plot analysis

	Topo To Raster		NN		Kriging		IDW		Spline	
ID	Standardised Residual	Distance to LiDAR Elevation	Standardised Residual	Distance to LiDAR Elevation	Standardised Residual	Distance to LiDAR Elevation	Standardised Residual	Distance to LiDAR Elevation	Standardised Residual	Distance to LiDAR Elevation
13	2.14	5.20	2.02	4.91	2.30	5.74	2.29	5.75	0.62	3.93
14	4.39	10.63	4.46	10.83	4.24	10.60	4.22	10.60	1.71	10.85
19	-1.61	-3.90	-1.61	-3.90	-2.16	-5.41	-2.17	-5.44	0.17	1.10
21	2.73	6.62	2.67	6.49	2.15	5.37	1.95	4.89	1.42	8.98
23	2.45	5.93	2.62	6.35	1.82	4.56	1.81	4.55	1.10	6.96
24	2.52	6.12	2.44	5.91	2.74	6.86	2.73	6.85	1.14	7.25
69	-0.69	-1.67	-1.18	-2.86	-1.51	-3.77	-1.49	-3.74	-2.17	-13.72
70	-1.06	-2.57	-1.13	-2.74	-0.13	-0.32	-0.12	-0.29	-2.07	-13.13
71	-1.38	-3.34	-1.17	-2.84	-0.80	-2.00	-0.78	-1.97	-2.14	-13.55
75	0.07	0.17	-0.51	-1.24	-0.54	-1.34	-0.52	-1.31	-2.09	-13.25

Figure 2.7 shows the identified locations of the significant residual outliers in the upper section of the tributary (Locations 11, 13, 14, 19, 21, 23 and 24). The downstream section of the tributary shows a higher correlation between the LiDAR elevation and interpolated algorithms that are within a 95% confidence level of vertical elevation difference. A large concentration of outliers can be seen in the upstream section of the tributary, where 5 of the 6 observation outliers identified are overestimations of elevation. The remainder of residual outliers identified (69, 70, 71 and 75) are all identified from the spline interpolation with significant elevation deviations (all 13 m under the LiDAR elevation).

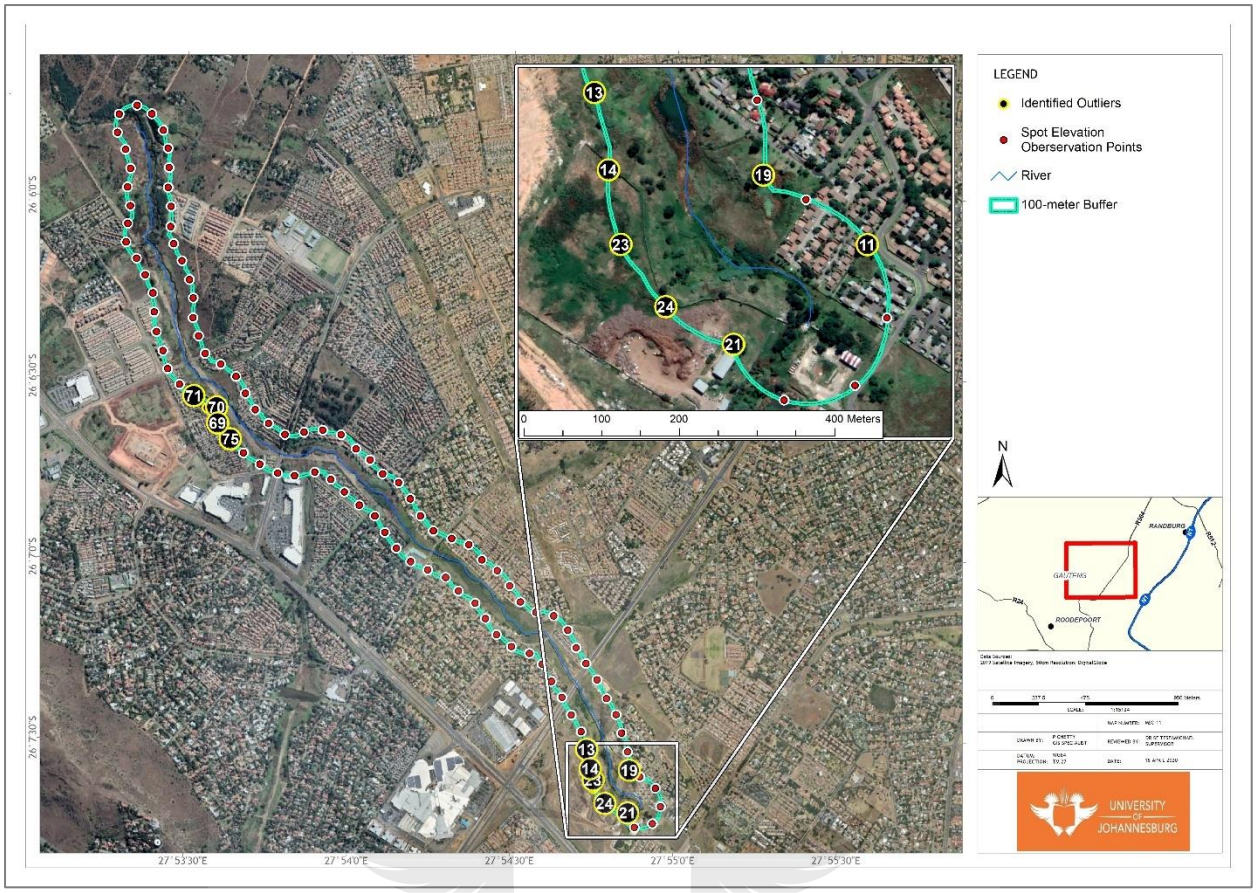

Figure 2.7: Identified standardised residual outlier locations, displayed in true colour RGB band combination

2.4 Discussion

The results obtained in the interpolation output compared against the reference LiDAR data indicate that the Topo to Raster interpolation technique yields marginally more accurate DEM surfaces than the other interpolators, based on the T-test. The Topo to Raster results agree with existing bodies of research (Arun, 2013; Salekin *et al.,* 2018) indicating that the Topo to Raster technique preserves critical components of the hydrological environment and by doing so, is the most accurate under these conditions. The spline interpolation technique was the most inaccurate and is unsuitable for the application on the 5 m NGI dataset to create a DEM. These results from the spline methodology are inconsistent with findings from Erdogan (2009) and Pavlova (2017) who found that the spline methodology yielded marginally more accurate results in comparison to other interpolations assessed. It must, however, be noted that Erdogan (2009) utilised a thin-plate spline algorithm which is a derivative of the original spline technique; this was not used in the research presented here, and Pavlova's (2017) findings are representative of an area with low topographical variations. All other interpolation

techniques assessed in the results presented as part of this research show good applicability with marginal differences in variation to the baseline LiDAR.

Spatial representations of the outliers as identified from the residual analysis reveal a large concentration of points to the upper part of the tributary which fall on a garden refuse site (Figure 2.7). Due to the differences in the temporal acquisition of the data, the garden refuse site would have undergone numerous topographical changes from the baseline LiDAR (acquired in June 2012) compared to the NGI (acquired in December 2009). Figure 2.8 illustrates the progression of the area, identified as the Weltevreden Park PickitUp garden refusal site, between 2006 and 2019 which shows the visible changes in topography over 13 years. Changes in the surface topography across this site over time have a direct influence on the elevation values observed during the LiDAR and NGI data acquisitions. These elevation value differences are prominent in the residual analysis, which shows a large concentration of residuals with a variance larger than 5 m in and around the refuse site. The residual interpretation further indicates the spline interpolation's output is unsuitable for accurate DEM interpolation from the 5 m NGI data source.

Figure 2.8: PickitUp garden refuse site surface changes: 2006-2019, displayed in true colour RGB band combination

The differences in elevation values between the NGI versus the LiDAR data reveals large differences in elevation values in the refuse site region, located in the upper section of the tributary (Figure 2.7). The NGI surface along this section is almost constantly below the LiDAR surface which shows clear definitions of a dump feature (Figure 2.8). This is indicative of changes in the surface between the acquisition of the 5 m NGI dataset (December 2009) and the LiDAR dataset (June 2012) which is statistically shown with the underestimation of the elevation values with the 5 m NGI dataset. The profile comparisons show a high degree of variance with regards to topographic changes that have occurred over the dumpsite, highlighting differences in temporal resolution as shown in Figure 2.9.

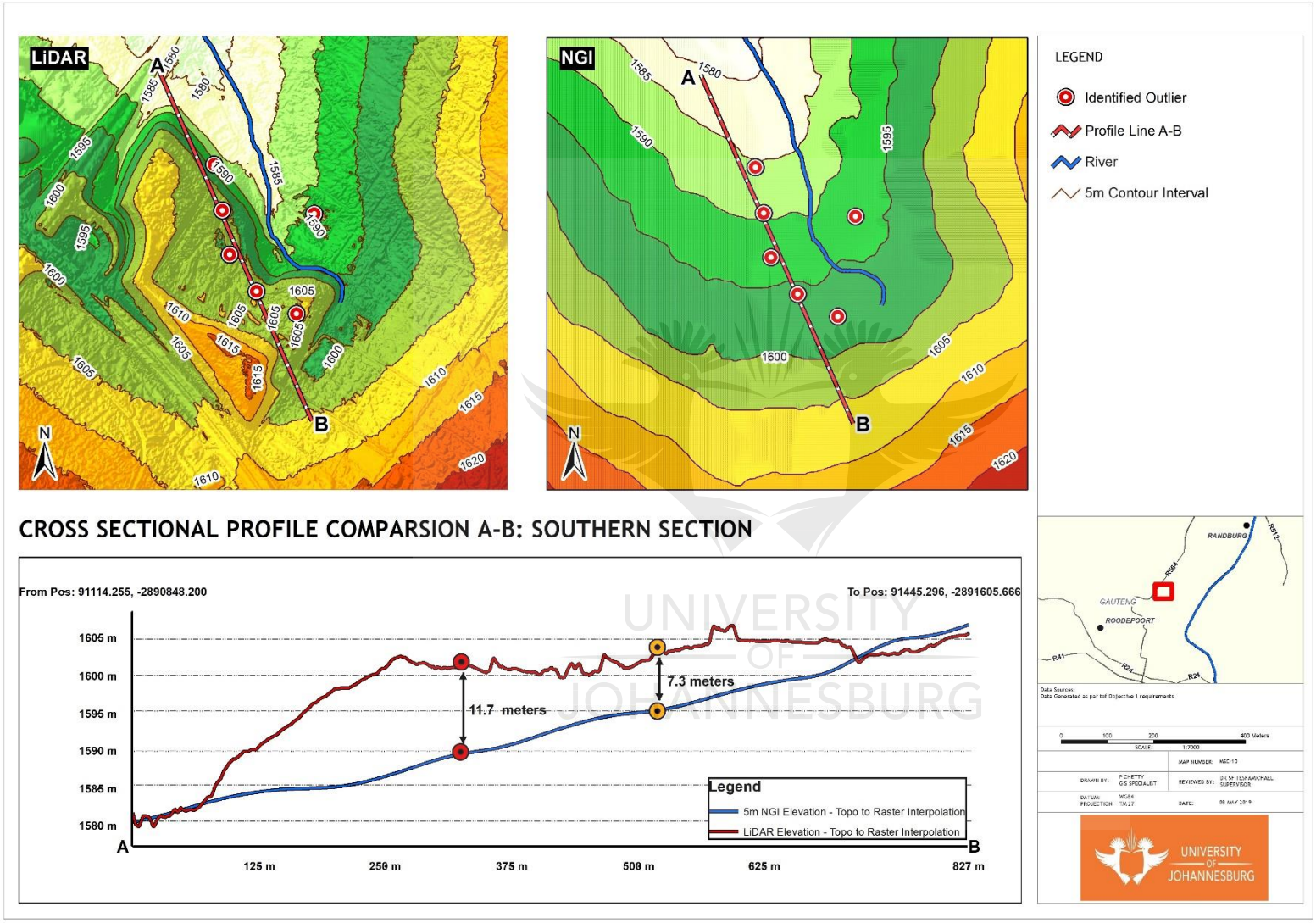

Figure 2.9: Profile comparisons for LiDAR (Left) versus NGI (Right) along A-B

2.5 Conclusion

The presented investigation's objective was to identify an optimal interpolation technique that can be applied to the 5 m NGI contour dataset in a hydrological environment with regards to spatial accuracy. The findings of this study indicate that for the most accurate interpolation of 5 m NGI contour data to create a DEM, the Topo to Raster interpolation technique is the most favourable. The results also indicate that while the application of the Topo to Raster technique yielded the most accurate results, the NN, kriging and IDW techniques were close to the Topo to Raster technique. These results imply that the application of the NN, kriging and IDW interpolation techniques to the 5 m NGI dataset will yield DEMs with similar vertical accuracy.

While the results indicate that the Topo to Raster technique is the most accurate, it must be acknowledged that certain interpolation techniques are likely to yield the most favourable results in the environments for which they were originally developed. The Topo to Raster interpolation algorithm was specifically formulated for its application in hydrological environments (Hutchinson, 1988), while the geostatistical method evaluated in this research (kriging) and local methods (NN and IDW) are limited by the resolution and spread of data (Al Mashagbah *et al.,* 2012*)*. Research into the interpolation technique to be applied and its favourability to different spatial distributions of data should always be taken into account when interpolating elevation datasets (Cellmer, 2014). Due to advancements in technology and information, it is also likely that the defining geometry (point, line or polygon) of the elevation data sources may change from line-based contour elevations to point-cloud elevation formats, which will also play a significant role in determining the ideal interpolation technique to apply.

The results presented in this research are specific to the application on the freely and nationally distributed South African NGI contour dataset. The residual analysis indicated substantial differences in elevation between areas for the reference LiDAR and NGI datasets, which is attributed to differences in temporal resolution. As access to spatial information in South Africa increases in association with advancements in survey techniques, future assessments should be performed on the most temporally relevant data available. The findings indicate that while the usage of lower spatial resolution datasets such as the 5 m data used in the present study may be acceptable in terms of RMSE, the need for access to more temporally relevant datasets is crucial to accurately represent topographical information for an area.

CHAPTER 3

A COMPARISON OF FLOOD-LINE MODELS DERIVED FROM MULTIPLE DEM SOURCES

3.1 Introduction

Rainfall trend studies done in South Africa from 1921– 2015 reveal that most of the country has undergone increases in the intensity of daily rainfall (Kruger & Nxumalo, 2017), corresponding to studies conducted on a global scale (Gentilucci *et al.,* 2019; Easterling *et al.,* 2000; Donat *et al.,* 2013). A pluvial flood event refers to the increased duration and/or intensity of rainfall that causes water to cover land areas that would otherwise have not been covered by water (Smith, 2013). The impacts from pluvial flooding are often compounded in urban areas because of landcover change and poor urban planning (Brockhoff *et al.,* 2019; Dawson *et al.,* 2008; Adeloye & Rustum, 2011). The results of flooding in urban areas include damage to property and built infrastructure, the displacement of people from their settlements, associated economic losses and in extreme cases, death (Nkwunonwo *et al.*, 2020). According to the South African Weather Service (SAWS), flooding accounts for the highest damage contributor amongst natural disasters. On 9 November 2016, the OR Tambo International Airport weather station in Johannesburg, South Africa received 89.6 mm of rain over 3 hours, while the historical monthly average for November is approximately 118 mm (SAWS, 2018). The recorded event caused significant amounts of damage to residential areas including Buccleuch, which was declared a disaster area. The 2018 Annual Climate Summary by the SAWS (SAWS, 2018) recorded a 77 mm rainfall event on the 22 March 2018 in Centurion, South Africa, during which numerous roads were damaged.

The flood-line modelling procedure is a numerical computer-aided technique which uses the return period volume to simulate a flood extent and associated area of inundation (Teng *et al., 2017)*. Flood-line modelling procedures are an important aspect of identifying which areas are prone to the negative impacts associated with flood events and often contribute towards preventative measures (Saksena & Merwade*,* 2015). The accuracy of the demarcated areas that are associated with the flood-line modelling outputs is therefore important in ensuring that the potential impacts from flood events are mitigated and avoided. Uncertainties in deriving the physical extent of the flood-line commonly result from the various data inputs that form part of the flood-line modelling process which includes the modelling procedure itself, model parametres and the topographic data that defines the geometry of the hydrological environment and its surroundings, referred to as a Digital Elevation Model (DEM). These

models are among the largest contributors to the accuracy of the extent of flood-line produced during the modelling process (Li & Wong*,* 2010; Zhang *et al.,* 2019).

Mashimbye *et al*. (2019) researched a sub-catchment of the Berg River in the Western Cape, South Africa, which aimed at assessing the influence that various DEM sources have on defining the accuracy of hydrological modelling. The study utilised popular data sources available locally in South Africa; these included the 30 and 90 m variants of the SRTM, the 30 m ASTER, the Stellenbosch University 5 m resolution DEM (SUDEM5) and the 2 m resolution DEM of South Africa (DEMSA2). The output data from the catchment and stream delineations were referenced to outputs from a GeoEye 1 m resolution DEM, with in-situ ground-truthing. The results showed that DEMs with a resolution below 30 m were better in delineating hydrological features. The findings also concluded that in the absence of high-resolution elevation data, the SRTM 30 m resolution source showed vertical accuracy that is conducive to generating hydrological features. While the research investigated the influence of DEM sources on the defining hydrological features, the research did not take the AW3D30 DEM into account.

Lim & Brandt (2019) conducted a sensitivity analysis on the Testebo River in Gavle, Sweden, to understand the influence of various DEM resolutions on the 2-D hydraulic modelling process. The study utilised a LiDAR point-cloud dataset, which was subjected to a series of processing techniques to produce a series of DTM's that were resampled from a range of 1 to 50 m resolutions. The hydraulic model was then run, with the only interchangeable parameter being the various resolution DTMs. The study found that while the lower resolution DTMs received better-quantified performances through the various statistical representations of the results, the physical flood-line outputs of the hydraulic model showed clear discrepancies.

Sanders (2007) conducted a study on a section of the North Carolina floodplains in the United States of America comparing flood-line outputs from the United States Geological Survey (USGS) National Elevation Dataset airborne LiDAR, Synthetic Aperture Radar (SAR) and the SRTM. The findings from the study indicated that the LiDAR DEM yielded the most accurate results, whereas the other DEMs overestimate the flood-line extent. The study found that the SRTM DSM performs well at moderately sloped topography. The study also concluded that the flood-line extents are highly dependent on the spatial resolution of the data. Jakovljevic *et al.* (2019) conducted a study on the difference of estimated flood extents using LiDAR, SRTM and the 30 m resolution ASTER inputs across four sites in Serbia with varying topographic conditions. The findings show that the ASTER outputs underestimate the flood-line extent by approximately 50%. More recently, Azizian & Brocca (2020) compared the applicability of DEM sources in an applied setting for flood inundation modelling in data-sparse regions, which

included assessments across ASTER, SRTM and ALOS sources. The study found that the ALOS DEM source yielded the most accurate results with the cross-sectional profile of the river being the closest to observed in-field measurements. For remote and inaccessible regions, remotely sensed data platforms may be the only source of elevation data. DEM data availability is often dependent on economic circumstances and site accessibility (Schumann *et al.,* 2008). The acquisition of high-resolution elevation data can be costly, which increases the appeal of lower resolution elevation data sources including SRTM and AW3D30. The potential applications of more readily available DEM sources need to be assessed in an environmental modelling and disaster management (Schumann, *et al.,* 2007).

Gurnell & Montgomery (2000) illustrated the advancements in hydrological modelling concerning the models and algorithms that were being developed for the incorporation of DEM data in GIS environments. While significant amounts of research have been applied to global scale elevation models and their suitability to flood-line mapping, there is a need for localised studies that compare the suitability of available elevation data with varying temporal and spatial resolution specifications. In the South African hydrological context, there is a need for a comparison of popularly utilised NGI, SRTMv3.0 and the relatively new AW3D30 elevation data sources and their associated flood-line extent outputs to understand the limitations associated with the usages of these data sources in deriving flood-line extents. The study presents the first instance where both the NGI and AW3D30 flood-line output delineations are compared against a baseline LiDAR flood-line delineation. The specific objectives of the study are to (1) compare flood-line outputs that are derived from the NGI, the 30 m SRTM and AW3D30 DEM sources in comparison to a LiDAR flood-line output and (2) identify limitations associated with each DEM source in its application in flood-line modelling. The performances of the NGI, SRTM and AW3D30 based flood-line outputs will be evaluated against a baseline high-resolution LiDAR-derived flood-line output. The comparisons of the various flood-line outputs could contribute to hydrological modelling in South Africa by listing recommendations towards the use of DEM inputs in the flood-line modelling environment.

3.2 Methods

3.2.1 Study area

The study area focuses on a 5 km length of a river that is a tributary of the Wilgespruit River, between Willowbrook and Strubens Valley in Roodepoort, Johannesburg. The study area was selected based on the available coverage overlap between the aerial and satellite-derived elevation data sources, of which the assessment of the various data sources forms part of the objectives. The study area is composed of an urban residential composition, which is amongst the highest affected land-use classes affected by the effects of flooding (Davis-Reddy & Vincent, 2017). Figure 3.1 shows the tributary and surrounding study area. According to the sub-quaternary catchment system by the DWS, the study area forms part of the A21E catchment area as shown in Figure 3.2 (DWS, 2017).

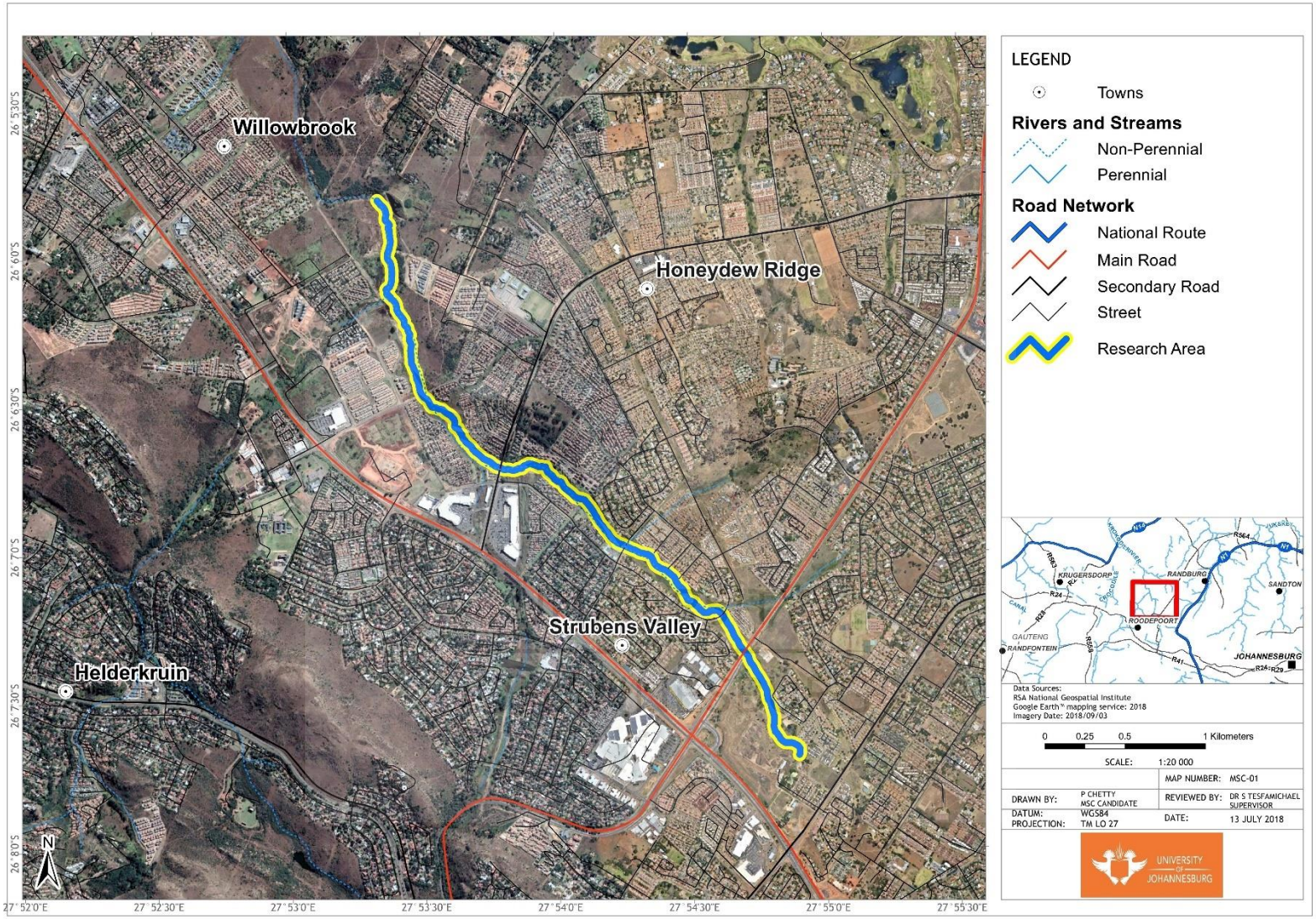

Figure 3.1: Research Area - Tributary of the Wilgespruit River, displayed in true colour Red-Greed-Blue (RGB) band combination

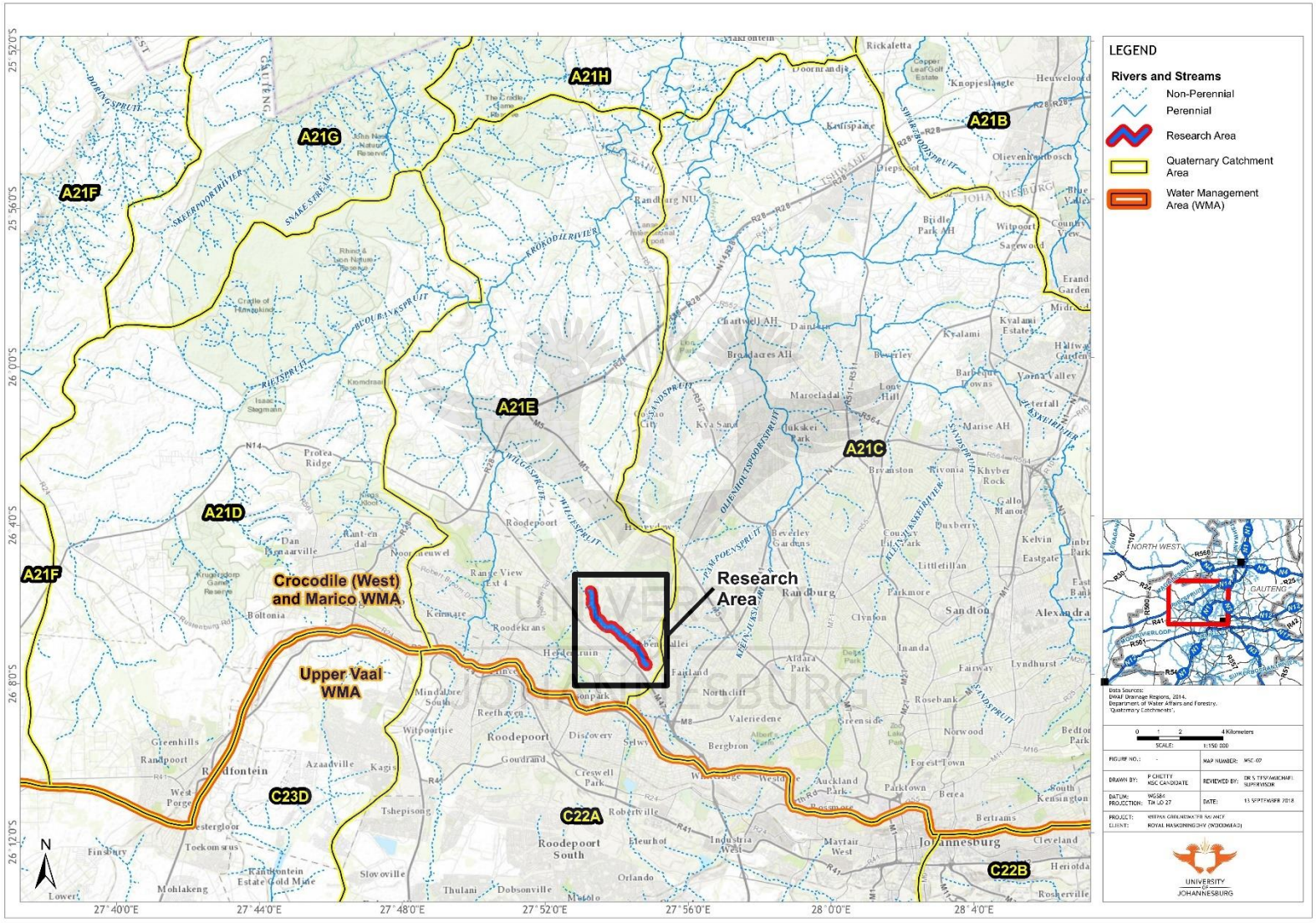

Figure 3.2: Research area - A21E catchment area

The Roodepoort region receives approximately 610 mm of rain per year, with the majority occurring during summer months from November to February (Climate-data.org, 2019). The region is classified as warm and temperate according to the Köppen and Geiger climate classification (Conradie, 2012). The warmest months by average temperature are between November to February. Figure 3.3 shows the annual rainfall and temperature for the Roodepoort region.

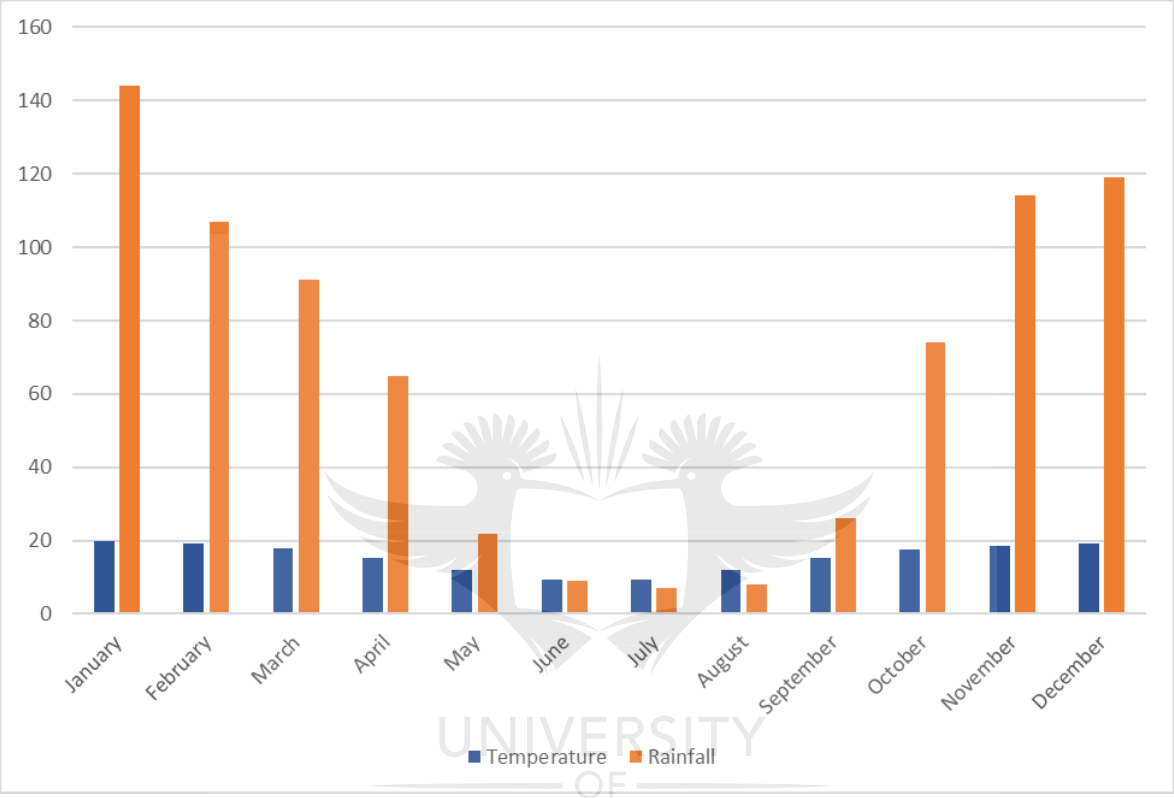

Figure 3.3: Roodepoort annual rainfall and average temperature

The geological material underlying the river and immediate area of interest includes Swazian era Halfway House granite formations that include ultramafic formations to the uppermost section of the tributary, followed by grey medium-grained porphyritic granodiorite in the remainder of the tributary heading in a northerly direction (Johnson *et al.,* 2006). A shear zone comes within approximately 100 metres of the northernmost section of the tributary (Johnson *et al.,* 2006).

The land-use of the region immediately surrounding the river under study is classified as a wetland surrounded by Urban Residential areas with small pockets of grasslands and thickets (GTI, 2014). Figure 3.4 shows the land-use classification of the study area and its surroundings.

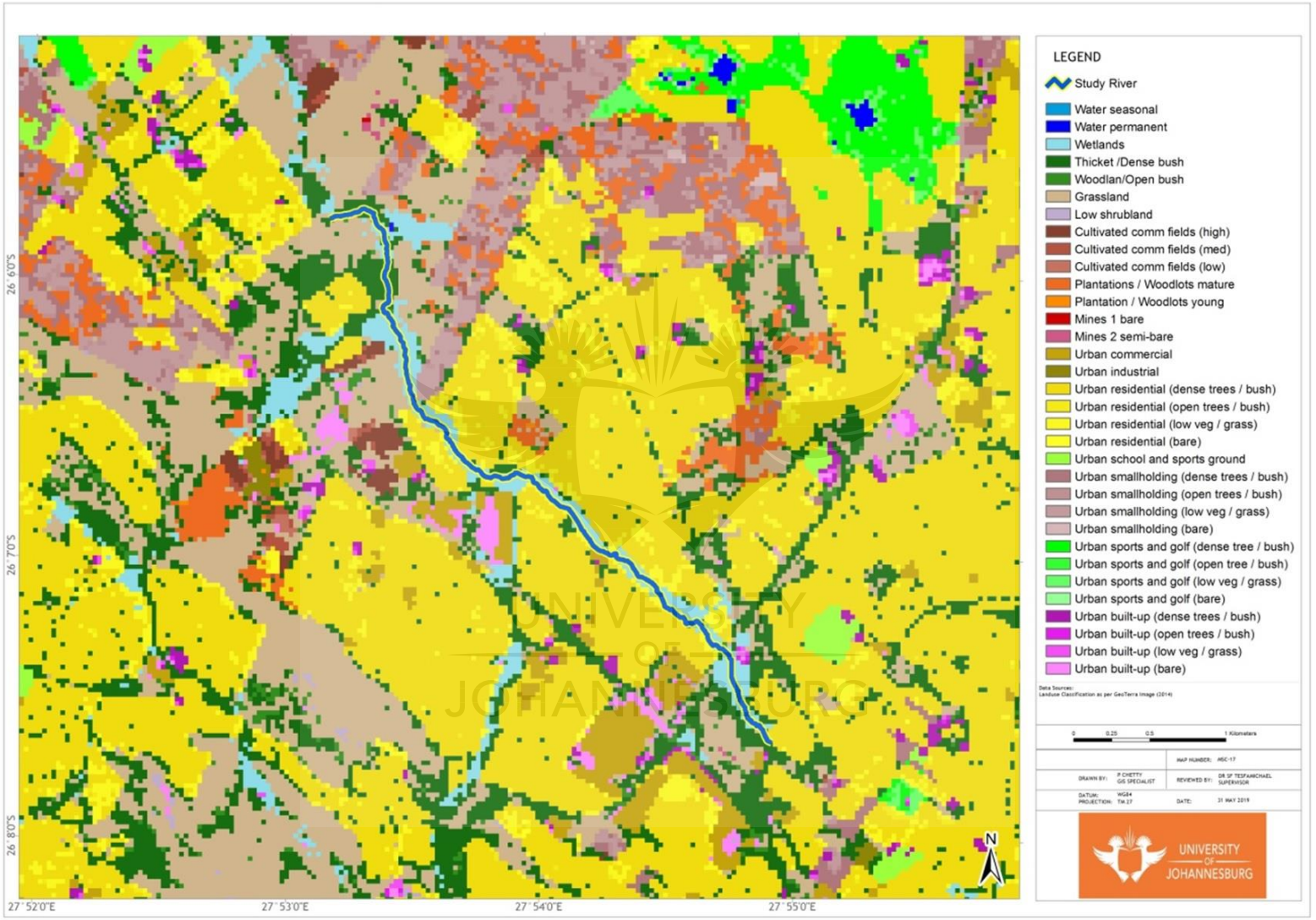

Figure 3.4: Regional land-use classification (Geo Terra Image, 2014)

3.2.2 Data

3.2.1.1 Elevation data sources

A DEM is a numerical data file representation of an areas topography (Erdogan, 2009) and can be differentiated into a DSM and a DTM. There are numerous remote sensing methods to generate DEM data which include photogrammetry, LiDAR and Interferometry (Takaku *et al.,* 2014). The representation of an area's topography is affected by two parameters: the temporal resolution and the spatial resolution, which characterise each DEM source (Erdogan, 2009).

3.2.2.2 5 m Chief Directorate National Geospatial Institute contours

The DRDLR through the NGI releases a 5 m resolution contour dataset to the public. The NGI owns and operates an Intergraph Dual Mass Camera (DMC) which captures stereo imagery at a GSD of 0.5 m (NGI, 2018). The NGI contracts service providers with similar camera specifications to acquire data owing to the large scale of the operation. The temporal resolution, or frequency of update for the NGI dataset is aimed at between every 3 years and 5 years. The dataset that will be included in this research is the 5 m NGI contour dataset, which was last updated on the 08/12/2009 for the study area.

Usage of the 5 m NGI is promoted by the Chief Directorate to South African studies and assessments that require topographical inputs, as per the National Spatial Data and Information act. While higher resolution datasets may be available for metropolitan areas in South Africa, areas that fall outside of the metropolitan area demarcations are at best covered by the 5 m contour offering. As such, the 5 m NGI dataset is a popular source amongst specialists who seek to apply topographical elements to their respective studies. The NGI contours were interpolated to obtain spatial continuity of the elevation data using the optimal interpolation technique, the Topo to Raster technique, as identified in Chapter 2 to produce a 5 m resolution DEM.

3.2.2.3 Light Detection and Ranging point cloud

The LiDAR data for the study area was obtained from the COJ) Municipality Corporate Geo-informatics Department. A target is illuminated by a light source through a laser beam and the time taken for the reflected beam to return to the sensor allows for the calculation of survey-grade measurements relating to the linear position of the target from the sensor (Vosselman, 2003). Advancements in optical and computing technologies have seen the emergence of

LiDAR as a rapid and accurate terrain mapping tool (Lohani & Ghosh, 2017). The COJ municipality region distributes an aerial-based LiDAR data that is acquired by a contracted service provider every three years. The data sourced for this study was acquired in June 2012.

The LiDAR point clouds used in the present study had a point density of 0.2 points per square metre with an approximate average spacing between neighbouring points being 2 m. The horizontal accuracy of the LiDAR data has a 0.048 m RMSE, and vertical accuracy of 0.32 m RMSE as verified with the usage of a network of seven ground control points. The points were classified into ground and non-ground points by the data supplier, with the ground points representing the physical ground level, while the non-ground point representing all features above ground including vegetation and structures. The ground points were used in the present study to serve as the baseline dataset to evaluate the accuracies of the different interpolation techniques applied to the 5 m elevation contour dataset.

3.2.3.4 Advanced Land Observation Satellite World 3D 30 m

In May 2016, the Japanese Aerospace Exploration Agency (JAXA) began freely distributing the World 3-D 30 m (AW3D30) dataset acquired by the ALOS. The AW3D30 combine inputs from three sensors on-board the ALOS which include the Panchromatic Remote-sensing Instrument for Stereo Mapping (PRISM), the Advanced Visible and Near Infrared Radiometer (AVNIR) and the Phased Array type L-band Synthetic Aperture Radar (PALSAR).

PRISM collected 2.5 m resolution imagery, which was processed using photogrammetric techniques to a 5 m resolution. AVNIR collected imagery at a 10 m resolution, while the PALSAR sensor collected radar data with resolution options ranging between 10 and 100 m. Each imaging option was sold commercially, with varying degrees of resolution outputs between 5 and 100 m. The ALOS satellite was successfully operated from 2006–2011 (JAXA, 2017). While the DEMs were commercially sold at a 5 m resolution as interpolated from the PRISM sensor, the DEM data was resampled to 1 arcsecond and released in 2016 to the public with no associated charges. Accuracy assessments conducted on the AW3D30 have yielded RMSE values of 4.40 m for control points located across numerous imagery tiles (Takaku *et al.,* 2016).

3.2.2.5 Shuttle Radar Topography Mission

The SRTM was launched in February 2000 by the United States National Aeronautics and Space Administration (NASA) and has been amongst the most complete sources of global

elevation information sources since. The SRTM version 3 (SRTM v3.0) global 1 arcsecond (approximately 30 m resolution in South Africa) product was used in this study. The dataset was published by NASA in 2015 and represents a void-filled 30 m resolution version of the dataset. The SRTM was flown on two Endeavour Missions in 1994 equipped with the C-Band Spaceborne Imaging Radar and the X-Band Synthetic Aperture Radar (SAR) to observe data on the Earth's surface (USGS, 2018). The dataset was revised from a 90 m resolution and released in 2015 to a finer 30 m resolution, revealing the full resolution of the satellite's original measurements (JPL, 2014). Accuracy assessments conducted using GPS measurements revealed that the absolute elevation errors range between 5.6 m and 9.0 m (Rodriguez *et al.,* 2006).

As the focus of the research is on evaluating the performance of elevation data sources for flood-line modelling, the 30 m SRTM was preferred to the 90 m SRTM. In addition, reference to previous literature indicates that for regions that do not show a high degree of topographical variation, the Advanced Spaceborne Thermal Emission and Reflection Radiometer (ASTER) 90 m resolution data source yields the lowest accuracy (Azizian & Brocca, 2020; Zhang *et al.,* 2019; Jakovljevic *et al.,* 2019). Therefore, the ASTER DEM source was not included as part of the assessment. Table 3.1 provides a summary of the elevation data sources with regards to the date of acquisition and spatial resolution.

Table 3.1: Summary of elevation data sources used

Elevation Source	Date of Acquisition	DEM Spatial Resolution
NGI	08/12/2009	5 m
LiDAR (Baseline Dataset)	06/2012	1 m
AW3D30	*2006–2011	30 m
SRTM v3.0	*2000	30 m

*Refers to the period of operation for the satellite

3.2.2.6 Rainfall data

Rainfall data plays an important role in determining the volume of water to be modelled as part of flood-line modelling. Rainfall data for the study area was obtained using the Design Rainfall Estimation software environment, as suggested by Gericke & Du Plessis (2012) for the A21 catchment area. The software provides a summary of the closest weather station in for the area being assessed and is entered through its set of centre coordinates. It is commonly applied and adopted in the hydrological modelling environment in South Africa due to its rich historical archive of rainfall data (SAWS, 2018; SAWB, 1956). The software allows for the

extraction of the duration of rainfall for each minutely defined graticule in South Africa. The Design Rainfall Estimation in South Africa database was also used to obtain rainfall depths for the Roodepoort region coded as 0475669_W. The data extracted from the database provided rainfall data ranging from five-minute increments up to a week of rainfall (known as the duration). The data for the duration for each return period is also provided which is broken down into 2-, 5-, 10-, 20-, 50-, 100- and 200-year periods (Schulze *et al.,* 2004). In the event of no recorded rainfall for a particular period, interpolation techniques are applied which also provides 90% upper and lower limits of the outputs for the particular region and its associated values (Smithers & Schulze, 2001).

3.2.3 Analysis

3.2.3.1 Digital Elevation Model input

The NGI contour and LiDAR point clouds were converted into continuous DEMs using the Topo to Raster interpolation technique that yielded the most accurate results as shown in Chapter 2. The resultant DEM from interpolation of the NGI was 5 m in resolution, while the LiDAR was interpolated to a 1 m resolution. The AW3D30 and SRTM DEMs were used at their native format supplied as gridded continuous surfaces at 30 m resolution. Therefore, no interpolation was needed for these datasets. The elevation model sources represent the only changing data source in the modelling environment for this research.

3.2.3.2 Water volume determination

The water volumes for a return period are commonly referred to as design flood peaks which correspond to specific periods which are generally broken into 10-year, 50-year and 100-year increments (Ongdas *et al.,* 2020; Saheed & Ndhlovu, 2019; Ullah *et al.,* 2016). The flood peaks are directly related to the characteristics of a rainfall event and the way in which the catchment area responds to the rainfall event (Gericke & Du Plessis, 2012). The calculation of flood peaks in a South African environment are either based on rainfall data or runoff data (Smithers, 2012). The 10-year and 100-year return periods were chosen for modelling as they are representative of two extreme conditions of return period modelling: a fine 10-year, and a liberal 100-year return period volume. By using two return period modelling scenarios, results can be assessed across each return period to establish if differences in volume are significant with regards to the flood-line extent outputs from the various DEM sources. The most common methods used in a South African hydrological environment include statistical, rational, unit hydrograph, standard design flood (SDF) and the empirical method (Smithers, 2012). The

statistical methodology is based on measured data, while the rational, unit hydrograph and SDF methodologies are based on a deterministic approach. The application of the various methods is also limited by the size of the catchment area where the determination is being performed.

The statistical method uses historical rainfall values to estimate the probability of a flood peak volume for a certain return period (HRU, 1972). This method, therefore, is limited to the catchments for which historical rainfall data is available. Usage of the statistical methodology is recommended where long archives of historical rainfall have been recorded due to its extrapolation nature, but with the limitation of the return period being less than double the length of record (Cullis *et al.,* 2007). The statistical method was therefore not used due to the historical archive of rainfall in the region not meeting the suggested limit. Rainfall volumes were calculated using the rational approach, the SDF approach and the empirical methodologies. The highest obtained volumes were used to ensure that the output model liberally represented the flood extents, as opposed to a conservative output which may have under-represented a potential flood.

Mulvaney (1851) was the first to propose the usage of the rational methodology that is based on the principle of the law of mass conservation, which implies that mass cannot be created or destroyed, but only rearranged or changed in form (Kuichling, 1889). The intensity of a rainfall event (how much rainfall is recorded over a particular time interval) is a key input into the rational method calculation. The method operates on the hypothesis that the rate of flow is directly proportional to the size of the catchment area and intensity of rainfall recorded (Kuichling, 1889). The usage of the rational method is recommended for catchments smaller than 15 km^2 due to its assumptions of uniform spatial and temporal rainfall distributions (Smithers, 2012). The formula for the rational methodology is given as follows.

$$Q = \frac{CIA}{3.6} \qquad \text{Equation 3. 1}$$

where Q is the flood peak (m^3/s);

C is the dimensionless calibrated runoff coefficient (where the C-value coefficients are shown in Table 3.2);

I is the average rainfall intensity (mm/hour); and

A is the catchment area (km^2).

The 3.6 value is a conversion factor. The rational methodology works on the assumption that the entire catchment area receives a uniform distribution of rainfall. The runoff coefficient C is also assumed to be constant throughout the duration of a rainfall event (Smithers *et al.,* 2013).

Table 3.2 C-value coefficients for rational method calculation (SANRAL, 2013)

Rural (C_1)					Urban (C_2)	
Component	Classification	Mean annual rainfall (mm)			Use	Factor
		< 600	600 - 900	> 900		
Surface slope (C_s)	Vleis and pans (<3%)	0,01	0,03	0,05	*Lawns*	
	Flat areas (3 to 10%)	0,06	0,08	0,11	- Sandy, flat (<2%)	0,05 – 0,10
	Hilly (10 to 30%)	0,12	0,16	0,20	- Sandy, steep (>7%)	0,15 – 0,20
	Steep areas (>30%)	0,22	0,26	0,30	- Heavy soil, flat (<2%)	0,13 – 0,17
					- Heavy soil, steep (>7%)	0,25 – 0,35
Permeability (C_p)	Very permeable	0,03	0,04	0,05	*Residential areas*	
	Permeable	0,06	0,08	0,10	- Houses	0,30 – 0,50
	Semi-permeable	0,12	0,16	0,20	- Flats	0,50 – 0,70
	Impermeable	0,21	0,26	0,30		
					Industry	
					- Light industry	0,50 – 0,80
Vegetation (C_v)	Thick bush and plantation	0,03	0,04	0,05	- Heavy industry	0,60 – 0,90
	Light bush and farm lands	0,07	0,11	0,15	*Business*	
					- City centre	0,70 – 0,95
	Grasslands	0,17	0,21	0,25	- Suburban	0,50 – 0,70
	No vegetation	0,26	0,28	0,30	- Streets	0,70 – 0,95
					- Maximum flood	1,00

Within the rational methodology, there are three common approaches in which rainfall intensity can be determined. The first approach uses a Depth-Duration-Frequency diagram, derived from studies conducted in 1978 by Midgley and Pitman (Smithers *et al.,* 2013). The second approach of the rational method applies the modified Hershfield equation to an updated rainfall database referred to as the TR102 representative rainfall dataset which was collected in 1981. The third approach uses a rainfall database with records for 1806–2000. Details of the dataset are presented in the rainfall dataset section of this research in Section 3.2.2.6. In this study, the third approach of the rational methodology was applied as one of the peak discharge calculations for the research because the rainfall records were more temporally relevant and complete for the study area.

The SDF developed by Alexander (2001), provides a uniform approach to flood peaks by using calibrated discharge coefficients for a recurring period of 2–100 years. The SDF method is one of the most popular methods of determining flood peaks in South Africa (SANRAL, 2013). The SDF method is based on the rational methodology (Schulze *et al.,* 2004), whereby calibrated coefficients were calculated across 29 basins in South Africa. Table 3.3 shows the basin details used to determine the C_t values. The SDF method is defined by the following formula.

$$Q_t = \frac{C_T I_T A}{3.6}$$ Equation 3. 2

The runoff coefficient differs from the rational method which uses a site-specific runoff coefficient by assessing the basin in which the assessment area falls as per Figure 3.5 and assigning a regional-level runoff value.

Table 3.3: Coefficient values based on basin assessment (SANRAL, 2013)

Basin	SAWS station number	SAWS site	M (mm)	R (days)	C2 (%)	C100 (%)	MAP (mm)	MAE (mm)
1	546204	Struan	56	30	10	40	55	1800
2	675125	Autoriteit	62	44	5	30	450	1900
3	760324	Siloam	64	28	5	10	470	1700
4	553351	Waterval	58	20	10	50	630	1600
5	680059	Leydsdorp	78	10	15	70	620	1600
6	369030	Siloam	51	54	15	60	640	1500
7	328726	Olivine	49	39	15	60	540	1700
8	322071	Danielskuil	47	39	5	20	380	2100
9	258452	Jacobsdal	43	47	15	60	380	1800
10	233049	Wonderboom	54	55	10	50	560	1600
11	236521	Mashai	39	66	40	80	430	1400
12	143258	Scheurfontein	39	52	5	30	890	2100
13	284631	Wilgenhoutsdrif	40	55	5	15	70	2600
14	110385	Middelpos	25	13	10	30	140	2400
15	157874	Garies	22	11	5	20	130	2100
16	160807	Loerisfontein	28	11	10	40	210	1900
17	84558	Elandspoort	45	1	40	80	500	1500
18	22113	La Motte	59	4	30	60	810	1400
19	69843	Letjiesbos	34	16	10	35	160	2200
20	34762	Uitenhage	53	12	15	60	480	1600
21	76884	Albertvale	45	23	10	35	460	1700
22	80569	Umzoniana	84	26	15	60	820	1200
23	180439	Insizwa	60	45	10	80	890	1200
24	240269	Newlands	76	15	15	80	910	1200
25	239138	Whitson	55	9	10	80	830	1200
26	336283	Nqutu	61	17	15	50	760	1500
27	339415	Hill Farm	85	17	30	80	890	1400
28	483193	Maliba Ranch	75	54	15	60	740	1400
29	556088	Mayfern	66	11	15	50	740	1600

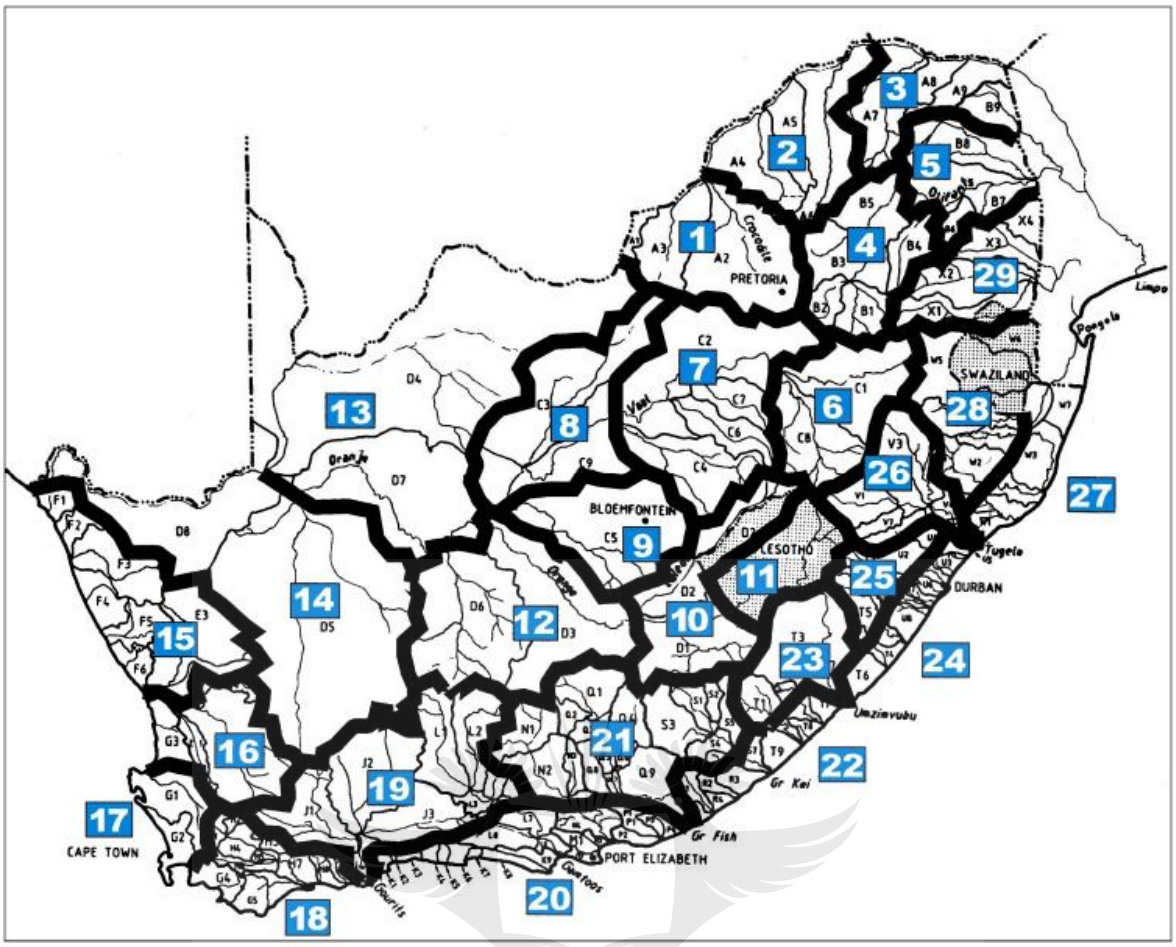

*

Figure 3.5: Basin locations for SDF method (SANRAL, 2013)

The empirical method includes an amalgamation of historical data, experience and the results of other methods. The empirical method is commonly used as a point of relativity to assess the other flood peak determination methodologies. The empirical method commonly applied in South African environments is the Midgley and Pitman model which is suitable for rural catchments larger than 100 km² (Smithers *et al.*, 2013). The frequency and distribution of peak flood events across 83 measuring stations in South Africa were studied. These areas were homogenised into veld type regions in South Africa as shown in Table 3.4. The formula for the Midgley Pitman model is given as follows.

$$Q_t = K_{rp} A^{0.5} \qquad \text{Equation 3. 3}$$

where K_{rp} is a constant for the return period T.

The K-values were established by grouping areas with similar topographic, rainfall, soils, drainage and vegetation cover into seven regions as shown in Figure 3.6. The K-value constants for the different regions are shown in Table 3.4.

Table 3.4: K-value constants for the empirical method (SANRAL, 2013)

Return Period T (Years)			10	20	50	100
Zone number and Veld type	1	Coastal Tropical Forest	0.17	0.23	0.32	0.40
	2	Schlerophyllous bush	0.42	0.52	0.68	0.80
	2	Schlerophyllous bush	0.83	1.04	1.36	1.60
	3	Mountain Sourveld	0.29	0.40	0.55	0.70
	4	Grasslands of interior plateau	0.59	0.68	0.95	1.20
	5	Highlands sourveld and Dohne sourveld	0.59	0.80	1.11	1.40
	5A	Zone 5 criteria – But soils weakly developed	0.59	0.68	0.95	1.20
	6	Karoo	0.33	0.45	0.63	0.80
	6	Karoo	0.67	0.91	1.26	1.60
	7	False Karoo	0.67	0.91	1.26	1.60
	8	Bushveld	0.42	0.57	0.79	1.00
	9	Tall sourveld	0.50	0.68	0.95	1.20

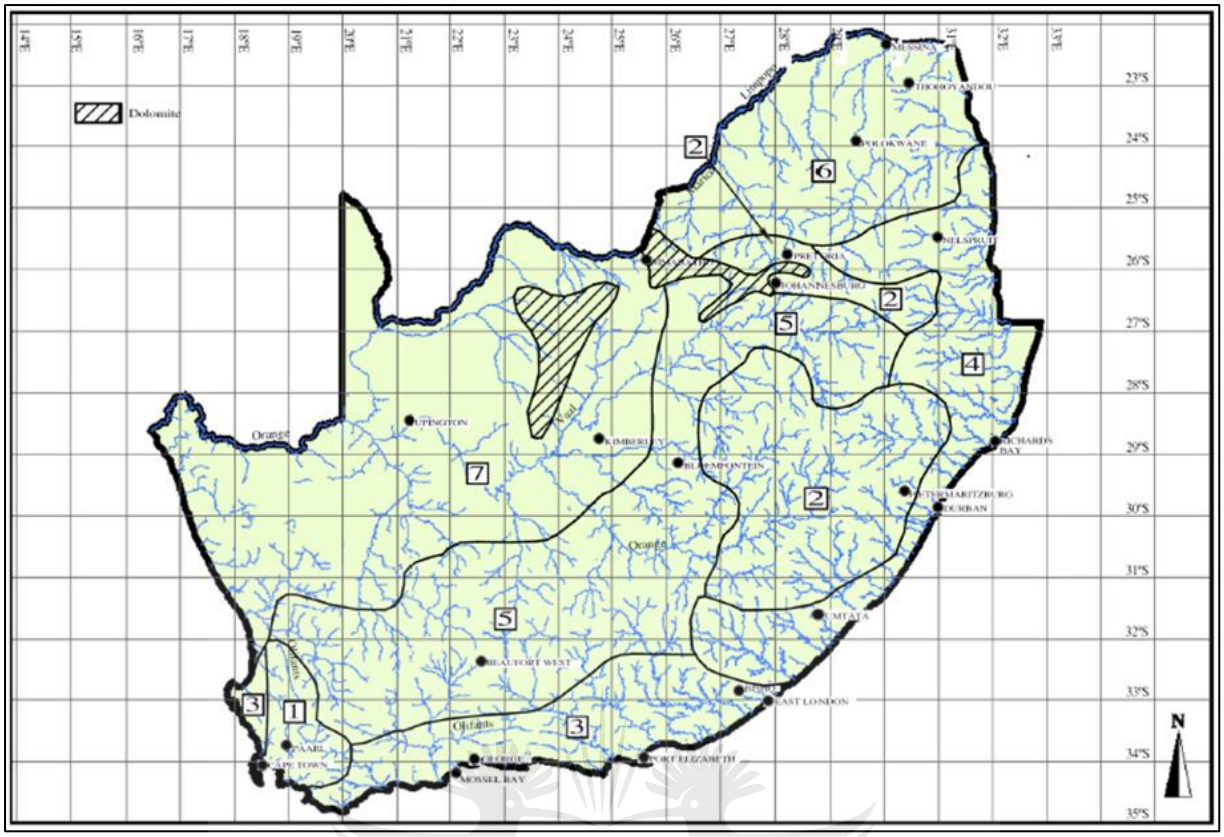

Figure 3.6: Vegetation region divisions used for the empirical method (SANRAL, 2013)

3.2.3.3 Definition of river geometry

The definition of the input river geometry is based on the centreline of the river and banklines on either side of the river (where the banklines define the river channel). The topology of the geometry is critical in the geometry definition to ensure that the model can calibrate the left and right bank, along the direction of the river flow (Teng *et al.,* 2017). Using the ArcGIS Spatial Analyst tool (ESRI, 2019), a flow accumulation analysis was performed on the most accurate elevation model data source, which in this research is represented by the LiDAR dataset. The flow accumulation uses the input elevation raster to identify the number of upslope cells that have the lowest value around them. The stream therefore always flows from a higher value to the lowest neighbouring value. The stream delineation is representative of the river centreline, which was kept constant throughout the modelling process as a stream centreline delineation on the LiDAR dataset served as the most accurate delineation. As part of the flow accumulation analysis procedure, sub-catchment delineation was also produced for the river being modelled.

3.2.3.4 Flood-line modelling process

The flood-line modelling software utilised by this study is the GeoHECRAS package, which is developed and distributed by the software company CivilGeo (CivilGEO, 2019). GeoHECRAS was chosen due to its ability to run multiple flood-line scenarios with interchangeable parametres. The river geometry definitions were kept constant, while the DEM inputs were interchanged in this study. The GeoHECRAS package also allows for full integration into GIS packages with the ability to export shapefile-based formats. The GeoHECRAS environment works on the principle that the flood-line and its associated velocities can be determined through hydraulic calculations that are based on the three key inputs: a DEM the project area with sufficient coverage around the course of the river being modelled, the volume(s) of water to be modelled per flood-line simulation and the definition of the river geometry to be modelled (CivilGEO, 2019). GeoHECRAS performs a calculation across each defined cross section, referred to as cross section (XS) cutlines. The XS cutline is drawn perpendicularly to the defined stream centreline across each bank with a fixed width of 150 m, ensuring that the full floodplain of the river system is captured. The XS cutline distance was defined at a regular interval of every 100 m in this study which provides a good balance between computational efficiency and flood-line output coverage. For the study area and river being modelled, the total number of XS cutlines is 50, which equates to 100 measurements (either side of each cutline) as shown in Figure 3.7.

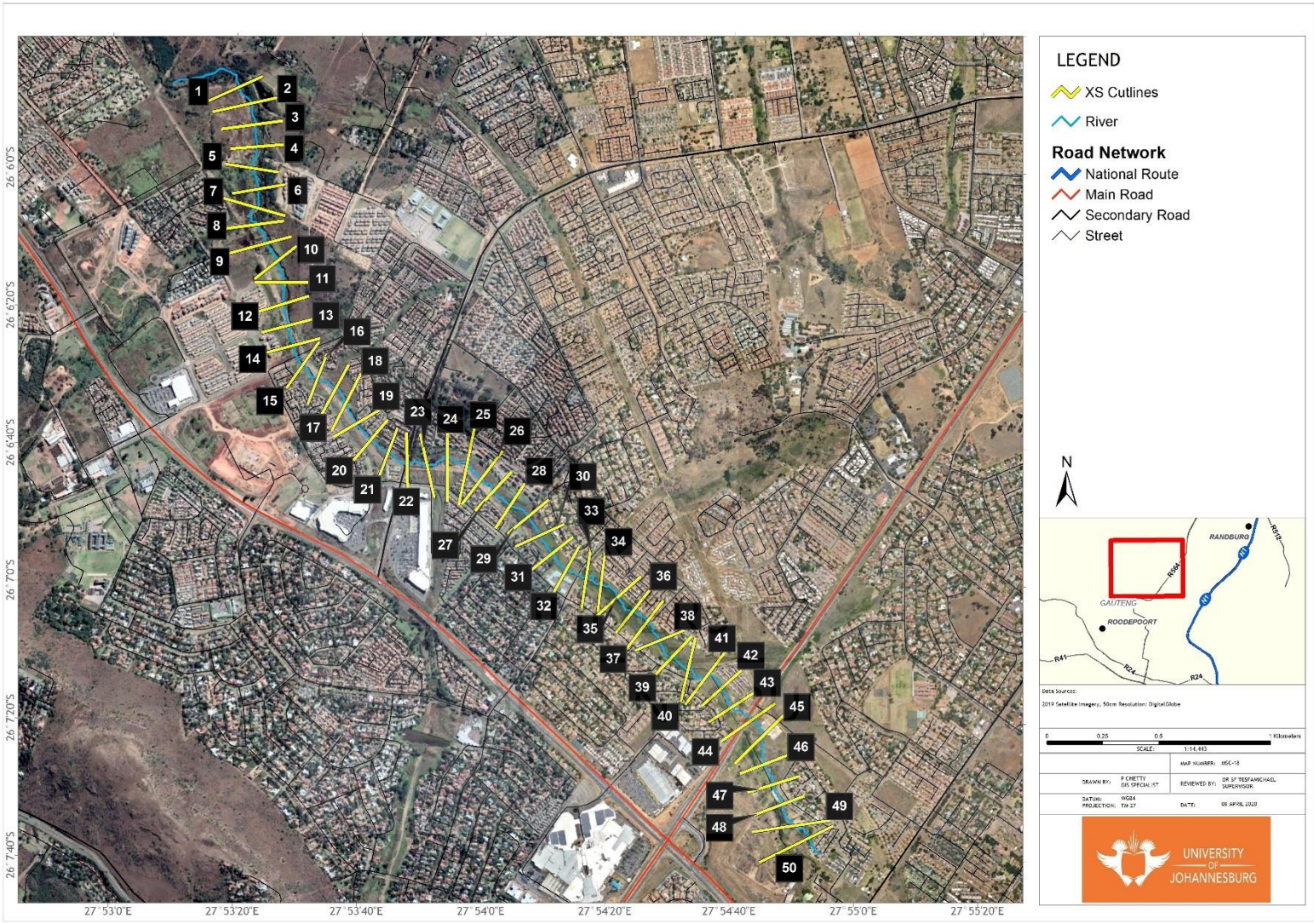

Figure 3.7: Cross section (XS) Cutline locations and associated locations of measurement along the tributary

The digital flood-line environment simulates a flood across each cross section, taking the volume of water, flow velocity and topography into account and recorded the maximum extent to which the water will flood along each defined XS cutline. Cumulatively, each cutline with its associated flood point creates a network of points which are joined to create a coverage representing the flood inundation area. Figure 8 illustrates the XS cutline, along with a cross section profile along the identified XS cutline showing a flood inundation extent.

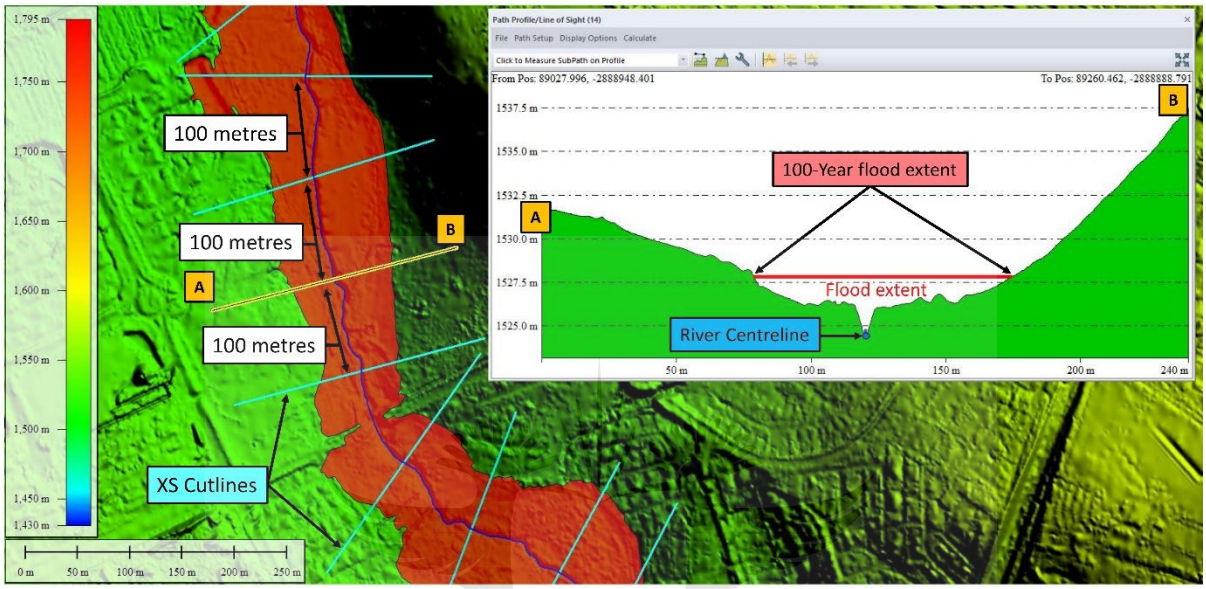

Figure 3.8: Cross sectional view of the river geometry as defined in GeoHECRAS

The LiDAR derived DTM, river geometry definition and rainfall volumes were run as a scenario for 10-Year and 100-Year flood events, producing baseline flood extents from which the subsequent outputs for the other DEM sources were compared against. The NGI, SRTM and AW3D30 elevation data sources were interchanged and modelled as the only variables in the modelling process, producing their own corresponding 10-Year and 100-Year flood line extent outputs. All outputs were exported in shapefile format to allow further analysis in a spatial context.

3.2.3.5 Extracting comparative flood extent data

The stream centreline and XS cutlines were kept uniform throughout the modelling process and therefore served as points of reference for the comparison of the different outputs. Using ArcGIS software (ESRI, 2019), the distance along each cutline was calculated from the stream centreline to either bank (the left bank and right bank). By extracting the respective “bank to stream centreline” distances, a total of 100 distance records were calculated and recorded for

further assessment to determine the accuracy of output from each DEM source. The bank to stream centreline distances are representative of the extent of the inundation model, with lower distances representing a small inundation extent, and higher distances representing a larger inundation extent.

3.2.4 Accuracy assessment

The distance from the river centreline to the flood extent for each scenario (10-Year and 100-Year) across all elevation model sources were measured in metres and defined as either the left bank or right bank as an attribute. The observed measurements from each DEM sources flood-line output to the river centreline were comparatively assessed using a T-Test and residual analysis. The T-test serves as a quantification of the amount of variance each output has to the baseline LiDAR, while the residual analysis allows for the geo-location of values beyond a defined 5 m threshold.

3.2.4.1 Comparing centreline—flood-line distance of LiDAR and DEM sources of interest

The T-test is a statistical procedure that is commonly used when investigating the relationship between variables by comparing the means on the dependent variables against the baseline or independent variable (Green & Salkind, 2012). The T-test was chosen due to the flood extent comparisons involved at each measurement station, where more than one dependent set of results will be compared to the baseline LiDAR flood-line extents. The P-value from the T-test output is used to assess the degree of difference between the means of the flood-line distance from the centreline versus the baseline LiDAR flood-line distances from the centreline. The T-test used is a generalisation of a two-sample T-test (Ostertagova & Ostertag, 2013) and is defined as follows.

$$F = \frac{Mean\ square\ between\ groups\ (MSG)}{Residual\ Mean\ Square(RMS)} \qquad \text{Equation 3. 4}$$

Where

$$MSG = \frac{\sum_{i=1}^{k}\left(\frac{T_i^2}{n_i}\right) - G^2/n}{k-1} \qquad \text{Equation 3. 5}$$

and

$$RMS = \frac{\sum_{i=1}^{k}\sum_{j=1}^{n_i} Y_{ij}^2 - \sum_{i=1}^{k}(\frac{T_i^2}{n_i})}{n-k}$$

Equation 3. 6

Where Y_{ij} is the observation distances from the stream centreline for each output;

T_i is the sum of each group of distances from the stream centreline;

G is the total of all observations being compared for the variance (model output being assessed versus baseline LiDAR output);

n_i is the number of observations in group I; and

n is the total number of observations being analysed for the variance.

The T-test and associated P-values were calculated using Microsoft Excel (Microsoft Corporation, 2019).

The Root Mean Square Error (RMSE) is a standardized statistical metric that is commonly used in model performance assessments where the computed value is a measure of the error between two datasets (Chai & Draxler, 2014). The usage of RMSE in the field of GIS is relatively widespread, where smaller RMSE values are indicative of observed values that are closer to the baseline values of assessment. The RMSE metric does not take direction in the form of negative and positive values into account, thus providing an absolute measure of error. The RMSE is calculated using the following formula.

$$RMSE = \sqrt{\frac{1}{n}\sum_{i=1}^{n}(P_i - O_i)^2}$$

Equation 3.7

Where n = number of observations;

P = Baseline or predicted value; and

O = Observed value.

Mean error (ME) is a statistical metric which refers to the average of all errors between a predicted and observed dataset (Khair *et al.,* 2017). Opposed to the RMSE metric, the ME takes positive and negative values into account. In the case of ME values, the results indicate instances where an observed model on average underestimates or overestimates a baseline predictive model and to what degree. The ME is calculated using the following formula.

$$ME = \frac{1}{n}\sum_{i=1}^{n}(P_i - O_i)$$ Equation 3.8

Where n = number of observations;

P = Baseline or predicted value; and

O = Observed value.

3.2.4.2 Residual analysis of the flood-lines generated from the DEM sources of interest

An analysis of residuals forms part of a regression analysis which is designed to assess model adequacy (Martin *et al.,* 2017). Due to the research purpose of accuracy assessment as opposed to model fitting, the regression analysis was therefore not chosen as an accuracy assessment tool in this research. However, components of the regression analysis remain useful tools in location-based analytics, such as the residual analysis which allows for the referencing to a specific observation and its associated spatial location. Residuals are defined as the vertical distance (r_i) between the observed measurement and the predicted measurement, represented by a linear regression line. The formula used is defined as follows.

$$r_i = \hat{y} - y_i$$ Equation 3. 7

where $\hat{y}$ represents the linear regression from the baseline LiDAR flood-line outputs and y_i represents the distance along the XS cutline from the stream centreline to the flood-line output of the model being assessed (NGI, SRTM & AW3D30).

Outlier identifications in data have been applied successfully through the usage of standardised residuals (Sousa *et al.,* 2012; Miller, 1993; Salekin *et al.,* 2018) and are defined by the following formula.

$$r_{s=} \frac{r_i}{s}$$ Equation 3. 8

The standardised residual is the residual value (r_i) divided by its standard deviation (s). At a 95% confidence level, it is expected that 95% of the data falls within 2 standard deviations of the mean (Sousa *et al.,* 2012). Data points falling lower than – 2 and higher than 2 on the standardised residual plot will therefore represent outliers, with increasing significance the further the point is from the 0 axes. The incorporation of a standardised residual analysis allows for the identification of interpolated elevation output observations that are significantly

different to the baseline LiDAR elevation values, which in turn allows for a spatial expression of the results observed. Negative values are representative of overestimations of the flood extent, while positive values are representative of underestimations of the flood extent. This component of the analysis allows for location-based interpretations of the results, which will offer insight into why certain variances and outliers exist.

Figure 3.9 represents a summary of the methodology followed to achieve the objectives set in this chapter. The methodology starts at the interpolation procedure application, which based on the recommendations and findings from Objective 1 is the Topo to Raster interpolation technique. The streamflow analysis is conducted to determine the stream centreline as per the baseline LiDAR dataset. The various elevation models subjected to the assessment were then prepared as modelling inputs by clipping the elevation datasets to match the regional extent that defines the topography of the modelling environment. The volume of water that is representative of the 10-year and 100-year return periods was calculated using a series of hydrological calculations that took parametres into account, including the area of the catchment and its landcover characteristics, as well as historical rainfall data. The modelling environment was then defined in a specialist software environment (CivilGEO, 2019), where cutline intervals were placed at every 100 m along the course of the river. The model was then run using the various data inputs, with iterations being run across each elevation data source. The outputs of the flood inundation models were exported as a shapefile, so that the distances from the centreline could be extracted and subjected to further analysis to determine which elevation data source is the most suitable in comparison to the baseline LiDAR. All GIS pre-processing and post-processing was conducted in ArcGIS (ESRI, 2019).

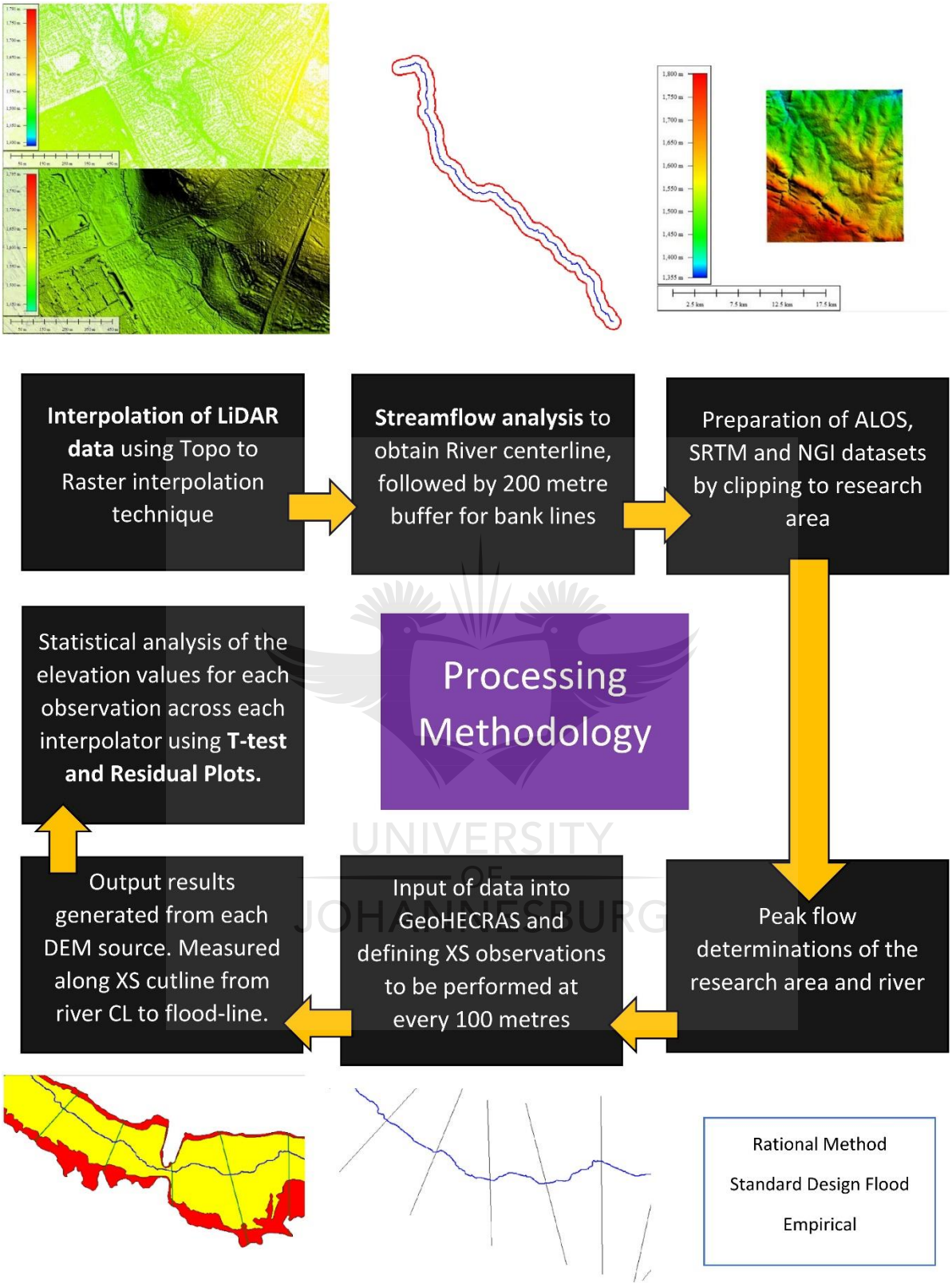

Figure 3.9: Summary of processing methodology used in the study

3.3 Results

3.3.1 Introduction

The flood peak value determinations for the 10-year and 100-year periods are presented as part of the results and were used as inputs to generate the flood inundation models for each DEM source. The physical outputs of the flood-line modelling process using the various DEM sources are presented as part of the results to visually depict the differences in the various flood inundation models. Distances from the stream centreline along each XS cutline were measured to each flood-line model's extent and form the basis of the accuracy assessments presented through a T-test and residuals analysis.

3.3.2 Peak flow determinations

Peak flow determinations were run for the rational approach, the SDF and the Midgley Pitman (empirical) methods. Out of the three assessments, the highest peak flow values were chosen from the 100-year period which is commonly practised in a hydrological modelling context to cater for a larger volume which accounts for a relaxed scenario opposed to a conservative approach. The 10-year volume was then used from the identified methodology as described for the 100-year volume. The results from the peak flow determinations show that the rational approaches results are preferred for the liberal approach for this study, measuring 192 m^3/s for the 10-year return period and 544 m^3/s for the 100-year return period. Table 3.5 shows a summary of the peak flow results obtained through the three methods applied, with the highlighted values indicating the volumes that were used in the modelling process.

Table 3.5: Peak flow volume results for 10-year and 100-year return periods

Catchment	Method					
	Rational method (alternative 3)		Standard design flood		Midgley Pitman (empirical)	
	1:10yr	1:100yr	1:10yr	1:100yr	1:10yr	1:100yr
	(m^3/s)					
Wilgespruit tributary (~75km²)	192	544	209	496	361	456

Flood-line model outputs were processed for each DEM source for the 10-year and 100-year return periods. Using the shapefile outputs from the flood-line model, the flood-line distance along each XS cutline was calculated as shown in Figure 3.10.

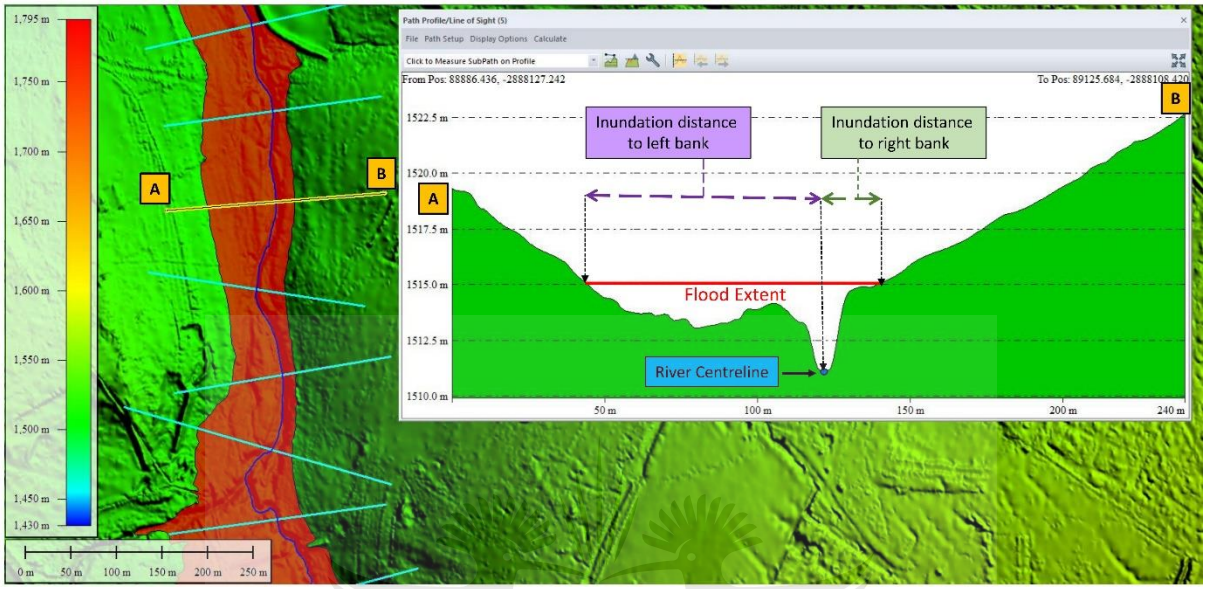

Figure 3.10: Illustration of distance to stream centreline measurements from either bank

Graphical illustrations of the flood-line model output extents are presented in Figure 3.11 for the 10-year return period and in Figure 3.12 for the 100-year return period. Immediate graphic outputs indicate that the SRTM return period outputs cover less than half of the modelling environment for the 10-year period and marginally over 50% for the 100-year period. In comparison, the NGI and AW3D30 outputs cover most of the LiDAR baseline flood-line output regions.

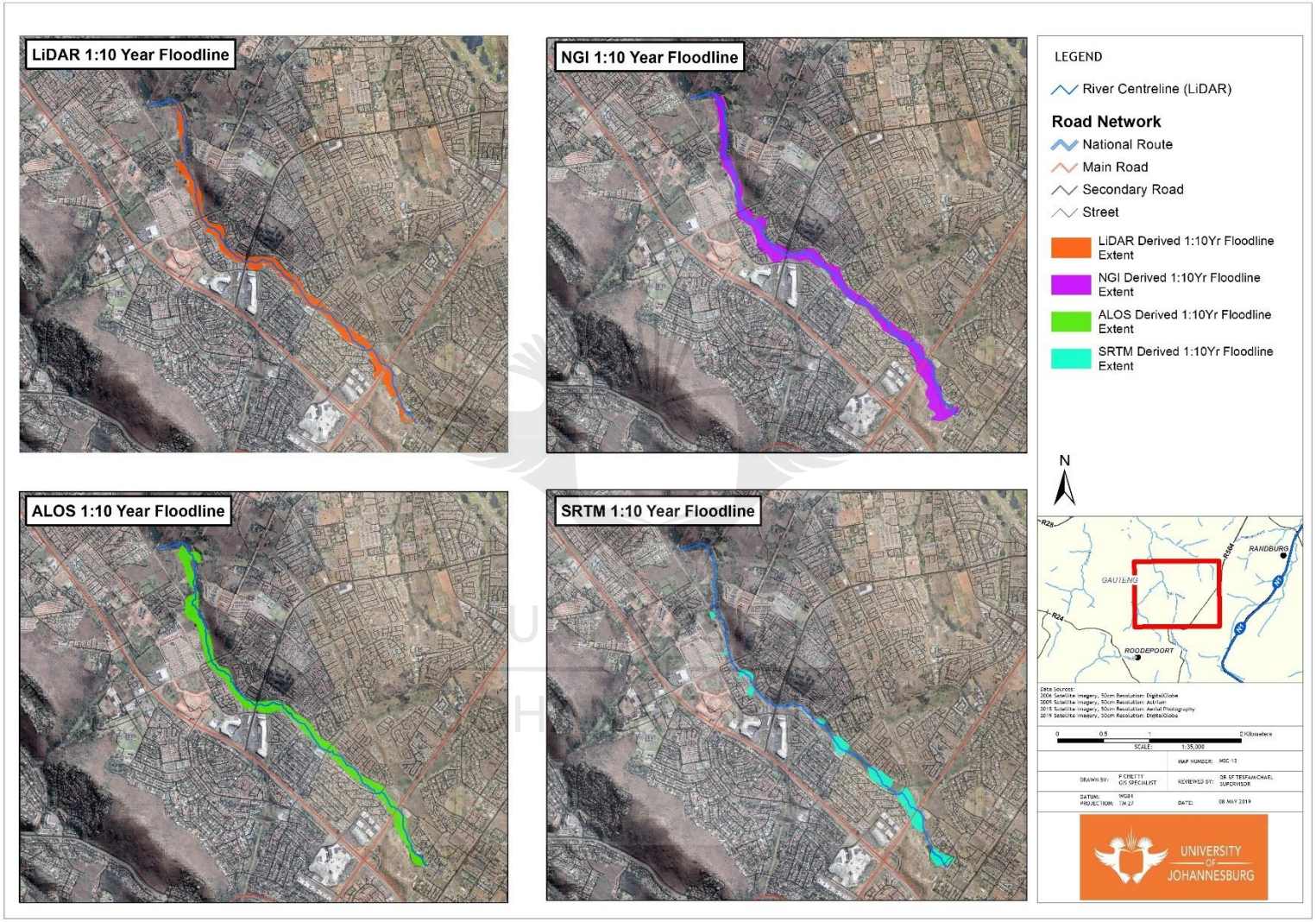

Figure 3.11: 10-year return period flood-line outputs for LiDAR, NGI, AW3D30 & SRTM DEM sources displayed in true colour RGB band combination

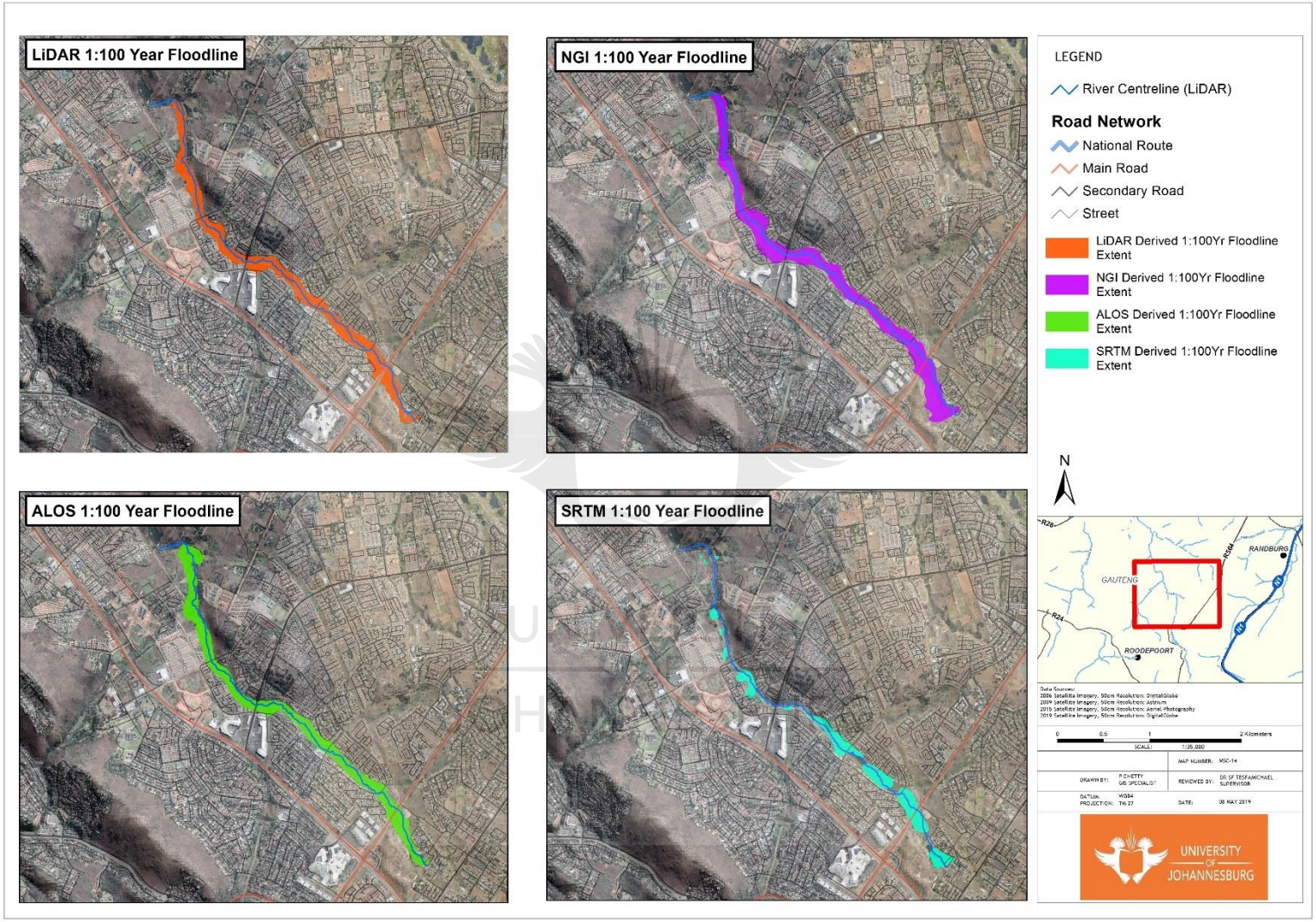

Figure 3.12: 100-year return period flood-line outputs for LiDAR, NGI, AW3D30 & SRTM DEM sources displayed in true colour RGB band combination

3.3.3 Distance differences between river centreline and flood-line for the DEM sources of interest

The results from the T-test, RMSE and ME analysis are presented in Table 3.6 for the output distances from each modelled DEM source for the 10-year and 100-year return period. Due to certain flood-line model outputs not covering the entire extent of the baseline LiDAR flood-line output, only areas of overlapping coverages across the XS cutlines are reported on. As a result, Table 3.6 also includes a quantification of the available overlapping records for comparison, along with a calculation of mean values based on the overlapping data. The overlapping record count is representative of the coverage of the model's output – the closer the count is to 100 (where 100 = a count of the baseline LiDAR flood-line XS value records), the more complete the coverage. The T-test was run at an alpha = 5%.

NGI-derived flood-line model for the 10-year return period indicates the highest number of comparable results against the baseline LiDAR-derived flood-line with a total of 92 output values. The 10-year NGI outputs show a significant difference (P-value of 0.01) to the baseline LiDAR for the 10-year return period. The mean distance from the LiDAR values that the NGI was compared against has the largest variation for the 10-year results, showing that the NGI outputs on average overestimate the extent of the flood-line by 15.43 m. The RMSE for the NGI-derived flood-line model for the 10-year return period shows the highest difference to the baseline LiDAR with an RMSE of 29.49 m. The NGI 100-year return period flood-line model results again show the highest number of comparable results against the baseline LiDAR outputs with a total of 99 output values. The 100-year NGI output shows a significant difference (P-value of 0.020) to the baseline LiDAR outputs. The mean distance from the LiDAR value that the NGI was compared against for the 100-year has the largest variation, showing that the NGI outputs generally overestimate the extent of the flood-line (as seen in the 10-year results) by 11.89 m. The RMSE for the NGI-derived flood-line model for the 100-year return period is 32.77 m.

The AW3D30 results for the 10-year return period flood-line model indicate the second-highest number of comparable results against the baseline LiDAR outputs with a total of 91 output values as shown in Table 3.6. The AW3D30 outputs show no significant difference (P-value of 0.16) to the baseline LiDAR for the 10-year return period. The mean distance from the LiDAR values that the AW3D30 was compared against has an intermediate level of difference for the 10-year results, showing that the AW3D30 outputs on average overestimate the extent of the flood-line by 7.3 m. The RMSE for the AW3D30-derived flood-line model for the 10-year return period shows the lowest difference to the baseline LiDAR with an RMSE of 25.06 m. The AW3D30 100-year return period flood-line model again shows the second-highest number of comparable results against the baseline LiDAR outputs with a total of 91 output values. The

100-year return period flood-line output also shows no significant difference (P-value of 0.07) to the baseline LiDAR outputs. The mean distance from the LiDAR values that the AW3D30 was compared against has an intermediate level of variation for the 100-year results, showing that the AW3D30 outputs on average underestimate the extent of the flood-line by 8.28 m. The RMSE for the AW3D30-derived flood-line model for the 100-year return period shows the lowest difference to the baseline LiDAR with an RMSE of 24.41 m.

The SRTM results for the 10-year return period flood-line model indicates the lowest number of comparable results against the baseline LiDAR outputs with a total of 32 output values as shown in Table 3.6. The SRTM output shows no significant difference (P-value of 0.70) to the baseline LiDAR for the 10-year return period. The mean distance from the LiDAR values that the SRTM was compared against has the lowest level of difference for the 10-year results, showing that the SRTM outputs on average overestimate the extent of the flood-line by 3.79 m. The RMSE for the SRTM-derived flood-line model for the 10-year return period shows an RMSE of 29.32 m. The SRTM 100-year return period flood-line model results also show the lowest level of difference against the LiDAR with a total of 56 output values. The 100-year return period flood-line output SRTM T-test results show no significant difference (P-value of 0.294) to the baseline LiDAR outputs for the 100-year return period. The mean distance from the LiDAR values that the SRTM was compared against has the lowest level of variation for the 100-year results, showing that the SRTM outputs on average underestimate the extent of the flood-line by 4.47 m. The RMSE for the SRTM-derived flood-line model for the 100-year return period shows the highest difference to the baseline LiDAR with an RMSE of 35.94 m.

Table 3.6: T-test, RMSE and ME results for 10-year and 100-year flood-line outputs

10-Year T-test Results						
DEM Source	Overlapping outputs (n)	Mean Distance from River: Varying DEM Source flood-line output (Metres)	Mean Distance from River: LiDAR baseline flood-line output (Metres)	*P-value	Mean Difference between LiDAR and Interpolator / ME	RMSE (metres)
NGI	92	59.71	44.28	0.01	-15.43	29.49
AW3D30	91	51.7	44.39	0.16	-7.3	25.06
SRTM	32	55.92	52.12	0.7	-3.79	29.32
100-Year T-test Results						
DEM Source	Overlapping outputs (n)	Mean Distance from River: Varying DEM Source flood-line output	Mean Distance from River: LiDAR baseline flood-line output	*P-value	*P Mean Difference between LiDAR and Interpolator / ME value	RMSE (metres)
NGI	99	71.42	59.53	0.02	-11.89	32.77
AW3D30	94	53.44	61.82	0.07	8.28	24.41
SRTM	56	60.32	64.79	0.29	4.47	35.94

*P value was measured using 95% confidence level

3.3.4 Identification of outliers from the flood-line outputs against the LiDAR reference flood-line output

An illustration of the plotted results from the residual analysis for a particular XS cutline output (XS Cutline 16) for each DEM source is presented in Figure 3.13. The results graphically illustrate outliers of significance that can be related to a spatial location shown in Figure 3.14, which forms a platform for the interpretation and subsequent discussion around the output data. Positive values indicate an underestimation of the flood extent, while negative values indicate an overestimation of the flood extent.

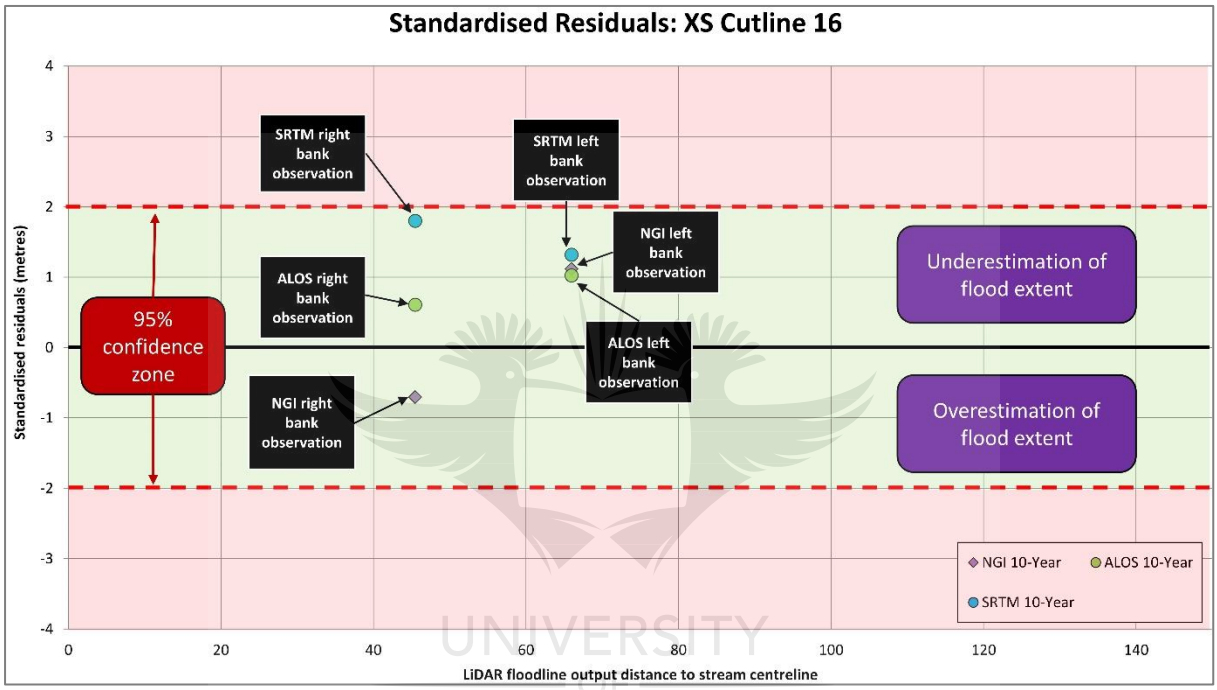

Figure 3.13: Standardised residual example for interpretation of plotted data

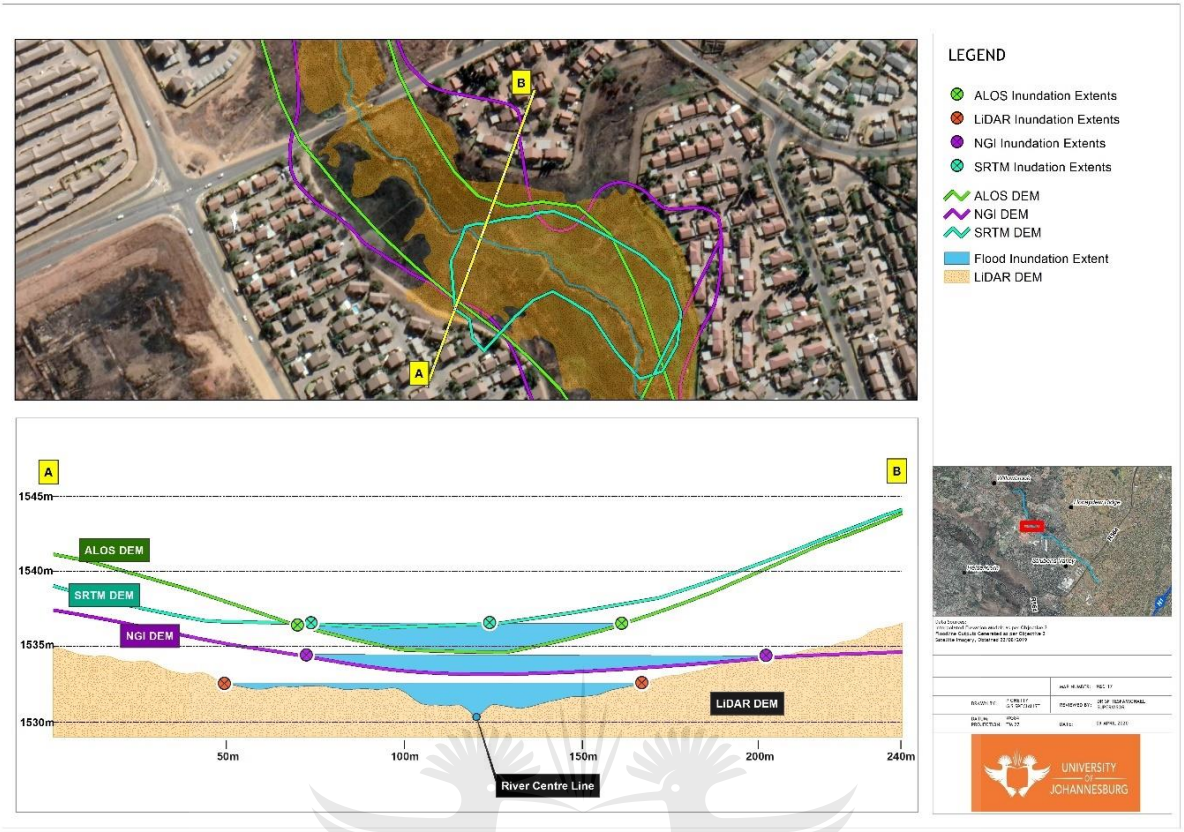

Figure 3.14: Spatial illustration of a residual outlier - XS Cutline 16

3.3.4.1 10-year flood-line outlier identification

Figure 3.15 illustrates the 10-year flood-line output residual analysis results, which represents the LiDAR-based flood-line output distance to the stream centreline on the X-axis, and the residual value outputs across the various DEM sources (AW3D30, SRTM & NGI) flood-line output distance to the stream centreline on the Y-axis. By using the residual plot analysis, individual records that were visual outliers from the distribution of residual values were identified. A total of 13 points was identified, each with its unique spatial location which was linked back to each XS cutline and bank side.

The values showed a gradual increase from negative standardised residual values indicative of overestimations in the lower flood inundation areas towards larger positive standardised residual values which are indicative of underestimations in the larger flood inundation areas (ranging between 60 m and 150 m). All DEM sources showed a good, randomised distribution about the Y-axis between 20 m and 60 m, with large deviations of underestimation and overestimation beyond these bounds. All outputs showed that the larger the flood inundation extent (by virtue of its increasing distance of the flood-line's distance to the centreline), the larger the overestimation of the extent of flood inundation.

Specifically, the NGI source overestimates the extent of the flood inundation model at various distances from the stream centreline with 63% of the recorded distances extending beyond the LiDAR baseline output shown in Figure 3.15. Instances of underestimation are recorded for a distance of approximately 90 m and 145 m away from the stream centreline. The AW3D30 outputs marginally overestimated the extent of the flood-line with 56% of the recorded measurements being larger than the LiDAR baseline output. Large overestimations of the inundation extent for the AW3D30 output occurred at the smaller inundation areas, whereas underestimations occurred at the larger inundation areas. The SRTM observations marginally overestimated the flood inundation extent, with 53% of the recorded measurements being larger than the LiDAR baseline output.

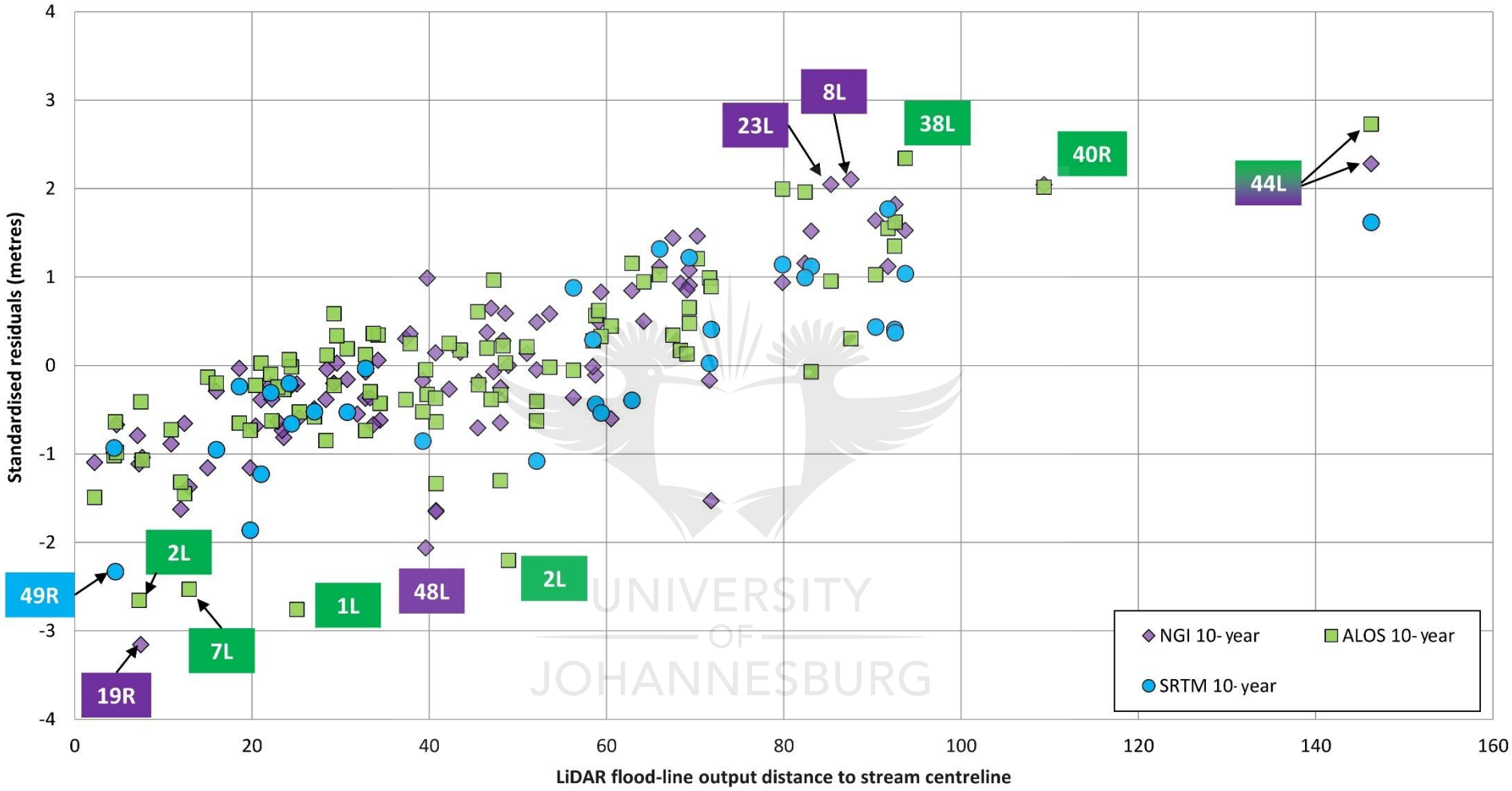

Figure 3.15: 10-year return period flood-line output standardised residuals plot across NGI, AW3D30 & SRTM DEM sources with significant outliers identified with a label

The identified XS cutlines where significant differences between the DEM source and LiDAR flood inundation outputs that are beyond the 95% confidence level are populated in Table 3.6, while Figure 3.16 shows the locations of the respectively identified XS cutlines associated with each outlier. The significant outliers identified as shown in Table 3.6 indicate that the majority of NGI outliers underestimate the flood-line extent, while the AW3D30 and SRTM sources show a mix of over and underestimation. The results show that the most significant outliers identified through the residual analysis for the 10-year period are on the left side of the river. The results also show that the NGI, AW3D30 and SRTM DEM sources tend to overestimate the flood extent in the smaller inundation areas (5 m to 50 m from the stream centreline) and underestimate the flood extent in larger inundation areas (80 m to 150 m from the stream centreline).

Table 3.7: Identified standardised residual outliers for 10-year return period flood-line outputs

XS Cutline ID	DEM Source	Bank (Left/Right)	Underestimation / Overestimation	Distance difference (metres)
49	SRTM	Right	Overestimation	65.55
2	AW3D30	Right	Overestimation	73.74
2	AW3D30	Left	Overestimation	88.19
19	NGI	Right	Underestimation	117.63
44	NGI	Left	Underestimation	145.78
44	AW3D30	Left	Underestimation	71.99
2	AW3D30	Left	Overestimation	90.58
48	NGI	Left	Overestimation	95.57
1	AW3D30	Left	Overestimation	90.577
38	AW3D30	Left	Underestimation	42.72
8	NGI	Left	Underestimation	50.97
23	NGI	Left	Underestimation	48.94
40	AW3D30	Right	Underestimation	19.33

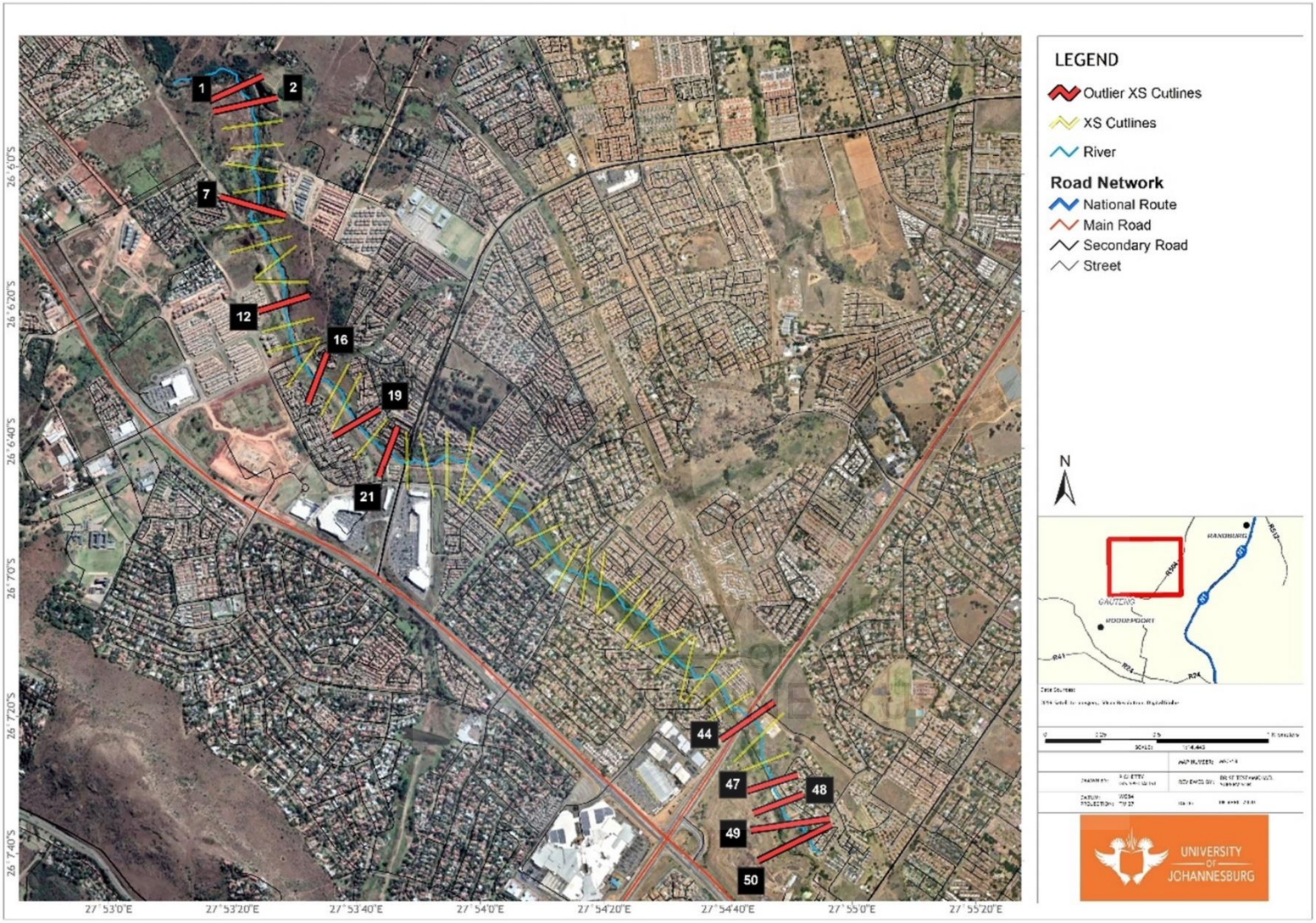

Figure 3.16: Identified standardised residual outliers for 10-year flood-line output locations displayed in true colour RGB band combination

3.3.4.2 100-year flood-line outlier identification

Figure 3.17 illustrates the 100-year flood-line output residual analysis results, which represents the LiDAR-based inundation distance to the stream centreline on the X-axis, and the residuals of inundation distance to the stream centreline derived from three DEM sources (AW3D30, SRTM & NGI) on the Y-axis. By using the residual plot analysis, individual records were identified that are visual outliers from the distribution of residual values. A total of ten points were identified, each with its unique spatial location that was linked back to each XS cutline.

The values showed a gradual increase from negative standardised residual values indicative of overestimations in the lower flood inundation areas towards larger positive standardised residual values that were indicative of underestimations in the larger flood inundation areas as shown in Figure 3.17. Like the 10-year residual outputs, the 100-year results showed that the larger the flood inundation extent, the larger the overestimation of the extent of flood inundation. The residual results indicate that the NGI source overestimated the extent of the flood inundation model at various distances from the stream centreline with 68% of the recorded distances extending beyond the LiDAR baseline output. Instances of underestimation were recorded at approximately 90 m and 120 m away from the stream centreline. The AW3D30 source showed a similar trend seen with the NGI values with larger deviations in general. The AW3D30 outputs generally underestimated the extent of the flood-line with 65% of the recorded measurements being lower than the LiDAR baseline output. Large overestimations of the inundation extent for the AW3D30 output occurred between 10 m and 70 m. The SRTM source showed an increasing trend in residual values with the extent of flood inundation, with large amounts of dispersion which represents larger averaged offsets from 5–50 m. The majority of the SRTM observations are underestimations of the LiDAR baseline output, with 63% of the recorded measurements being lower than the LiDAR baseline output.

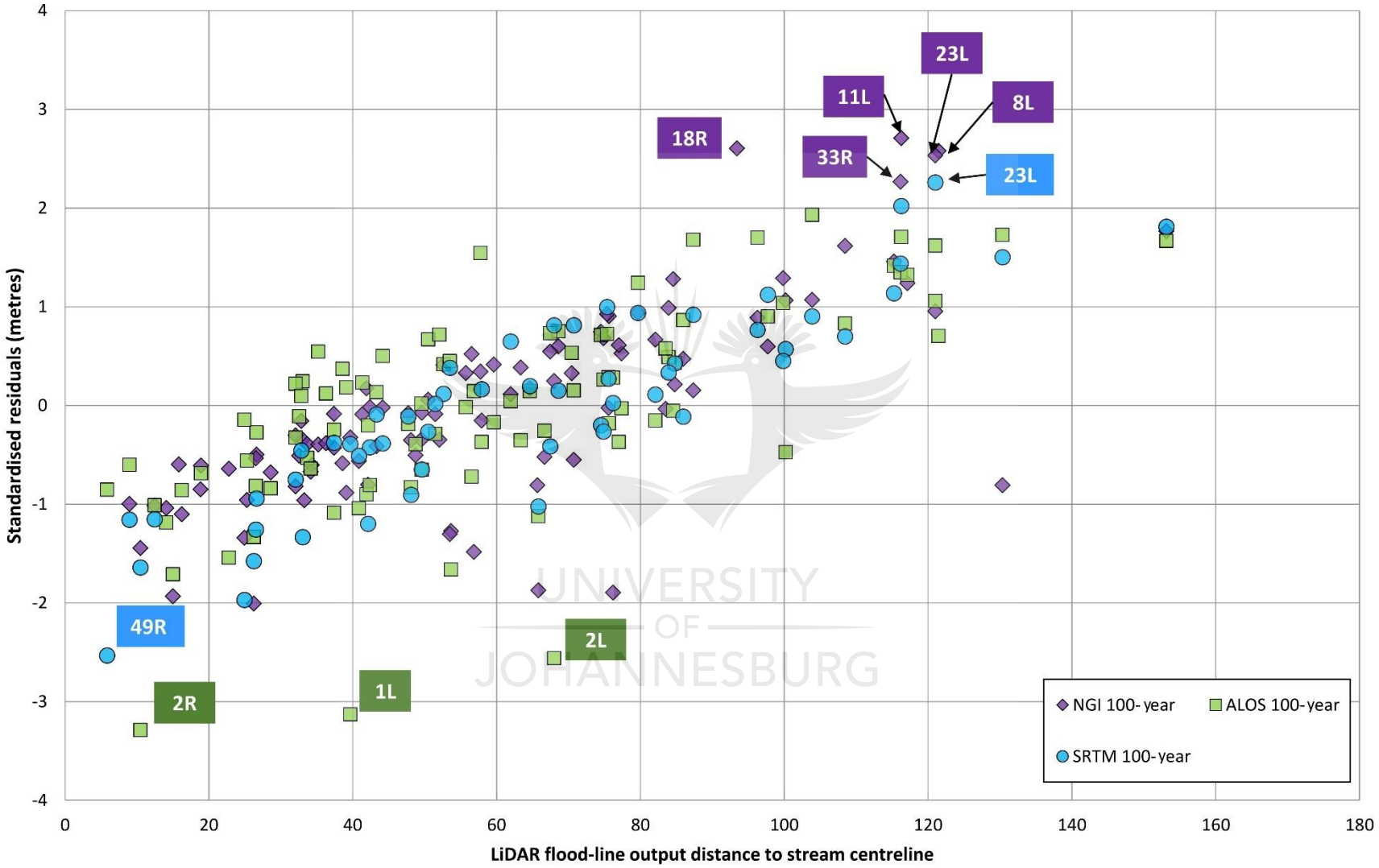

Figure 3.17: 100-year return period flood-line output standardised residuals plot across NGI, AW3D30 & SRTM DEM sources with significant outliers identified with a label

The identified XS cutlines where deviations significant differences between the DEM source and LiDAR flood inundation outputs are populated in Table 3.8 which shows that the NGI source had the largest outlier count (5), followed by the AW3D30 (3) and then SRTM (2), which had the least significant outliers. Figure 3.18 shows the identification of the standardised residual outliers which were larger than 2 and lower than -2, corresponding with a 95% confidence level.

Table 3.8: Identified standardised residual outliers for 100-year return period flood-line outputs

XS Cutline	DEM Source	Bank (Left/Right)	Underestimation / Overestimation	Distance difference (metres)
1	AW3D30	Left	Overestimation	75.97
2	AW3D30	Left	Overestimation	69.132
2	AW3D30	Right	Overestimation	70.53
8	NGI	Left	Underestimation	49.28
11	NGI	Left	Underestimation	60.275
18	NGI	Right	Underestimation	77.17
23	SRTM	Left	Underestimation	86.93
23	NGI	Left	Underestimation	47.614
33	NGI	Right	Underestimation	39.74
49	SRTM	Right	Overestimation	87.06

The results show that the most significant outliers identified through the residual analysis for the 100-year period were on the left side of the river. All NGI identified outliers were underestimations of the food extent, while all AW3D30 outliers were overestimations. The SRTM identified outliers were representative of overestimates and underestimates. The results also show that the NGI, AW3D30 and SRTM DEM sources tended to overestimate the flood extent in the smaller to medium scale inundation areas (5 m to 80 m from the stream centreline) and underestimate the flood extent in larger inundation areas (90 m to 130 m).

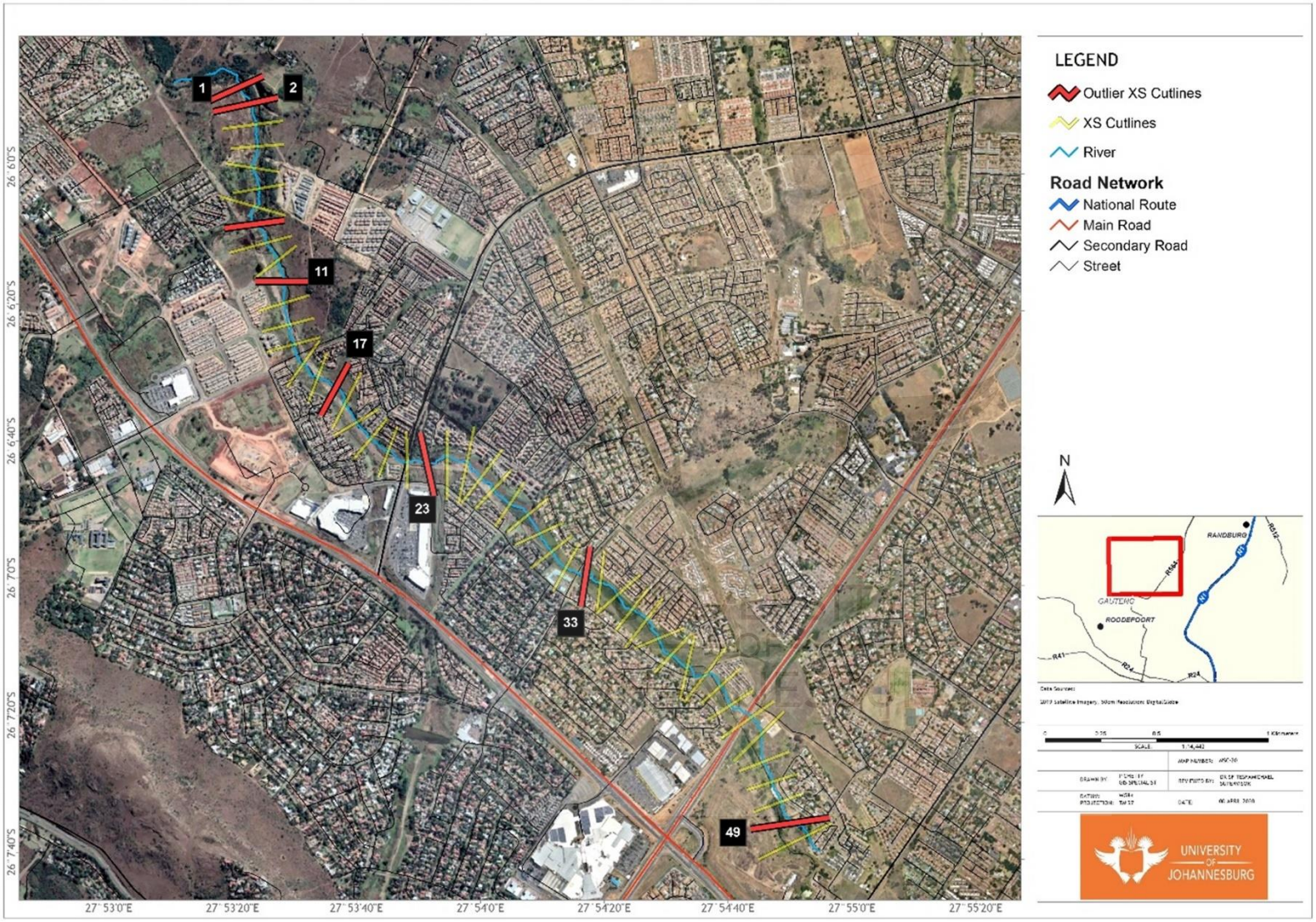

Figure 3.18: Identified standardised residual outliers for 100-year flood-line output locations displayed in true colour RGB band combination

3.4 Discussion

3.4.1 DEM source accuracy

The results show that for the 10- and 100-year return periods, the NGI DEM yields marginally the most complete flood-line delineations, in agreement with research findings by Sanders (2007) who found that accurate and coherent depictions of flood-line extents are highly dependent on high spatial resolution data used as input. Interestingly, the difference between the NGI and baseline LiDAR outputs were the highest of the assessed DEM sources, indicating that while the NGI DEM produces flood-line outputs with the best level of coverage, the accuracy of the flood-line output itself is relatively low. This is further shown in the results obtained from the RMSE analysis where the RMSE values for the 10-year period show the largest differnece to the baselibe LiDAR, and a signficantly high difference in RMSE for the 100-year period. The SRTM DEM outputs yielded the poorest coverage for the 10-year and 100-year flood-line outputs but showed the least difference to the LiDAR outputs. These findings are consistent with findings by Lim & Brandt (2019) who found that while a lower resolution DEM input may yield quantifiably improved results, the general error in the form of discrepancies on the flood-line output is significant. The findings on SRTM are also in agreement with previous research by Mashimbye *et al*. (2019) who showed that SRTM produced good vertical accurcy levels. The AW3D30 DEM source results performed significantly better than the SRTM DEM source in terms of coverage area across both return periods which is in agreement with findings by Azizian & Brocca (2020). While the results indicate that the AW3D30 DEM source falls between the SRTM and LiDAR DEM sources in terms of accuracy, the holistic overview taking into account the significant spatial coverage provided by the AW3D30 DEM along with the best RMSE results obtained means that the AW3D30 DEM source can be regarded as quite promising for flood-line modelling.

Comparisons of the river profile between the various sources as shown in Figure 3.19 indicate numerous incline features moving in a downstream direction; these are not characteristic of a smooth-flowing hydrological system. Due to the processing nature of the GeoHECRas system which takes flow volumes and velocity into account from a cumulative perspective, any artificial incline features or misrepresentations of the river system in the DEM has the potential to lead to areas of poor model outputs (CivilGEO, 2019). It is also important to note the key differences between the DEM sources being assessed. A DEM can be differentiated into a DTM which provides elevation on terrestrial features only, and a DSM which provided elevation information on both terrestrial and any ancillary features located on the surface at the time of the data collection (Lohani & Ghosh, 2017). The methodology used during the elevation data collection process and its associated post-processing categorises the DEM product into either

a DSM or DTM. The LiDAR dataset served as the only true DTM since it was generated utilising a well-refined ground elevation point cloud. Therefore, influences such as tree and vegetation canopy in the DSM surfaces can potentially lead to inaccurate representations of the elevation that defines the hydrological environment around the river.

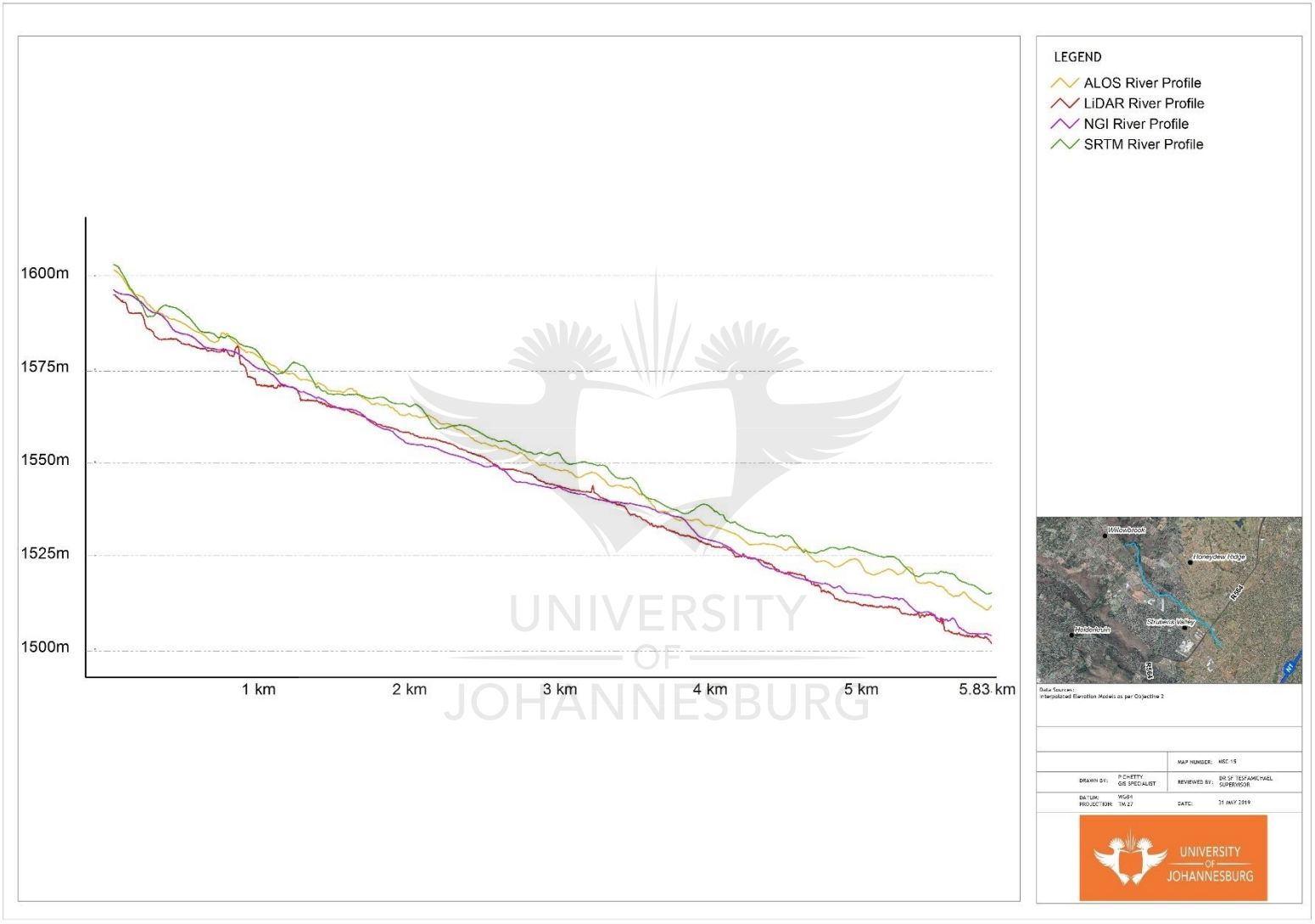

Figure 3.19: River profile comparison between LiDAR, NGI, AW3D30 & SRTM DEM sources

3.4.2 Flood-line extent coverages between the DEM sources

The NGI results show the largest number of overlapping data points in both return periods (n = 92 for 10-year; n = 99 for 100-year), which implies that the NGI DEM source covered the largest flood inundation extent when compared to the baseline LiDAR output. The AW3D30 DEM source showed good levels of flood inundation coverage (n = 94 for 10-year and 100-year) while the SRTM source outputs indicate that the application of this source is unsuitable for short-term use, localised flood-line assessments (10-year n = 35%; 100-year n = 56). The water volume determination results between the 10-year and 100-year return period increased by a factor of 2.8 (10-year: 192 m^3; 100-year: 544 m^3) as shown in Table 3.5. The number of overlapping results across all DEM sources and the baseline LiDAR increased in the 100-year flood-line outputs when compared to the 10-year flood-line results, indicating that increases in a return period's water volume yield increasingly coherent flood inundation outputs. The SRTM DEM source showed the largest increase in its flood-line area of coverage results in the 100-year return period when compared to the 10-year return period. The AW3D30 source showed good levels of consistency and applicability between both return periods.

The difference between each DEM source and the baseline LiDAR outputs were expressed by the T-test (Table 3.6). The NGI flood-line output showed the largest significant difference to the LiDAR flood-line output for both 10- and 100-year return periods. The AW3D30 assessment showed an increase in performance for the 100-year period in terms of the area of coverage a mean difference to the LiDAR output. The SRTM DEM source which represents a resolution offering similar to that of the AW3D30 source also showed an increase in performance in terms of coverage area and mean difference, but nowhere near the performance of the AW3D30 DEM source outputs. A significant difference between the AW3D30 and SRTM elevation sources is their respective date of data acquisition, with the AW3D30 being the more recently acquired dataset as shown in Table 3.1. Differences in the acquistion dates for the area resulted in significantly different flood inundation outputs, highlighting the importance of temporally relevant data in flood-line assessments as shown in previous research by Sanders (2007). These temporal differences, for instance, as highlighted between the NGI and LiDAR DEM sources, affect the flood-line extents, with the difference between the two models shown in Figure 3.21. A large number of outliers were identified along the left bank using the residual analysis. The cross sectional profile shown in Figure 3.20 indicates that the NGI DEM is significantly lower in elevation than the LiDAR DEM. Figure 3.21 shows temporal satellite imagery from 2006, 2010, 2015 and 2019 for the same identified area, revealing a PickitUp garden refuse dumpsite. Results from the 10-year return period volume returned a large number of observations that were identified as outliers in the standardised residual analysis. Typically, garden refuse dumpsites undergo constant

reshaping, as confirmed by the historical imagery assessment shown in Figure 3.21. This further highlights the importance of using timely data in addition to taking into consideration the spatial resolution of a DEM.

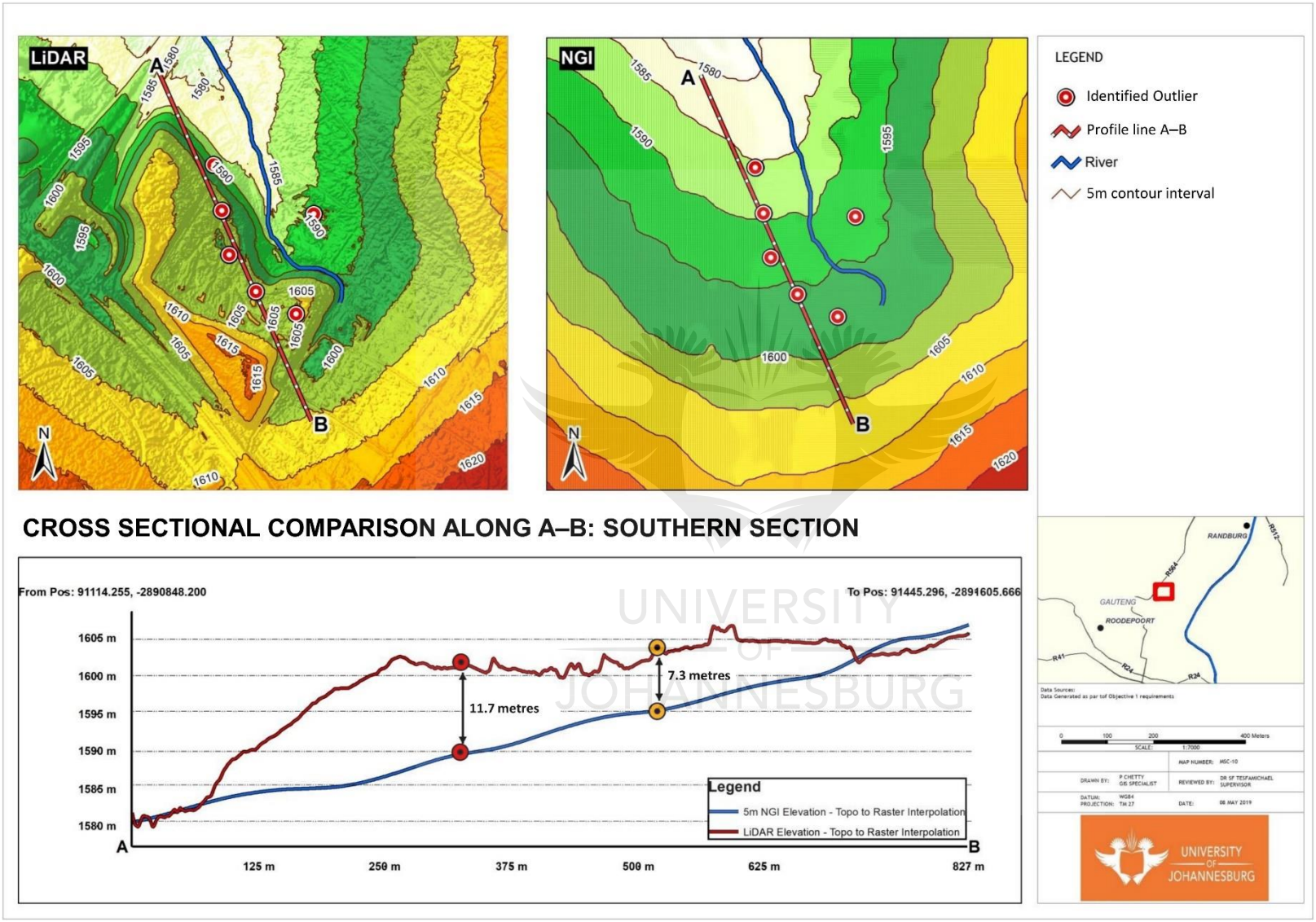

Figure 3.20: DEM cross sectional comparison along A–B: southern section

Figure 3.21 PickitUp garden refuse site surface changes from 2006–2019 displayed in true colour RGB band combination

3.4.3 Limitations associated with the various DEM sources

Overestimations of flood extent result in overly aggressive baselines for development activity along the banks of a river course that translate to land that is incorrectly categorised as a flood hazard area. In contrast, underestimations of flood extents results can lead to significant property damage and in extreme circumstances the loss of life. The 10-year and 100-year return period LiDAR flood-line outputs indicate that in areas where potential flood inundation areas have been identified, these areas have not been developed in accordance with the CSIR guidelines for development along a hydrological system (CSIR, 1999). Areas, where the flood inundation extent overlaps with the urban and residential developments, were measured for each DEM source output for the 10-year and 100-year outputs. For the 10-year return period, the NGI DEM source shows the largest area intersection with the established urban and residential developments in the study area, followed by AW3D30, SRTM and then the baseline LiDAR. For the 100-year return period, the NGI DEM source again shows the largest area intersection with the established urban and residential developments in the study area, followed by SRTM, AW3D30 and the baseline LiDAR. Based on these observations, the NGI source can be concluded to have the highest degree of overestimation that leads to the encroachment of the flood inundation model into the already developed urban and residential areas.

While the AW3D30 and SRTM data sources share a similar spatial resolution of 30 m, the results from the two sources differ vastly. Differences in the output statistics can be attributed to the acquisition date differences, where the SRTM was acquired in 2000 and the AW3D30 data acquired in the 2006–2011 period. The results consistently show that the DEM sources that were acquired closer to the LiDAR acquisition date have a closer flood-line output. The underlying spatial resolution associations with the data sources needs consideration. The SRTM utilised a single sensor using SAR techniques to acquire its elevation data and process this to an approximate 30 m resolution offering for southern Africa. In contrast, the AW3D30 utilised a combination of three sensors which operated on photogrammetry and SAR-based principles to acquire elevation data. The resultant AW3D30 DSM was processed by combining the archive data that were collected through the three sensors, including coverage from the 2.5 m resolution PRISM sensor which resulted in a final 30 m resolution DSM. While the resolution was resampled from a 5 m pixel to a larger 30 m pixel in areas where PRISM coverage was available, the accuracy of the 5 m PRISM-based DSM is still inherent in the AW3D30 DSM product and is therefore superior to the 30 m SRTM product.

3.5 Conclusion

The goal of this research was to look at the influence of various DEM sources that were applied in hydrological modelling of flood-lines in a localised river system. The DEM sources used in this study are representative of datasets that are widely used globally, excepting for the 5 m photogrammetric contour-derived NGI dataset. While the existing body of research places emphasis on spatial resolution and its influences on flood-line delineations, the timely acquisition of DEM data plays a significant role in the accurate delineation of flood-line extents.

The results indicate that for the 10-year return period, the SRTM flood-line outputs showed the smallest difference from the baseline LiDAR flood-line outputs, but were severely deficient regarding flood-line output coverage. The SRTM flood-line outputs yielded the lowest flood inundation area and are therefore not recommended for application in short term flood-line modelling applications. Interestingly, the 10-year return period NGI flood-line output showed the largest difference from the baseline LiDAR, but in contrast, covers the largest flood-line output area. The results for the 10-year return period for the AW3D30 flood-line results indicate relatively good results in comparison with the baseline LiDAR and indicate that both NGI and AW3D30 DEM sources can be applied to effectively model flood inundation areas in similar topographic scenarios.

The results for the 100-year return period show the same pattern of results, where the SRTM output shows the smallest difference to the baseline LiDAR, but also covers the smallest area. The NGI flood-line output showed the largest difference to the LiDAR flood-line outputs, but marginally covers the largest area of the flood-line. The AW3D30 output falls between the SRTM and NGI in terms of difference but produces a large coverage area that makes the AW3D30 DEM source favourable for application in longer-term return period flood-line modelling. The applicability of SRTM for longer-term return periods should be approached with caution and avoided where possible in the said environment due to its inability to produce an acceptable area of coverage. Based on the performance from the NGI and AW3D30, both DEM sources can be applied successfully to model flood inundation extents in the longer return periods.

The findings presented in this study highlight the need for improved access to more recently acquired medium- to high-resolution elevation data sources to effectively and accurately model flood inundation extents. Intense rainfall events have the potential to alter the topography surrounding a river system. Increasing trends both in rainfall and the intensity of rainfall in South Africa validate the need for temporally relevant elevation data sources that can represent the topography of a region as accurately as possible. The results indicate that while a medium 5 m resolution NGI data source yielded the most complete results in terms of

coverage, a more recently acquired, coarser 30 m resolution AW3D30 data source was able to yield results which showed good levels of accuracy with outputs that are acceptable within a flood-line modelling context.

CHAPTER 4

CONCLUSIONS AND RECOMMENDATIONS

4.1 Revisiting the objectives of the study

Flood-line delineations are an integral component in ensuring that any potential impacts associated with floods along a river are avoided and mitigated. The river and the surrounding topography that contributes to the flow of water is commonly expressed as a DEM file in GIS software, which allows the river to be represented in a spatial framework. This in turn enables the assessment of multiple flooding scenarios. The accurate representation of the river and its surrounding topography therefore play an important role in ensuring that flood-line modelling procedures/ generate accurate results.

In South Africa, popular DEM sources that are utilised in hydrological modelling includes the NGI (of which the elevation data is interpolated from contours), SRTM, LiDAR in certain regions, and more recently, the AW3D30. The NGI source was produced by the NGI through a photogrammetric processing environment resulting in a 5 m resolution contour dataset that can be interpolated into a DSM. The SRTM was produced by NASA through interferometric radar techniques, resulting in an eventual 30 m resolution DSM product. The AW3D30 dataset from ALOS is a relatively new, offering a similar technical specification to the SRTM with a 30 m resolution DSM; however, it was collected with a range of three elevation sensors of differing resolution capability. The three sensors included the PALSAR sensor which collected radar data between 10 and 100 m resolution, the AVNIR sensor which collected data at 10 m resolution and the PRISM sensor which collected stereo imagery at 2.5 m resolution. LiDAR data in South Africa is amongst the most accurate remotely sensed elevation sources and is commonly produced with sub-metre elevation resolution that is representative of a DTM. The research aimed to identify the most accurate elevation source from the most commonly available and applied DEM sources in terms of the output accuracy in a flood-line modelling environment. The LiDAR DEM source was utilised as a baseline dataset, from which the SRTM, NGI and AW3D30 DEM source outputs from the flood-line modelling environment would be assessed against. The findings would therefore quantify the applicability of each DEM source and make recommendations on the ideal DEM source to utilise for flood-line modelling applications.

This dissertation aimed to investigate the role that the elevation data source has on the flood-line modelling procedure in terms of (1) comparing various interpolation techniques conducted on the NGI elevation data source which includes the IDW, NN, kriging, spline and Topo to

Raster techniques, (2) identifying limitations associated with the interpolation accuracy of the NGI dataset, (3) comparing flood-line outputs that are derived from the NGI, SRTM and AW3D30 DEM sources in comparison to a LiDAR flood-line output and lastly (4) identifying limitations associated with each DEM source in its application in flood-line modelling. The objectives that the study was based on aimed to provide context to the local hydrological modelling environments, where access to high-resolution remotely sensed data may be restricted. The study therefore utilised datasets which are commonly utilised internationally, and a local photogrammetric dataset, equivalent to those of various other countries. The study aimed at providing suggestions on the optimal interpolation procedure for hydrological modelling environments with similar data, along with recommendations of a DEM source where access to high-resolution information is restricted.

4.2 Comparison of interpolation techniques

To utilise elevation data as an input into the flood-line modelling process, the elevation data needed to be a continuous surface of values created from a network of elevation points or contours (a DEM). The creation of a continuous surface required that the unknown areas in between the known points or contours were approximated through interpolation. A review of existing literature on interpolation applications in elevation values showed that a multitude of commonly used interpolation techniques is used to generate DEM data (Chaplot *et al.,* 2006). The existing body of literature also shows that extensive research has been performed to assess the accuracy of these interpolation techniques. These include the NN, IDW, kriging, Topo to Raster (ANUDEM) and spline methodologies evaluated against highly accurate baseline elevation measurements (Erdogan, 2009; Zimmerman *et al.,* 1999; Aguilar *et al*., 2005; Pavlova, 2017; Salekin *et al.*, 2018; Chaplot *et al.*, 2006).

As part of this dissertation, the commonly utilised 5 m resolution NGI dataset was considered and subjected to the IDW, NN, kriging, spline and Topo to Raster techniques. The resulting outputs were then assessed against a baseline LiDAR point-cloud elevation dataset at a series of observation points along a hydrological setting. The Topo to Raster interpolation technique yielded the most accurate result, while the spline technique was unsuitable for DEM interpolation from the NGI data source. The findings are aligned to previous research findings (Arun, 2013; Callow *et al*., 2007) that indicate the suitability of Topo to Raster techniques for hydrological environments at a 1:20 000 scale. Based on the quantitative T-test and residuals analysis, it is suggested that the Topo to Raster interpolation technique be applied to the NGI dataset or elevation data sources that share a common resolution of 5 m with a

photogrammetric source origin for small to medium sized hydrological research areas of interest that share similar topographic characteristics.

4.3 Comparison of flood-line models derived from multiple DEM sources

A digital flood-line modelling approach was used to simulate the extent to which a tributary would flood, where the only variables that were interchanged in each model were the DEM source inputs. Reviews of literature show that there are numerous sources of DEM data that can be utilised for environmental modelling applications, such as flood-line generation (Grayson *et al.,* 1991; Sanders, 2007; Jakovljevic *et al*., 2019; Schumann *et al.* 2008). The accuracy of the output models generated by the various DEM sources is affected by the spatial resolution (pixel size), temporal resolution (acquisition date) and the nature of the DEM, being distinguished into being either a Digital Surface Model (DSM) or Digital Terrain Model (DTM). DSM's take all ground and non-ground features into account simultaneously when expressing the elevation in an area, whereas DTM's only take the ground elevation values and disregard all non-ground features such as vegetation and buildings (Lohani & Ghosh, 2017). From a flood-line modelling perspective, the process has increased benefit from utilising a DTM opposed to a DSM, as the DTM provides a better representation of the hydrological environment. The acquisition of elevation data that represents a DTM is more time-consuming, and as a result, is often more costly owing to the additional processing requirements. This includes the need to filter all non-ground features out of the data in photogrammetric environments; there is also the requirement for classification in LiDAR point-cloud datasets. As a result of the time and cost constraints, the utility and access to high-end DTM inputs is not always a feasible approach which leads to the adoption of more readily available DEM sources. The DEM sources assessed as part of this study included the NGI, SRTM, AW3D30 and a LiDAR DEM which served as a baseline dataset.

Based on the results obtained across two volumetric scenarios representative of the 10-year and 100-year return periods, the most complete coverage area flood-line outputs originate from the NGI source of data, followed by the AW3D30, while the SRTM yielded the least covered area. Interestingly, an analysis of the mean difference in distances from the centreline of the stream showed that the NGI-derived flood-line outputs were the least accurate, while the SRTM derived flood-line outputs returned values closer to the LiDAR output mean. It must be noted that the statistical analysis of mean values could only be conducted across areas of data overlap; that is, where flood-line outputs occur for both the baseline LiDAR DEM source, and the DEM source being compared. As such, the SRTM DEM source flood-line outputs returned the best accuracy amongst the areas of overlapping coverage only, which is why the

area of coverage produced needs to be considered. Using the holistic approach, the AW3D30 derived flood-line results showed an accuracy closer to the SRTM, with a coverage area closer to the NGI-derived flood-lines too which makes the AW3D30 source favourable. The findings indicate the importance of taking both spatial resolution and timely acquired data into account when considering which dataset to utilise.

The flood-line output assessment results also indicated with the increased water volume modelled for the 100-year versus the 10-year return period, the coarser-resolution DEM sources (AW3D30 and SRTM) performed significantly better. This indicates that in instances where larger volumes are used as input into the generation of flood-lines, the appeal of coarser-resolution DEM sources increases. For shorter duration (such as the 10-year) return periods, the lower resolution DEM sources should be applied to capture significant hydrology defining topographic features that may otherwise be missed when using larger resolution sources. In areas where the DEM source may not represent topographic features correctly, such as mining environments or rapidly changing urban environments, the results show the use of recently acquired data is preferred.

4.4 Limitations associated with each assessed DEM source in flood-line modelling

The performance of the NGI versus the baseline LiDAR can be attributed to spatial resolution differences and the acquisition date of the data. For the study area, the acquisition of timely data was the greatest limitation identified associated with the accuracy of the NGI data. By analysing residual values, the locations of significant differences between the NGI and LiDAR datasets were identified spatially. Assessment of historical imagery confirmed the limitation associated with the need for timely data acquisition. The NGI dataset provides poor estimations of elevation in areas that frequently undergo topographical change, including mining environments, dumpsites, landfills and urban areas that are undergoing development.

The limitations encountered for the various DEM sources are attributed to spatial resolution differences, the timely acquisition of data, and differentiations between a DSM and DTM. The results indicate that in the absence of high-resolution DEM source inputs in flood-line modelling environments for urban and residential environments, the AW3D30 yields the best combination of accurate and complete results overall. In areas where there have been substantial changes in topography, special consideration needs to be given to the acquisition dates from which the DEM data has been derived. In such environments, the application of the AW3D30 DEM source has shown good applicability that increases with larger volumes of water. The SRTM results indicate its unsuitability for short term return period modelling with poor coverage of the inundation area. In extreme circumstances, the SRTM DEM source can

be utilised for longer-term return periods (100-year), but preference is shown towards the AW3D30 which has proven to return more accurate results in an urban environment.

Significance also needs to be placed on the compilation of the AW3D30 dataset, which has resampled versions of data produced by the various on-board sensors of the satellite. In instances where 5 m resolution PRISM elevations were resampled to 30 m resolution, the positional accuracy of the data would still inherently be representative of the original PRISM elevation product, further differentiating the ALSO-based AW3D30 DEM source from the SRTM source.

4.5 Recommendations

The research showed significant differences between the SRTM and AW3D30 DEM source outputs which are attributed to differences in temporal resolution at the least. Further accuracy assessments need to be conducted on the AW3D30 data source with particular focus on the influence of the data specific composition of the AW3D30 in the region of assessment. This assessment will allow for the differentiation of accuracy differences between PALSAR and PRISM sensor-derived information in comparison to the SRTM.

There are procedures in which the vertical and horizontal accuracy of an elevation model can be improved by incorporating local ground control points and re-rectifying the data. It is recommended that research is conducted into the incorporation of ground control points and the related outputs for NGI, SRTM and AW3D30. Incorporation of ground control points can be made into the interpolation assessments for NGI data along with accuracy assessments for NGI, AW3D30 and SRTM DEM sources.

The research conducted was aimed at conducting an accuracy assessment of popularly utilised DEM sources in South Africa against LiDAR, assuming the absence of high-resolution LiDAR data. In the case of flood-line outputs, the LiDAR flood-line output is representative of the most accurate output and served as the baseline against which all DEM source outputs were compared. As access to technology improves, it is envisaged that the availability of LiDAR data in the hydrological environment will improve. It is therefore suggested that the field demarcation methodology for determining a flood-line extent, which involves the measurement of a flood-line after a significant rainfall period, be compared against a deterministic LiDAR-derived flood-line output by running a flood inundation model with the same rainfall volume. This can then be assessed against the in-situ recorded extent, which will enable the LiDAR data to also become a DEM source for accuracy comparison. The LiDAR data utilised in this research was flown in 2012, although the latest LiDAR survey (yet to be released by COJ) was flown in 2019. This presents an opportunity to utilise a more temporally relevant LiDAR dataset with the possibility of performing a temporal output assessment of LiDAR 2012 versus LiDAR 2019. This research will allow for comparative assessment based strictly on the date of acquisition of data.

While this research was specifically applied to an urban environment, it is recommended that further research be conducted on a variety of settings to evaluate the consistency of the results produced. Understanding the limitations of DEM sources in specific environments is key to their successful application.

REFERENCES

Adeloye, A.J., R. Rustum. (2011). Lagos (Nigeria) flooding and influence of urban planning. *Urban Design and Planning,* 164(3): 53-68.

Aguilar, F.J., F. Agu¨era, M.A. Aguilar. & F. Carvajal. (2005). Effects of terrain morphology, sampling density, and interpolation methods on grid DEM accuracy. *Photogrammetric Engineering and Remote Sensing*, 71: 805–816.

Al Mashagbah, A., R. Al-Adamat. & E. Salameh. (2012). The use of Kriging Techniques within GIS Environment to Investigate Groundwater Quality in the Amman-Zarqa Basin/Jordan*. Research Journal of Environmental and Earth Sciences*, 4: 177-185.

Alexander, W.J.R. (2001). The Standard Flood – Theory and Practice. Available from: http://www.up.ac.za/academic/civil/divisions/ water/upflood.html (Accessed 18/10/2018).

Arun, P. V. (2013). A comparative analysis of different DEM interpolation methods. *The Egyptian Journal of Remote Sensing and Space Sciences*, 16(2): 133-139.

Academy of Science of South Africa (ASSAf), (2020). Quest: Science for South Africa, 16(2).

Azizian, A. & L. Brocca. (2020). Determining the best remotely sensed DEM for flood inundation mapping in data sparse regions. *International Journal of Remote Sensing,* 41(5): 1884-1906.

Belayneh, M. W., S. K. Matthai, M. J. Bluntands. & F. Rogers, (2009). Comparison of deterministic with stochastic fracture models in water- flooding numerical simulations. *AAPG Bulletin*, 93(11):1633–1648.

Brockhoff, R.C., S.H.A. Koop. & A.W. Snel. (2019). Pluvial flooding in Utrecht: On its way to a flood-proof city. *Water*,11:1501–1518.

Brunner, G.W. (2008). HEC-RAS: River Analysis System; Hydraulic Reference Manual, Version 4: US Army Corps of Engineers: Hydrological Engineering Centre, CPD-69: 411.

Callow, J, N., G.S Boggs. & K. P van Niel. (2007). How does modifying a DEM to reflect known hydrology affect subsequent terrain analysis? *Journal of Hydrology*, 332(1–2): 30–39.

Cellmer, R. (2014). The possibilities and limitations of geostatistical methods in real estate market analyses. *Real Estate and Valuation*, 22(3): 54–62.

Chai, T. & R.R. Draxler. (2014). Root mean square error (RMSE) or mean absolute error (MAE)? – Arguments against avoiding RMSE in the literature. *Geoscientific Model Development*, 7:1247-1250.

Chaplot, V., F. Darboux, H. Bourennane, S. Leguedois, N. Silvera. & K. Phachomphon. (2006). Accuracy of Interpolation Techniques for the Derivation of Digital Elevation Models in Relation to Landform Types and Data Density. *Geomorphology*, 77: 126–141.

CivilGEO 2019. GeoHECRAS: Release V2.0. Middleton, WI.

Climate-data.org. (2019). Roodepoort Climate. Available from https://en.climate-data.org/africa/south-africa/gauteng/roodepoort-232/.

Conradie, D. C. U. (2012). South Africa's Climatic Zones: Today, Tomorrow. International Green Building Conference and Exhibition, Future Trends and Issues Impacting on the Built Environment, Sandton, July 25–26.

Council for Scientific and Industrial Research (CSIR). (1999). Ecologically Sound Urban Development. Available from https://www.csir.co.za/sites/default/files/Documents/Chapter_05_08_02_-Vol _I.pdf.

Csanyi, N. & C.K. Toth. (2007). Point positioning accuracy of airborne lidar systems: A rigorous analysis. *International Archives of Photogrammetry*, *Remote Sensing and Spatial Information Systems,* 36(1):107–111.

Cullis, J., A.H.M Gorgens., S. Lyons. (2007). Review of the selection of acceptable flood capacity dams in South African in the context of dam safety. *WRC Report No. 1420/1/07, Water Research Commission*, Pretoria.

Dawson, R.J., J. Hall., L. Speight., S. Djordjević. (2008). Attribution of flood risk in urban areas. *Journal of Hydroinformatics,* 10(4): 275–288.

Davis-Reddy, C.L. & K. Vincent. (2017). Climate risk and vulnerability: A handbook for Southern Africa (2nd Edition), CSIR, Pretoria, South Africa.
Department of Water and Sanitation (DWS). 2017. The quaternary drainage regions. Available from http://www.dwa.gov.za/iwqs/wms/data/000key2data.asp.

Donat, M.G., L.V. Alexander., H. Yang., I. Durre., R. Vose., R.J.H. Dunn., K.M. Willet., E. Aguilar., M. Brunet. & J. Caesar. (2013). Updated analyses of temperature and precipitation extreme indices since the beginning of the twentieth century: the HadEX2 dataset. *Journal of Geophysical Research Atmospheres*, 118:2098–2118.

Easterling, E.J.L., P.Y. Groisman., T.R. Karl., K.E. Kunkel. & P. Ambenje. (2000). Observed variability and trends in extreme climate events: A brief review. *American Meteorological Society,* 81(3):417–425.

Elkhrachy, I. (2017). Vertical accuracy assessment for SRTM and ASTER Digital Elevation Models: A case study of Najran city, Saudi Arabia. *Ain Shams Engineering Journal*, 9(4): 1807–1817.

Erdogan, S. (2009). A comparison of interpolation methods for producing digital elevation models at the field scale. *Earth Surface Processes and Landforms*, 34: 366-376.

ESRI 2019. ArcGIS Desktop: Release 10.7. Redlands, CA: Environmental Systems Research Institute.

Gentilucci, M., B. Maurizio., H.S. Lee. & D. Zardi. (2019). Analysis of rainfall trends and extreme precipitation in the middle Adriatic side, March region (Central Italy). *Water,*11: 1948–1962.

Geo Terra Image (GTI). (2014). South African National Landcover Dataset. Pretoria.

Gericke, O. J. & J.A. du Plessis. (2012). Catchment parameter analysis in flood hydrology using GIS applications. *Journal of the South African Institutions of Civil Engineering*, 54(2): 15–26.

Grayson, R.B., I.D. Moore. & A.R. Ladson. (1991). Digital terrain modelling: A review of hydrological, geomorphological, and biological applications. *Hydrological Processes*, 5(1): 3–30.

Green, S.B. & N.J. Salkind. (2012). Using SPSS for Windows and Macintosh: Analysing and understanding data (5th Edition). Upper Saddle River, New Jersey: Pearson Education Incorporated.

Gurnell, A. M. & D.R. Montgomery. (2000). Hydrological Applications of GIS. Advances in Hydrological Processes Series*. Wiley*. 18:176.

Hydrological Research Unit (HRU). (1972). Design flood determination in South Africa, Department of Civil Engineering, University of Witwatersrand, Johannesburg.

Hu, P., X. Liu. & H. Hu. (2009). Accuracy assessment of digital elevation models based on approximation theory. *Photogrammetry, Engineering and Remote Sensing. 75:* 49–56

Hutchinson, M.F. (1988). Calculation of hydrologically sound digital elevation models, Third International Symposium on Spatial Data Handling at Sydney, Australia, vol. 3, no. 1, pp.120–127.

Jakovljevic, G., M. Govedarica, F. Alvarez-Taboada. & V. Pajic. (2019). Accuracy assessment of deep learning-based classification of LiDAR and UAV points clouds for DTM creation and flood risk mapping. *Geosciences*, 9: 323–327.

Japan Aerospace Exploration Agency (JAXA). (2017). ALOS Global Digital Surface Model (DSM), “ALOS World 3D-30m” (AW3D30). Available from: http://www.eorc.jaxa .jp/ALOS/en/aw3d30/aw3d30v11_format_e.pdf.

Jenkins, W.A. (1927). Graduation based on a modification of osculatory interpolation. *Transactions of the Actuarial Society of American,* 28:198–215.

Johnson, M. R., C.R. Anhaeusser. & R.J. Thomas. (2006). The Geology of South Africa. Council for Geoscience.

JPL (2014). U.S. Releases enhanced shuttle land elevation data, viewed 07 May 2020, Available from: https://www.jpl.nasa.gov/news/news.php?release=2014–321

Khair, U., H. Fahmi., S. Al Hakim., R. Rahim. (2017). Forecasting error calculation with mean absolute deviation and mean absolute percentage error. *Journal of Physics conference series,* 930(1): 0012002.

Krige, D.G. (1951). A statistical approach to some basic mine valuation problem on the Witwatersrand. *Journal of the Chemical, Metallurgical and Mining Society of South Africa*. 12: 119–139.

Krige, D.G. (1952). A statistical analysis of some of the borehole values in the Orange Free State goldfield. *Journal of the Chemical, Metallurgical and Mining Society of South Africa*, 9: 47–64.

Kruger, A.C. & M.P. Nxumalo. (2017). Historical rainfall trends in South Africa: 1921-2015. *Water SA,* 43(2): 285–297.

Kuichling, E. (1889). The relation between the rainfall and the discharge of sewers in populous areas. *Transactions, American Society of Civil Engineers,* 20: 1– 56.

Li, J. & D.W.S. Wong. (2010). Effects of DEM sources on hydrologic applications. *Computers, Environment and Urban Systems*, 34: 252-261.

Lim, N.J., S.A. Brandt. (2019). Flood map boundary sensitivity due to combined effects of DEM resolution and roughness in relation to model performance. *Geomatics, Natural Hazards and Risk,* 10(1): 1613–1647.

Liu, X., H. Peng. & H. Hai. (2015). Accuracy assessment of LiDAR-derived digital elevation models based on approximation theory. *Photogrammetric Engineering and Remote Sensing*, 7(6):7062–7079.

Lohani, B. & S. Ghosh. (2017). Airborne LiDAR technology: A review of data collection and processing systems. *Proceedings of the National Academy of Sciences, India Section A: Physical Sciences,* 87(1):567–579.

Manuel, P. (2004). Influence of DEM interpolation methods in drainage analysis. *GIS in Water Resources,* 8: 32–28.

Mark, D.M. (1984). Automatic detection of drainage networks from digital elevation models. *Cartographica*, 21(2-3): 168–178.

Martin, J., A. David. & A. Garcia Asuero. (2017). Fitting Models to Data: Residual Analysis, a Primer. Intech. Available from: http://dx.doi.org/10.5772/68049.

Mashimbye, Z.E., W.P. De Clercq. & A. Van Niekerk. (2019). Assessing the influence of DEM source in derived streamline and catchment boundary accuracy. *Water SA*, 45(4): 672–384.

Matheron, G. (1963). Principles of geostatistics. *Economic Geology,* 58: 1246–1266.

Meijering, E. (2002). A chronology of interpolation: From ancient astronomy to modern signal and image processing. *Proceedings of the IEEE,* 90(3): 319–342.

Merolla, S. (2012). The effect of floods and high rainfall on the water quality in selected sub-areas of the upper Vaal Catchment. University of Johannesburg.

Merz, R. & G. Blöschl. (2008). Flood frequency hydrology: Temporal, spatial, and causal expansion of information. *Water Resources Research*, 3:13–20.

Microsoft Corporation, 2019. Microsoft Excel (Windows 10 version), Available at: https://office.microsoft. com/ excel.

Miller, J.N. (1993). Outliers in experimental data and their treatment. *Analyst*, 118(5):455–461.

Mulvaney, T.J. (1851). On the use of self-registering rain and flood gauges in making observations of the relations of rainfall and flood discharges in a given catchment. *Proceedings of the Institution of Civil Engineers of Ireland*, 4, 19–31.

Nkwunonwo, U.C., M. Whitworth. & B. Baily. (2020). A review of the current flood modelling for urban flood risk management in the developing countries. *Scientific African*. 7: e00269.

Ongdas, N., F. Akiyanova., Y. Karakulov., A. Muratbayeva. & N. Zinabdin. (2020). Application of HEC-RAS (2D) for flood hazard maps generation for Yesil (Ishim) river in Kazakhstan. *Water, 12:2672.*

Ostertagova, E. & O. Ostertag. (2013). Methodology and application of one-way ANOVA. *American Journal of Mechanical Engineering*, 1(7):256–261.

Pavlova, A.I. (2017). Analysis of elevation interpolation methods for creating digital elevation models. *Optoelectron. Instrument. Proc,* 53(2):171–177.

Robinson, T. B. & G. Metternicht. (2003). A comparison of inverse distance weighting and ordinary kriging for characterizing within-paddock spatial variability of soil properties in Western Australia. *Cartography,* 32(1):11–24.

Rodriguez, E., J.E. Belz. & C.S. Morris. (2006). A global assessment of the SRTM performance. *Photogrammetric Engineering and Remote Sensing,* 72:249–260.

Rukundo, O. & H. Cao. (2012). Nearest Neighbor Value Interpolation. *International Journal of Advanced Computer Science and Applications*, 3: 25–30.

Saheed, O. & G. Ndhlovu. (2019). Floodline Delineation for Brandfort Area of South Africa: An Integrated Approach. *Advances in Sustainable and Environmental Hydrology, Hydrogeology, Hydrochemistry and Water Resources,* 10:405–407.

Saksena, S. & V. Merwade. (2015). Incorporating the effect of DEM resolution and accuracy for improved flood inundation mapping. *Journal of Hydrology*, 530(1):80–194.

Salekin, S., J.H. Burgess., J. Morgenroth., E.G. Mason., D.F. Meason. (2018). A comparative study of three non-geostatistical methods for optimising digital elevation model interpolation. *ISPRS International Journal of Geoinformatics,* 7: 300–308.

Sanders, B. F. (2007). Evaluation of on-line DEMs for flood inundation modelling. *Advances in Water Resources,* 30(8):1831–1843.

Schoenberg, I.J. (1946). Contributions to the problem of approximation of equidistant data by analytic functions. Part A—on the problem of smoothing or graduation. A first class of analytic approximation formulae. *Quart. Appl. Math*., 4(1): 45–99.

Schulze, R.E., E.J. Schmidt. & J.C. Smithers. (2004). Visual SCS-SA User Manual (Version 1.0). ACRUcons Report, School of Bioresources Engineering and Environmental Hydrology, University of KwaZulu-Natal. 52.

Schumann, G., P. Matgen., M. Cutler., A. Black., L. Hoffmann. & L. Pfister. (2008). Comparison of remotely sensed water stages from LiDAR, topographic contours and SRTM. *ISPRS Journal of Photogrammetry and Remote Sensing*, 63: 283-296.

Shepard, D. (1968). A two-dimensional interpolation for irregularly-spaced data. 23rd ACM National Conference, Brandon Systems Press, Princeton, New Jersey, pp. 517–524.

Sibson, R. (1980). Interpolating Multivariate Data: A Brief Description of Natural Neighbour Interpolation. New York: Wiley.

Smith, K. (2013). *Environmental hazards: Assessing risk and reducing disaster*, Routledge, London.

Smithers, J. C. (2012). Methods for design flood estimation in South Africa, *Water SA*, 38(4): 633–646.

Smithers, J.C. & R.E. Schulze. (2001) Design Runoff Estimation: A Review with Reference to Practices in South Africa. *Proceedings from the Tenth South African National Hydrology Symposium,* 26–28 September 2001, School of BEEH, University of Natal, Pietermaritzburg, South Africa.

Smithers, J., K. Chetty, M. Frezghi, D. Knoesen, M. Tewolde. & J. Mesfin. (2013). Development and assessment of a daily time-step continuous simulation modelling approach for design flood estimation at ungauged locations: ACRU model and Thukela Catchment case study. *Water S.A.,* 39:467-475.

Sousa, J.A., A.M. Reynolds. & A.S. Ribeiro. (2012). A comparison in the evaluation of measurement uncertainty in analytical chemistry testing between the use of quality control data and a regression analysis. *Accredited Quality Assurance*, 17(1):207–214.

South Africa. Department of Rural Development and Land Reform, Chief Directorate: National Geo-spatial Information (NGI). (2018). *Chief Directorate for Surveys and Mapping*. Available from: http://www.cdsm.gov.za.

South Africa. Department of Rural Development and Land Reform, Chief Directorate: National Geo-spatial Information (NGI). (2014). National Landcover Classification – Geo Terra Image. Available from http://www.geoterraimage.com/uploads/GTI%202013-14%20SA%20LANDCOVER%20REPORT%20-%20CONTENTS%20vs%2005%20DEA%20OPEN%20ACCESS%20vs2b.pdf.

South African National Roads Agency SOC Limited (SANRAL). (2013). Drainage Manual. 6th ed. Pretoria: The South African Roads Agency SOC Limited.

South African Weather Bureau (SAWB). (1956). Climate of South Africa. Part 3: Maximum 24-hour Rainfall. *South African Weather Bureau Publication WB 21*. South African Weather Bureau, Pretoria, RSA.

South African Weather Services (SAWS) (2018). Annual Climate Summary for South Africa. SAWS. Available from: http://www.weathersa.co.za/Documents/Corporate/Annual%20Climate%20Summary%202018%20FINAL.pdf.

Stal, C., A. De Wulf., P. De Maeyer., R. Goosens., T. Nuttens., F. Tack. (2012). Statistical comparison of urban 3D models from photo modelling and airborne laser scanning. *International Multidisciplinary Scientific GeoConference-SGEM,* 12:901–908.

Takaku, J., K. Ichikawa., T. Tadono. & K. Tsutsui. (2016). Validation of “AW3D” global DSM generated from ALOS PRISM. *The International Archives of the Photogrammetry, Remote Sensing and Spatial Information Sciences*, 3:25–36.

Takaku, J., T. Tadono. & K. Tsutsui. (2014). Generation of high-resolution global DSM from ALOS PRISM. *The International Archives of the Photogrammetry*, *Remote Sensing and Spatial Information Sciences,* 40:243–244.

Teng, J., A.J. Jakeman, J. Vaze, S. Kim, B. Croke. & D. Dutta. (2017). Flood inundation modelling: A review of methods, recent advances and uncertainty analysis. *Environmental Modelling and Software,* 90:201–216.

Ullah, S., M. Farooq., T. Sarwar., M. Tareen. & M. Wahid. (2016). Flood modeling and simulations using hydrodynamic model and ASTER DEM—A case study of Kalpani River. *Arabian Journal of Geosciences*. 9:439–449.

Vosselman, G. (2003). 3D reconstruction of roads and trees for city modelling. *The International Archives of the Photogrammetry, Remote Sensing and Spatial Information Sciences*, 34(1):211–216.

Zhang, K., C. Fritz., D. Gann., Q. Robertson., J. Rhome., M. Ross., J. Sarmiento. & S. Santana. (2019). Accuracy assessment of ASTER, SRTM, ALOS, and TDX DEMs for Hispaniola and implications for mapping vulnerability to coastal flooding. *Remote Sensing of Environment*, 225:290–306.

Zimmerman, D., C. Pavlik, A. Ruggles. & M. Armstrong. (1999). An experimental comparison of ordinary and universal kriging and inverse distance weighting. *Mathematical Geology,* 31:475–390.